

International
Progress Report

IPR-06-24

Äspö Hard Rock Laboratory

A transformational, structural and natural occurrence study of green rust

Bo C. Christiansen

Master Thesis accepted by the
Geological Institute
University of Copenhagen

March 2004

Svensk Kärnbränslehantering AB

Swedish Nuclear Fuel
and Waste Management Co
Box 5864
SE-102 40 Stockholm Sweden
Tel 08-459 84 00
+46 8 459 84 00
Fax 08-661 57 19
+46 8 661 57 19



**Äspö Hard Rock
Laboratory**

Report no.
IPR-06-24

Author
Bo C. Christiansen

Checked by
John Smellie

Approved
Anders Sjöland

No.
F123K

Date
March 2004

Date
November 2006

Date
2006-11-29

Äspö Hard Rock Laboratory

A transformational, structural and natural occurrence study of green rust

Bo C. Christiansen

Master Thesis accepted by the
Geological Institute
University of Copenhagen

March 2004

Keywords: Green Rust, Redox, Structure, AFM, XRD

This report was made in cooperation with SKB but the conclusions and viewpoints presented are those of the author(s) and do not necessarily coincide with those of the client.

A Transformational, Structural and Natural Occurrence Study of Green Rust

Master Thesis in Geology
Bo C. Christiansen

Advisor
Susan L. S. Stipp

Geological Institute
University of Copenhagen
March 2004

Sammanfattning

Grundvatten-ytan och den kemiska sammansättningen hos grundvattnet varierar över året. De kemiska miljöerna ändrar sig mellan oxiderande och reducerande förhållanden varvid järnförande mineral omvandlas. När dessa omvandlingar sker blir tidigare sorberade ämnen inkorporerade eller frigjorda. Det är därför viktigt att förstå övergången mellan olika järnföreningar. I denna studie har jag undersökt oxideringen av $\text{Fe}(\text{OH})_{2(s)}$ till grön rost sulfat (GRso_4) och vidare till götit med hjälp av Atomic Force Mikroskopi (AFM), kapillärrörs-röntgendifraktometri (CT-XRD) och Mössbauer-spektroskopi.

Grön rost är en grupp av föreningar med brucitliknande lager av ferro- och ferrihydroxid med anjoner och vatten inlagrade. Den kan bildas genom oxidation av en ferrolösning i neutral till lätt basisk miljö. Föreningarna studerades redan 1948 av Keller som beskrev den reducerande förmågan hos grön rost med inlagrade kloridjoner. Först under de senare 20 åren har forskning skett på möjligheten att använda grön rost till att bekämpa föroreningar.

Jag har med hjälp av CT-XRD kunnat producera diffraktogram av GRso_4 med större detaljeringsgrad än tidigare. Genom att placera GRso_4 i en handskbox har jag kunnat ta AFM-bilder utan oxidationsproblem. Användandet av CT-XRD eliminerade influensen från syre och gav röntgendiffraktogram av GR-sulfatet med nya toppar. Resultaten visar att monovalenta katjoner ingår i strukturen. Med hjälp av AFM upptäckte jag en $\sqrt{3} \times \sqrt{3}$ superstruktur på kristallytorna som överensstämmer med Fe(III) i hydroxylagret, eventuellt kombinerat med en anjonpåverkan från sulfatjonerna. Jag tog prover från grundvatten på Bornholm, Danmark och Äspö, Sverige och fann, med hjälp av XRD och AFM, starka indikationer på att GR finns i det ytnära grundvattnet. Mina resultat visar att man behöver känna till de termodynamiska egenskaperna, strukturella modellerna och naturliga förekomsterna av GR-föreningar. Jag kommer att fortsätta att arbeta med dessa frågeställningar och i en nära framtid etablera en strukturell modell av GR-sulfat samt bestämma de termodynamiska egenskaperna.

Contents

1	RESUME.....	3
2	ABSTRACT.....	4
3	INTRODUCTION.....	5
4	LITERATURE REVIEW.....	6
4.1	INTRODUCTION.....	6
4.1.1	<i>Green Rust 1</i>	9
4.1.1.1	Green Rust chloride.....	10
4.1.1.2	Green Rust carbonate.....	10
4.1.1.3	Green Rust halides.....	12
4.1.1.4	Green Rust hydroxide (fougerite).....	12
4.1.1.5	Green Rust oxalate.....	15
4.1.1.6	Green Rust sulphite.....	16
4.1.2	<i>Green Rust 2</i>	16
4.1.2.1	Green Rust sulphate.....	16
4.1.2.2	Green Rust nitrate.....	18
4.1.2.3	Green Rust selenate.....	19
4.1.2.4	Green Rust phosphate.....	19
4.1.2.5	Green Rust perchlorate.....	20
4.1.2.6	Other Green Rust compounds.....	20
4.2	OVERVIEW OF GREEN RUST PARAMETERS.....	21
4.3	THE ROLE OF GREEN RUST IN THE TRANSFORMATION PROCESS OF IRON COMPOUNDS.....	22
4.3.1	<i>Fe(OH)₂</i>	22
4.3.2	<i>Goethite</i>	23
4.3.3	<i>Lepidocrocite</i>	25
4.3.4	<i>Ferrosulphate and δ-FeOOH</i>	25
4.3.5	<i>Magnetite and Maghemite</i>	26
4.3.6	<i>Hematite</i>	26
4.3.7	<i>Ferrihydrite</i>	27
4.3.8	<i>Siderite</i>	27
4.3.9	<i>Summary</i>	27
4.4	BIOGENICALLY FORMED GREEN RUST.....	29
4.5	THE ROLE OF GREEN RUST IN IMMOBILISING TOXIC COMPOUNDS.....	30
4.5.1	<i>Inorganic compounds</i>	30
4.5.1.1	Nitrite.....	30
4.5.1.2	Nitrate.....	31
4.5.1.3	Selenium.....	32
4.5.1.4	Arsenium.....	34
4.5.1.5	Chromium.....	36
4.5.1.6	Other inorganic compounds.....	39
4.5.2	<i>Radioactive compounds</i>	40
4.5.2.1	Technetium.....	40
4.5.2.2	Uranium.....	41
4.5.3	<i>Organic compounds</i>	43
4.5.3.1	Trichloroethene.....	43
4.5.3.2	1,1,1-Trichloroethane.....	43
4.5.3.3	Carbon tetrachloride.....	43
5	EXPERIMENTAL DETAILS.....	45
5.1	GLOVE BOX.....	45
5.2	SYNTHESIS.....	45
5.3	SAMPLING.....	47
6	TECHNIQUES.....	49
6.1	X-RAY DIFFRACTION.....	49

6.2	CAPILLARY TUBE X-RAY DIFFRACTION	50
6.3	ATOMIC FORCE MICROSCOPY	52
6.4	TRANSMISSION MÖSSBAUER SPECTROSCOPY	53
6.5	REPRODUCIBILITY AND UNCERTAINTY	56
6.5.1	<i>Atomic Force Microscopy</i>	56
6.5.2	<i>X-ray diffraction</i>	56
6.5.3	<i>Mössbauer spectroscopy</i>	57
7	RESULTS AND DISCUSSION.....	58
7.1	TRANSFORMATION STUDY	58
7.1.1	<i>Mineralogical and morphological changes</i>	61
7.1.2	<i>Chemical changes</i>	80
7.1.3	<i>Atomic resolution of GR_{SO₄}</i>	85
7.2	QUANTIFICATION	88
7.3	STRUCTURAL STUDY	89
7.4	NATURAL OCCURRENCE OF GREEN RUST	95
8	CONCLUSIONS	99
9	FUTURE WORK.....	100
10	ACKNOWLEDGEMENTS.....	101
11	LITERATURE CITED.....	102

1 Resume

Grundvandszonens øverste grænse fluktuerer i løbet af året, herved ændres ilt forholdene. Som følge af de ændrede ilt forhold kan der ske en omdannelse af jernforbindelser i dette område som følge af reduktion eller oxidation. Ved en sådan omdannelse kan sorberede stoffer blive inkorporeret eller frigivet. Det er derfor vigtigt at forstå overgangen mellem forskellige jernforbindelser. I dette studium har jeg undersøgt transformationen af $\text{Fe}(\text{OH})_{2(s)}$ under iltning til sulfat grøn rust (GR_{SO_4}) og videre til goethit ved hjælp af Atomic Force Microscopy, kapillærrørs røntgen diffraktometri og Mössbauer spektroskopi.

Grøn rust er en gruppe af forbindelser der består af brucit lignende lag af ferro-ferri hydroxyd med anioner og vand som mellemlag. Det kan dannes ved oxidation af en ferro opløsning i neutralt til let basisk medium. Grøn rust er blevet undersøgt siden 1948 hvor Keller beskrev den reductive kapacitet af den klorid indskudte type. Inden for de sidste 20 år og specielt de sidste 10 år er det forskningsmæssige fokus øget for at undersøge grøn rusts muligheder inden for forureningsbekæmpelse. Jeg har ved hjælp af kapillærrørs røntgen diffraktometri formået at producere diffraktogrammer af grøn rust sulfat der viser en større detaljerigdom end hidtil.

Derudover har jeg ved at placere et Atomic Force Mikroskop (AFM) i en handskeboks og optaget billeder af den morfologiske forandring i forbindelse med dannelse og omdannelse ved iltning af grøn rust sulfat. Som følge af uoverensstemmelser i litteraturen og mine resultater undersøgte jeg indflydelsen af monovalente kationer og dannelsen af GR_{SO_4} og ved hjælp af XRD fandt jeg at de monovalente kationer må være en del af GR strukturen. Ved hjælp af AFM fandt jeg at der findes en $\sqrt{3} \times \sqrt{3}$ superstruktur på krystaloverfladerne der stemmer overens med en ordning af Fe(III) i hydroxydlaget, eventuelt kombineret med en interaktion af sulfat anionerne. Jeg tog prøver af grundvand på Bornholm, Danmark og Äspö, Sverige og fandt med XRD og AFM stærke indikationer at GR findes i grundvandszonen. Mine resultater har vist at der er et stort behov for at finde de termodynamiske egenskaber, strukturelle modeller og naturlige forekomst af grøn rust materialer. Jeg vil i den nærmeste fremtid foretage beregninger samt yderligere prøver få at nå til bunds i disse spørgsmål.

2 Abstract

The upper groundwater zone boundary defined by redox behaviour fluctuates during season shifts. The chemical environment changes between oxidative and reductive. Iron containing minerals in this zone thus transform because of the changes. When such transformations take place, sorbed compounds may release to the groundwater zone. In this study, I have used Atomic Force Microscopy (AFM) and capillary-tube X-ray diffraction (CT-XRD) to examine the transformation of $\text{Fe}(\text{OH})_{2(s)}$ to Green Rust Sulphate (GR_{SO_4}) and further, to goethite during oxidation.

Green Rust (GR) is a family of compounds consisting of brucite-like layers of mixed ferrous-ferric hydroxide with anions and water molecules incorporated. The compounds were first investigated by Keller in 1948 who described the reductive capacity of the chloride-intercalated type. I have shown using AFM that the transformation from $\text{Fe}(\text{OH})_{2(s)}$ to GR_{SO_4} is topotactic. The compound's sensitivity to oxygen has been a challenge when investigating them using techniques operated under oxic conditions. X-ray diffraction data of GR presented in the literature have not been produced under careful protection against oxidation and preferred orientation to produce well-defined structural data.

I placed the AFM in a glove box and obtained images of GR_{SO_4} without oxidation problems. My use of CT-XRD eliminated the influence of oxygen and produced XRD traces of GR_{SO_4} with new peaks. The results indicate that monovalent cations are also part of the structure. I investigated this possibility. The results proved that monovalent cations are part of the GR_{SO_4} structure. Atomic resolution images of the GR_{SO_4} surface taken with AFM exhibited the expected unit cell parameters for the surface layer, but I found also a $\sqrt{3} \times \sqrt{3}$ superstructure that can be explained by ordering of the Fe(III) and possibly by interaction of the anions. In the this study I used AFM and XRD to identify a GR_{CO_3} type compound coming from Fe(II)-rich ground waters located in Sweden and on Bornholm. My results have shown that there needs to be done more work to determine the thermodynamic properties, structural models and natural occurrence of GR-compound. I will continue working on these problems and establish a structural model for GR_{SO_4} and determine the new thermodynamic properties in the near future.

3 Introduction

Iron (oxy)hydroxides are known to adsorb trace metals and organic compounds. In environments where the redox conditions change frequently, it is important to understand the processes that could alter the iron (oxy)hydroxide mineralogy. Green Rust (GR) is believed to be an important intermediate compound between ferrous and ferric mineral phases formed in neutral to slightly basic environments where oxidation or reduction processes take place. It has been shown that GR can immobilise and/or degrade potentially dangerous compounds such as Cr(VI), Se(VI), U(IV) and Trichloroethene (TCE) by reducing them and/or incorporating them into the structure. Changes in morphology associated with transformation and incorporation are important to examine because they can offer valuable clues about the potential for release of sorbed substances. It is important to study the behaviour of GR in a carefully controlled, pure system to establish a base against which to compare Green Rust behaviour in contaminated environments.

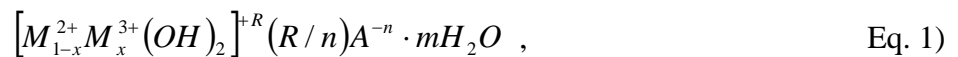
The existing literature concerning GR compounds is extensive and covers a variety of science professions: material science, corrosion science, industrial application, soil chemistry, remediation research, geology and crossovers. During interpretation of my experimental results, it became apparent that a number of the previously published reports on GR are incomplete or wrong. It was, thus, important to establish a thorough literature review of what is known and especially what is not known about the properties of GR compounds. Two experiment series were conducted to examine the structure and changes in morphology during transformation caused by oxidation. Therefore, a thorough and critical literature review was made.. The first series consisted of two experiments: one was planned for slow oxidation with an airflow rate of 142 ml min^{-1} and the other, at double the oxidation rate, 284 ml min^{-1} . The aim was to gain simultaneous and complementary information about morphology from Atomic Force Microscopy (AFM), structure from Capillary Tube X-Ray Diffraction (CT-XRD) and oxidation state from Transmission Mössbauer Spectroscopy (TMS). The second series consisted of three experiments where the effect of the presence of metal hydroxides was tested: Lithium hydroxide, sodium hydroxide and potassium hydroxide. The aim was to investigate the effect of cation size on structure and to determine if a monovalent cation influenced the formation and/or structure of Green Rust. Two additional experiments were also conducted: one to quantify the phases present in the first set of experiments and second to identify GR in natural environments.

4 Literature review

4.1 Introduction

Green Rust (GR) is the generic name originally given by Bernal et al. (1959), to a family of Fe(II)-Fe(III) hydroxy-compounds. They consist of brucite-like layers of Fe(II)-Fe(III) hydroxide that are interlayered with water and anions. This type of layered structure places GR in the subclass of layered double metal hydroxides (LDH). The GR family is divided into two groups based on the structure characterised by XRD: Green Rust 1 (GR-1) and Green Rust 2 (GR-2). The structure is determined by the geometry of the anion, so that spherical and planar anions cause a rhombohedral unit cell (GR-1) and tetrahedral anions cause a hexagonal unit cell (GR-2). As a result of these unit cell characteristics, the GR compounds resemble another LDH series, the pyroaurite/sjögrenite (Py/Sj) group. This resemblance makes it possible to associate the chemical structure of GR with that of the Py/Sj group.

The chemical composition for the Py/Sj group was given by Hashi et al. (1983) as:



where M^{2+} =Mg, Fe, Ni; M^{3+} =Al, Fe, Cr; A^{-n} = CO_3^{2-} , SO_4^{2-} , NO_3^- ; R is the ratio M^{3+}/M^{2+} and m is the amount of crystal water. In GR, the metal ions are by definition Fe(II) and Fe(III). Recent research (Chapter 4.2 for data and references) has shown that other additional anions can be incorporated in GR than was originally reported by Allmann et al. (1968). The anions that intercalate GR-1 compounds are: Br^- , Cl^- , CO_3^{2-} , $C_2O_4^{2-}$, F^- , I^- and SO_3^{2-} . Originally the GR-2 group included only SO_4^{2-} , NO_3^- and perhaps PO_4^{3-} but XRD data have not been produced for the last (Hansen and Poulsen, 1999; and Parmar, 2001). Recently SeO_4^{2-} has also been reported (Refait et al., 2000). ClO_4^- has been observed in GR compounds (Vinš et al., 1987; and Lewis, 1997), but without further specification of structural type because strongly the oxidising nature of ClO_4^- results in an unstable compound. GR_{ClO_4} probably belongs to the GR-2 group.

GR is believed to be an important actor in reduction and oxidation processes that control the composition of Fe-containing compounds, whether it is in the corrosion of steel or the oxidation of soils and groundwater containing reduced iron species. Stampfl (1969) identified the first occurrence of natural GR on corroded municipal water pipes. GR has since been found in neutral to

slightly basic environments where reinforced steel corrodes in medium to high ionic strength brines (Kounde et al., 1989; Wang et al., 2001), in soils (Trolard et al., 1997) and in an ochre sludge from a water treatment plant (Bender Koch and Mørup, 1991). Abiotic processes, however, are not the only way that GR can form. Ona-Nguema et al., (2002) found GR as a product from bioreduction of lepidocrocite (γ -FeOOH) by *Shewanella putrefaciens*. Because GR can be found in these environments, it is also believed that it exists in the upper groundwater zone, where redox conditions change seasonally. In the groundwater zone, potentially toxic components that are redox dependent such as Cr(VI) can exist. It is important to understand the structure and behaviour of the various GR types and the processes that alter them, because they can act as reductants, reducing the compound to a less toxic form and thereby decreasing the risk of pollution. Incorporation of $\text{Fe}(\text{CN})_6^{4-}$ and aldehydes in Py/Sj compounds and, especially, in GR is thought to have played an important role in the formation of RNA precursor components in the Archean oceans (Arrhenius et al., 1989). The known GR species are described in the first part of this thesis in order to give the necessary background for interpreting the experimental results. A summary of their composition are given in chapter 4.2 and crystallographic details, such as lattice plane distances (d_{hkl}) are given in Tables 1 and 2.

Table 1. X-ray diffraction data of GR-1 compounds. Prefix defines precipitation media.

GR-1														
hkl	NH ₄ -GR _{Br}		NH ₄ -GR _I		Na-GR _{Cl}		NH ₄ -GR _{Cl}		Na-GR _{C₂O₄}		Na-GR _{SO₃}		Na-GR _{CO₃}	
	Vinš et al. (1987)		Vinš et al. (1987)		Refait et al. (1998a)		Vinš et al. (1987)		Refait et al. (1998b)		Simon et al. (1997)		Drissi et al. (1995)	
	d _{hkl} (Å)	I/I _t ⁽¹⁾	d _{hkl} (Å)	I/I _t ⁽¹⁾	d _{hkl} (Å)	I/I _t ⁽¹⁾	d _{hkl} (Å)	I/I _t ⁽¹⁾	d _{hkl} (Å)	I/I _t ⁽¹⁾	d _{hkl} (Å)	I/I _t ⁽¹⁾	d _{hkl} (Å)	I/I _t ⁽¹⁾
003	7.97	80	8.29	20	7.97	100	7.93	90	7.9	100	7.81	100	7.510	100
006	3.97	100	4.14	100	3.966	31.5	3.79	100	3.89	50	3.89	80	3.736	50
101	2.75	5	2.75 ⁽²⁾		2.744		2.76	5	-		-		2.73	2
012	2.69	60	2.70 ⁽²⁾	5	2.692	34	2.71	50	2.69	40	2.68	50	2.652	25
009	2.69		2.75 ⁽²⁾	5	2.64						-			
104					2.53				2.51	15	-		2.457	2
015	2.39	40	2.45	20	2.392	4.5	2.40	10	2.38	30	2.39	60	2.333	25
107					2.16	21			-		-		2.085	2
018					2.027	2	2.03	10			2.01	40	1.961	22
00,12					1.98	19.2							1.88	2
10,10					1.808								1.736	8
10,11					1.702	5.5							1.636	5
211							1.60	30						
110	1.59	20	1.60	5	1.595	4.5							1.579	10
113	1.57	20	1.57	5	1.563	9	1.57	10					1.547	13
10,13					1.526	10.4							1.459	7
116					1.479	5								
01,14					1.448	4.3								
00,18							1.32	5						
202					1.375	3								
119					1.364									

¹Relative intensity in % referring to the strongest intensity.

²Notice d-spacing switch compared to the other GR-1 compounds.

Table 2. X-ray diffraction data of GR-2 compounds. Prefix defines precipitation media.

GR-2											
?-GR _{SO₄}			Na-GR _{SO₄}		NH ₄ -GR _{SO₄}			NH ₄ -GR _{NO₃}		Na-GR _{SeO₄}	
Bernal et al. (1959)			Simon et al. (2003) ⁽¹⁾		Vinš et al. (1987)			Gancedo et al. (1983)		Refait et al. (2000)	
hkl ⁽²⁾	d _{hkl} (Å)	I ⁽³⁾	d _{hkl} (Å)	I/I ₁ ⁽⁴⁾	Hkl	d _{hkl} (Å)	I/I ₁ ⁽⁴⁾	d _{hkl} (Å)	I ⁽³⁾	d _{hkl} (Å)	I ⁽³⁾
0001	10.92	vs	10.89	100	001	11.2	80	10.28	vs	10.9	s
0002	5.48	s	5.442	40.9	002	5.58	40	5.91	s	5.48	m
	-		4.728	11.1				4.770	w		
	-		4.326	7.0				4.353	w		
	-		3.953	4.1							
0003	3.65	s	3.610	33.3	003	3.77	100	3.723	s	3.65	m
	-		3.084	9.4					ms		
0004, 10 $\bar{1}$ 0	2.747	m	2.759	31.0	100	2.76	20	2.754	ms		
10 $\bar{1}$ 1	2.660	ms	2.640	36.3	101	2.69	20	2.671	ms		
10 $\bar{1}$ 2	2.459	ms	2.455	32.7	102	2.48	40	2.468	m		
0005, 10 $\bar{1}$ 3	2.195	ms	2.201	21.1	103	2.22	5	2.222	m		
10 $\bar{1}$ 4	1.938	ms	1.945	15.5	104	1.94	5	1.970	m		
	-		1.793	5.0					w		
10 $\bar{1}$ 5	1.712	w	1.719	9.4	105	1.74	5	1.746	w		
11 $\bar{2}$ 0	1.587	w	1.592	23.4	110	1.59	10	1.600	w		
11 $\bar{2}$ 1	1.570	w	1.575	25.7	111	1.58	10	1.576	w		
								1.555	w		
11 $\bar{2}$ 2	1.525	w	1.530	21.9	112	1.53	5	1.532	w		
	-		1.465	7.6	113	1.46	5	1.466			

¹ d-spacing and intensities are determined from Figure 2 in Simon et al. (2003), indices are not given in the reference.

² Indices based on a hexagonal cell; a = 3.174 Å and c = 10.94 Å.

³ v = very, s = strong, m = medium, w = weak

⁴ Relative intensity in % referring to the strongest intensity.

4.1.1 Green Rust 1

The study of GR began with investigation of Green Rust Chloride (GR_{Cl}) a member of the GR-1 group, which was the first type identified by Keller in 1948 and Feitknecht and Keller in 1950. The GR-1 compounds have been more extensively studied compared, to the GR-2 compounds, probably because some GR-1 anions are more common in nature: Cl⁻ in seawater and groundwater associated with waste disposal sites in northern urban environments and CO₃²⁻ from equilibrium with calcite and CO₂. It also may be attributed to the greater variety of GR-1 anions. All species in the GR-1 group have characteristic XRD d-spacings of approximately 7.9 Å and 3.9 Å, (see Table 1 for XRD

parameters). The compounds of GR-1 are all classified in the hexagonal crystal system with space group $R\bar{3}m$.

4.1.1.1 *Green Rust chloride*

Green Rust chloride (GR_{Cl}) was the first type of GR, described originally by Keller in 1948 and Feitknecht and Keller (1950), and has been studied in detail thereafter (Detournay et al., 1975; Taylor, 1984a, b; Vinš et al., 1987; Kounde et al., 1989; Refait and Génin, 1993; Schwertmann and Fechter, 1994; Refait et al., 1997; Génin et al., 1998; and Refait et al., 1998a). It has been observed that the Fe(II):Fe(III) ratio in this form can vary from 3 to 2.2 (Schwertmann and Fechter, 1994; and Refait et al., 1998a).

Using XRD, Refait et al. (1998a) found that the material's resemblance with the pyroaurite group could be used to propose a structural model for GR_{Cl} . The crystal structure of GR_{Cl} resembles that of iowaite ($Mg^{II}_3Fe^{III}(OH)_8Cl \cdot 2H_2O$). Various researchers have proposed different crystallographic parameters for GR_{Cl} obtained from XRD: Refait et al. (1998a) found $a=3.190 \text{ \AA}$ and $c=23.85 \text{ \AA}$, where Dasgupta and Mackay, (1959) found $a=3.198 \text{ \AA}$ and $c=24.2 \text{ \AA}$, both structures based on a rhombohedral unit cell.

4.1.1.2 *Green Rust carbonate*

This type of GR has been identified on corroded municipal water supply pipes (Stampfl, 1969). It forms under conditions where dissolved carbonate species are present. In iron corrosion, Legrand et al. (2000) found that when pH was above 9.5 or when $[HCO_3^-]$ was below 0.3 M, GR_{CO_3} was the sole product even at temperatures up to 90°C. At lower pH or higher $[HCO_3^-]$, GR_{CO_3} may still precipitate, but depending on the temperature, siderite ($FeCO_3$) or what the authors called amorphous $FeOOH$ could be the sole product formed.

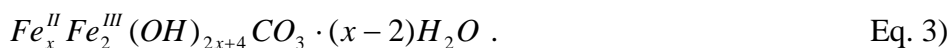
McGill et al. (1976a and b) examined a GR-1 compound formed by corrosion of cast iron in aerated water with various salts and NaOH and found it to have hexagonal lattice parameters, with $a=3.181 \text{ \AA}$ and $c=21.82 \text{ \AA}$. This GR compound was later identified as GR_{CO_3} by Taylor (1980). The crystal lattice parameters of GR_{CO_3} , based on the space group $R\bar{3}m$ for GR-1, have been reported to be 3.17 \AA for the a-axis with c-axis dimensions varying between 22.46 and 22.72 \AA (Brindley and

Bish, 1976; Taylor, 1980 and Drissi et al., 1994) and up to 23.61 Å (Legrand et al., 2001). The difference in c-axis dimension was associated with differences in the synthesis procedure of GR_{CO₃} and probably results from varying amounts of intercalated water (Legrand et al., 2001).

The way GR_{CO₃} precipitates is important for the composition of the compound. Based on data from Carbon-Hydrogen-Nitrogen-analyses (CHN), Stampfl (1969) found that the average composition of GR_{CO₃} was:



but the Fe(II)/Fe(III) ratio was variable. Murad and Taylor (1986) (as cited by Drissi et al., 1995) proposed a general formula for the composition of GR_{CO₃} as:



Omitting crystal water, the stoichiometric composition shown in Equation 3 with x=4 was found to describe GR_{CO₃} synthesised by Hansen (1989). Drissi et al. (1995) found the same composition of chemically synthesised GR_{CO₃} and estimated the amount of crystal water in the general formula (Eq. 3) setting it to 2.

Electrochemically precipitated GR_{CO₃} (Legrand et al., 2001) was found to have a composition with x=2:



The c-axis of this GR_{CO₃} compound is larger than that observed for other GR_{CO₃} species: 23.61 Å compared to 22.52 and 22.72 Å. The presence of some chloride in the structure, may explain why electrochemically formed GR_{CO₃} has larger c-axis dimensions (Legrand et al., 2001) than other GR_{CO₃}. The chloride originates from the solutions used for synthesising GR_{CO₃}. The compositions described in this section agree with the general formula proposed by Murad and Taylor (1986) (as

cited by Drissi et al., 1995) (Eq. 3) with the exception of the crystal water content proposed by Stampfl (1969) (Eq. 2).

In competition with SO_4^{2-} and Cl^- , CO_3^{2-} is the preferred anion of incorporation in GR (Refait et al., 1997). Miyata (1983) and Mendiboure and Schöllhorn (1986) found that CO_3^{2-} could also exchange for SO_4^{2-} in hydrotalcite-like compounds (pyroaurite type compounds). Both research groups (Miyata, 1983; and Mendiboure and Schöllhorn, 1986) found that divalent anions, in general, are preferred over monovalent anions in the hydrotalcite-like compounds. In preliminary studies in our group (Sonne Larsen, Skovbjerg and Christiansen), it was found that CO_3^{2-} could exchange for SO_4^{2-} in GR_{SO_4} at concentrations as low as 0.5 M $[\text{HCO}_3^-]$.

4.1.1.3 Green Rust halides

When Bernal et al. (1959) made a classification of the GR-1 compounds, they based it on four species: Green Rust-fluoride (GR_F), -bromide (GR_{Br}), -chloride (GR_{Cl}) and -sulphate (GR_{SO_4}). The last was also classified as GR-2. No one has challenged the Bernal et al. (1959) classification of GR_{SO_4} as a GR-1 type since. Vinš et al. (1987) examined a number of GR compounds and added Green Rust iodide (GR_I) as a GR-1 compound. A specific formula for the chemical composition of GR_I , GR_{Br} and GR_F has not been given in either study.

Bernal et al. (1959) showed that GR_{Br} has crystal-dimensions of: $a = 3.18 \text{ \AA}$ and $c = 22.8 \text{ \AA}$, but they provided no new information about GR_F except additional evidence that the compound does belong to the GR-1 category. A linear relationship between anion type and the length of the c-axis was presented by Vinš et al. (1987). The crystal lattice dimensions of GR_I are $a = 3.18 \text{ \AA}$ and $c = 24.8 \text{ \AA}$. Their GR_{Br} dimensions resemble the data published by Bernal et al. (1959); the a-axis dimensions are identical but Vinš et al. (1987) estimated the c-axis dimension to be larger, i.e. 24.1 \AA . These halide compounds and their relative stability with respect to anion replacement or transformation to other compounds during oxidation have not been investigated further.

4.1.1.4 Green Rust hydroxide (fougerite)

Originally, Trolard et al. (1997) and Abdelmoula et al. (1998) described a GR phase from hydromorphic soils (e.g. beneath the forest of Fougères). Based on TMS, they concluded that the phase resembled GR_{Cl} , but contained no anion other than OH^- . However, they did not analyse for

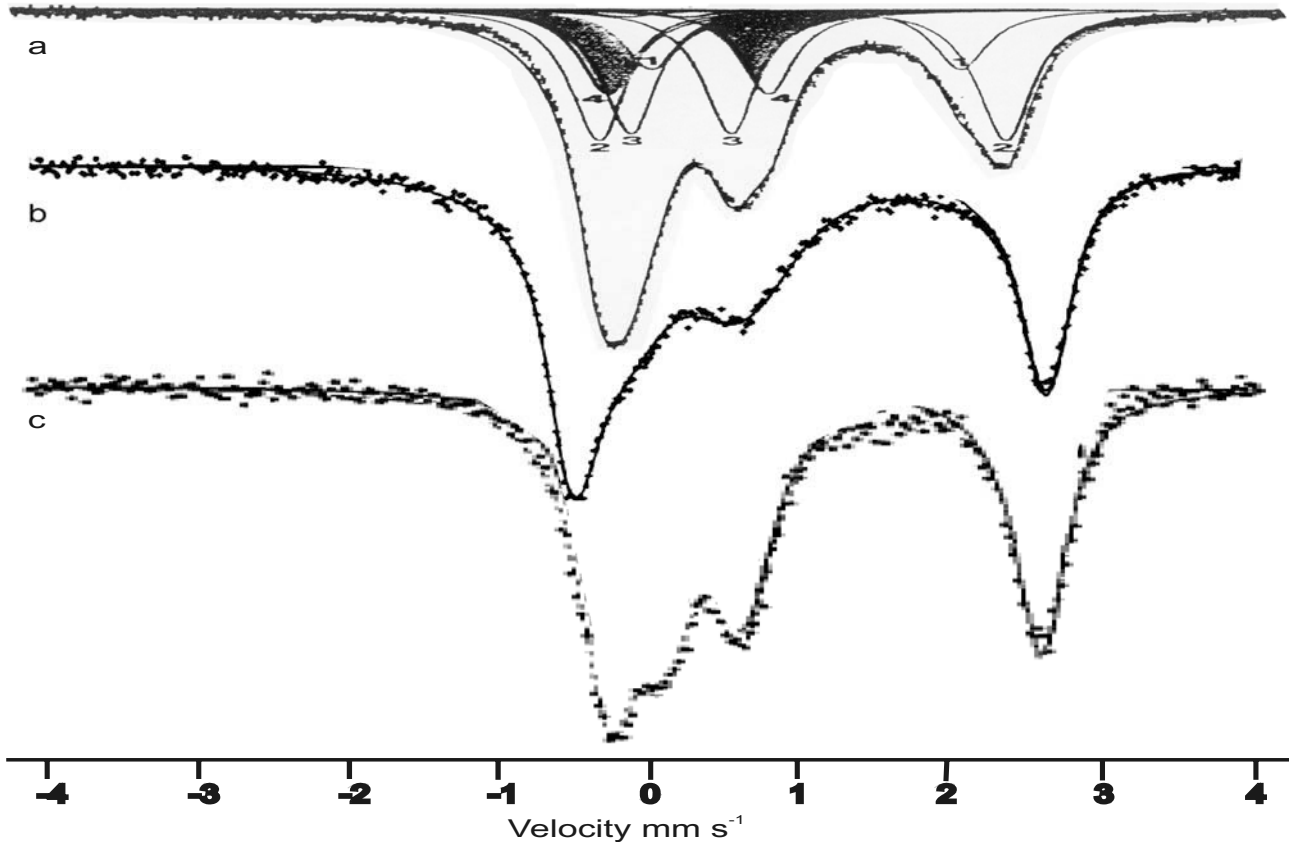
the presence of OH⁻. The identification of this phase as Green Rust hydroxide (GR_{OH}) relied only on Raman Spectroscopy (RS) and TMS data, and it was the Fe(II)/Fe(III) ratio that led to the exclusion of GR_{CO₃} as the possible identity of the phase. To determine the existence of GR_{OH}, Trolard et al. (1997) used indirect evidence from an experiment by Refait et al. (1994), where a hydrous Ni-containing Fe(III) GR-1 compound was precipitated at high pH. Refait et al. (1994), however, did not supply any chemical data for the hydrous compound that could prove the absence of CO₃²⁻ or SO₄²⁻ in the interlayer. In later work (Génin et al., 1998a, b; Bourrié et al., 1999; and Génin et al., 2001), the thermodynamic properties of the GR_{OH} compound were determined based on the observations and calculations from early studies of ferrosferric hydroxides, Fe₂OH₅ and Fe₃(OH)₈ (Arden, 1950; and Ponnampereuma, 1967), but no structural proof by XRD has ever been presented.

Although Transmission Mössbauer Spectroscopy (TMS) is useful for identifying Fe-phases, it is more reliable when used as a complement to other bulk analytical tools, such as X-ray diffraction and chemical analysis. In their studies of various green rusts compounds, the group of Génin used TMS and XRD as the primary bulk analytical methods. However Abdelmoula et al. (1998) excluded their XRD data “because of the small presumed amount of iron-containing compound in soils (...) X ray diffraction is not relevant for identification”. Thus, their definition of a GR_{OH} phase is, based primarily on TMS, RS and chemical data. Although TMS results resemble those from synthetic GR data quite well, with the exception of the relative area ratio of the doublets in the spectra, a reliable identification of the soil mineral assemblage cannot be made without some structural information. In a recent study by Feder et al. (2002), in-situ Mössbauer spectroscopy (MS) was used to examine the soil composition beneath the forest of Fougères. They interpreted their MS results only in terms of GR-like phases and did not at all consider the possibility of any other ferrous or ferric silicate or other phases.

The hydromorphic soil in which Génin and colleagues have interpreted the presence of GR_{OH} has developed from a saprolitic granodiorite containing cordierite (Trolard et al., 1997; Abdelmoula et al., 1998; Refait et al., 2001; and Feder et al., 2002). Thus it is certain that other Fe-bearing minerals are also present, especially biotite (K(Mg, Fe^{II})₃(Al, Fe^{III})Si₃O₁₀(OH)₂) and as transformation products of mafic minerals, ferrous chlorite (chamosite), (Fe^{II}₅Al)(Si₃Al)O₁₀(OH)₈ (Bailey, 1988). This last phase is particularly interesting because it has Fe(II) bound in brucite-like interlayers. The Mössbauer parameters would certainly resemble GR because the coordination

environment of Fe is almost identical in the two phases. Comparison of TMS spectra published for weathered muscovite by Farrow (2002) and annite (ferric-rich biotite) by Dyar and Burns (1986) with spectra of the phase reported by the group of Génin (Fig. 1) shows that the spectra of the samples are almost identical. The fitting of doublets is dependent of the eye of beholder, because e.g. the doublets of the GR_{OH} could be split in two (at about $\text{IS}=0.5 \text{ mm s}^{-1}$). The position of, and the number of fitted doublets needed to fit the curves influence the Mössbauer parameters. Murad and Taylor (1984) discussed the problem of using TMS as an identification tool in soils because of the resemblance of GR and Fe-bearing clay minerals (Heller-Kallai and Rozenson, 1981) and recommended to test the sample by exposing it to atmospheric oxygen.

Figure 1. Mössbauer spectra of a) annite (Dyar and Burns, 1986) possibly obtained at room temperature, fitted with 4 doublets (numbers applied for each), b) muscovite weathered in water (Farrow, 2002) obtained at room temperature and c) fougérite obtained at 78 K (Trolard et al., 1997). The temperature difference is expected to shift the quadrupole split of the absorption lines by approximately $+0.12 \text{ mm s}^{-1}$ for the 78 K sample.



In the light of this evidence, the interpretation of a GR_{OH} phase in the soil is doubtful, especially because the possible presence of chlorite or other iron-bearing silicate phases in the soils is not considered. They readily assume that the green rust originates from microbial reduction of ferric mineral phases (Trolard et al., 1997; Abdelmoula et al., 1998; and Bourrié et al., 1999) but forget that other Fe-bearing minerals can also result from weathering of granodiorite. Secondly, the calculation of thermodynamic properties was based on the ferrosferric hydroxide examined by Arden (1950) and the ferrousferric hydroxide observed by Ponnampereuma (1967), but these phases were later classified as GR_{SO₄} by Hansen et al. (1994) and possibly as GR_{CO₃} by Taylor (1980), respectively. Thirdly, the hydrous Ni-Fe(III) GR-1 compound (Refait et al., 1994), which Trolard et al. (1997) used as an analogue for GR_{OH}, was precipitated at high pH and was not chemically analysed to determine the interlayer anion. Finally because the pH of soil water beneath Fougères is between 5 and 6 (Bourrié et al., 1999), [OH⁻] is low, so it is difficult to accept a possible incorporation of OH⁻ in the GR structure. The Ni-bearing analogue for GR_{OH} is therefore not so obvious as implied. Finally, the authors excluded GR_{CO₃} simply because their interpreted TMS results exhibited a Fe(II)/Fe(III) ratio of 1:1 and they assumed that GR_{CO₃} cannot exist with other Fe(II)/Fe(III) ratios than 2:1. The group has recently, however, questioned their own exclusion argumentation for GR_{OH} (Ona-Nguema et al., 2002). They reported that GR_{CO₃} can exist with other Fe(II)/Fe(III) ratios than previously believed, but a correction for the thermodynamic data and, indeed, doubt about the existence of GR_{OH}, has not been addressed. Some of these disagreements have already been pointed out by Hansen (2001), but it seems that the International Mineralogical Association has approved fougérite as a mineral anyway (Génin pers. comm., 2004).

4.1.1.5 Green Rust oxalate

Refait et al. (1998b) examined GR incorporation of organic anions by using oxalate (C₂O₄²⁻) as a representative. Based on TMS data, they found the Fe(II)/Fe(III) ratio to be around 3:1. Because the number of anions in the structure depends on the proportion Fe(III), they proposed the chemical formula for GR_{C₂O₄} to be:



XRD showed crystal lattice parameters for $\text{GR}_{\text{C}_2\text{O}_4}$ to be $a=3.195 \text{ \AA}$ and $c= 23.4 \text{ \AA}$, consistent with the unit-cell dimensions of the GR-1 group.

4.1.1.6 Green Rust sulphite

Simon et al. (1997) precipitated GR with SO_3^{2-} in the interlayer (GR_{SO_3}) and using TMS, found the Fe(II)/Fe(III) ratio to be 3:1. On the basis of these and XRD data, the formula for GR_{SO_3} was deduced to be:



Based on XRD, GR_{SO_3} is placed in the GR-1 group and classified to be in the $\text{R}\bar{3}\text{m}$ space group with lattice parameters $a = 3.22 \text{ \AA}$ and $c = 23.40 \text{ \AA}$. Simon et al. (1997) observed that GR_{SO_3} transforms to GR_{SO_4} under oxidising conditions.

4.1.2 Green Rust 2

Anions with a tetrahedral shape, such as SO_4^{2-} , SeO_4^{2-} , NO_3^{2-} and possibly ClO_4^{2-} and PO_4^{3-} take more space in the interlayer, causing a different structural relationship. They form a second group. All members can be recognised by their XRD patterns, where the peaks of the three basal planes are most characteristic at values of 10.9 \AA , 5.5 \AA and 3.7 \AA compared to GR-1 where the spacings of the two basal planes are $7.5\text{-}7.9 \text{ \AA}$ and 3.9 \AA . All GR-2 compounds belong to the hexagonal crystal system with space group varying as a function of anion size and charge.

4.1.2.1 Green Rust sulphate

Green Rust sulphate (GR_{SO_4}) was originally described by Dasgupta and Mackay (1959) and Bernal et al. (1959). During the last decade or so, investigation of this compound has intensified because of its role in formation of goethite, ease of preparation and possible occurrence in nature. There is also evidence that it plays a role in the function of iron-wall remediation techniques (Roh et al., 2000a).

Originally, based partly on the thesis of Keller (1948), Bernal et al. (1959) and Dasgupta and Mackay (1959) proposed that GR_{SO_4} evolves *via* a GR-1 stage. However, no evidence has been found in later work that a GR-1 sulphate phase exists. Based on the similarity between the XRD

data from Bernal et al. (1959) and from Drissi et al. (1994) (Table 3), it is more likely that the compound found by Bernal et al. (1959) was in fact GR_{CO_3} and not a group 1 GR_{SO_4} compound. The GR_{SO_4} was precipitated in a buffered system but because Dasgupta and Mackay (1959) and Bernal et al. (1959) did not describe their experiments in detail, it is not possible to deduce the development pathway. The chemical formula for the phase has been determined with the use of TMS and chemical analysis. Based on these analytical tools, several authors (Hansen et al., 1994 and 1996; Génin et al., 1996; Refait et al., 1999; and Simon et al., 2003) have determined the same formula:



The amount of crystal water in the structure, n , is proposed by Hansen et al. (1994 and 1996) and Génin et al. (1996) to be 2 or 3.

Table 3. Comparison of GR-1 GR_{SO_4} and GR_{CO_3} XRD data.

GR-1 GR_{SO_4}			GR_{CO_3}		
Bernal et al. (1959)			Drissi et al. (1995)		
hkl ⁽¹⁾	d_{hkl} (Å)	$I^{(2)}$	hkl ⁽³⁾	d_{hkl} (Å)	I/I_t
0003	7.49	vs	003	7.510	100
0006	3.84	s	006	3.736	50
$10\bar{1}2$	2.72	m	101	2.73	2
			012	2.652	25
$10\bar{1}5$	2.47	m	104	2.457	2
			015	2.333	25
$10\bar{1}8$	2.029	w	107	2.085	2
			018	1.961	22
			0012	1.88	2
			1010	1.736	8
$11\bar{2}0$	1.616	mw	1011	1.636	5
$11\bar{2}3$	1.579	mw	110	1.579	10
			113	1.547	13
			1013	1.459	7

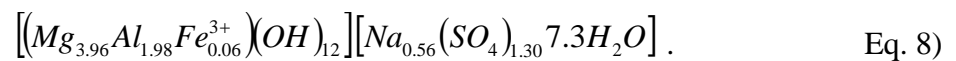
¹ Indices based on a rhombohedral lattice with $a = 3.23 \text{ \AA}$ and $c = 22.5 \text{ \AA}$.

² v = very, s = strong, m = medium, w = weak.

³ Indices based on a hexagonal lattice with $a = 3.160 \text{ \AA}$ and $c = 22.45 \text{ \AA}$.

Recent studies (Géhin et al., 2002; and Simon et al., 2003) have suggested new crystallographic properties of GR_{SO_4} . The characterisation was done with TMS and XRD. The XRD was made on material in capillary tubes and structure was determined by Rietveld analysis. In their study, however, certain peaks were omitted because they were believed to result from contamination. The new structure determination placed GR_{SO_4} in the trigonal $\text{P}\bar{3}m1$ space group with axis parameters of $a = 5.524 \text{ \AA}$ and $c = 11.011 \text{ \AA}$. Simon et al. (2003) used differential scanning calorimetry to estimate the amount of crystal water at approximately 8.

Some years ago, Hansen et al. (1994) suggested that Na^+ could be incorporated in the GR_{SO_4} structure based on work by Drits et al. (1987), who found a layered double hydroxide with Na^+ incorporated:



The unit-cell parameters were: $a = \sqrt{3}a_0 = 5.28 \text{ \AA}$ and $c = 11.16 \text{ \AA}$, where a_0 represents the shortest distance between neighbouring Fe atoms. A literature review of GR_{SO_4} and the possible incorporation of Na^+ and other monovalent cations in its structure will be discussed further in connection with the Experimental Details in Chapter 7.3.

4.1.2.2 Green Rust nitrate

Gancedo et al. (1983) found a NO_3^- interlayered GR (GR_{NO_3}) forming during corrosion of iron in an NH_4NO_3 -rich environment. The XRD data from their study indicates a GR-2 type structure. Even though NO_3^- is not body-centred, its shape is tetrahedral because a lone pair orbital takes up space; therefore it is likely to generate a GR-2 structure. From TMS parameters, it was found that the Fe(II)/Fe(III) ratio was 1.15 ± 0.26 . Lewis (1997) succeeded in producing GR_{NO_3} and found that X-ray data of the compound gave $d\{001\} = 10.97 \text{ \AA}$, $d\{002\} = 5.48 \text{ \AA}$ and $d\{003\} = 0.366 \text{ \AA}$. The discrepancy between the XRD data (Table 4) from Lewis (1997) and Gancedo et al. (1983) has not been addressed. The formation media used in the two studies was different, Gancedo et al. (1983) used a NH_4/NH_3 buffered system whereas Lewis (1997) used either NaOH or KOH to precipitate GR_{NO_3} .

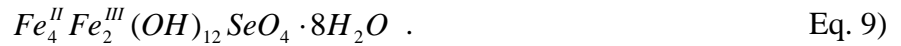
Table 4. XRD data of the three basal planes in GR_{NO₃⁻}.

hkl	Gancedo et al. (1983)	Lewis (1997)
	d _{hkl} (Å)	d _{hkl} (Å)
001	10.28	10.97
002	5.91	5.48
003	3.723	3.66

Hansen et al. (2001) observed that even though NO₃⁻ could exchange with an anion already incorporated in the GR structure, NO₃⁻ could not exist as an interlayer anion long enough to give an XRD pattern, because its reduction by GR is too rapid.

4.1.2.3 Green Rust selenate

In a study to investigate GR ability to reduce selenate, Refait et al. (2000) discovered that SeO₄²⁻ was incorporated in the interlayer. Using Transmission Mössbauer Spectroscopy (TMS) and XRD, they found that it resembles GR_{SO₄} in that the chemical formula also has Fe(II):Fe(III) = 2:1. So based on the data from TMS, Refait et al. (2000) defined the stoichiometric formula of GR_{SeO₄} to be:



Even though XRD showed the three basic lines of a GR-2 compound (i.e. 10.9 Å, 5.48 Å and 3.65 Å) no crystallographic information about GR_{SeO₄} was provided.

4.1.2.4 Green Rust phosphate

Hansen and Poulsen (1999) examined the interaction of orthophosphate (HPO₄²⁻) with GR_{SO₄} using XRD and found that the interplanar distance decreased upon exposure to phosphate from 10.86 Å, to a stable distance of ~10.4 Å, which was taken as evidence for an exchange of anions in the interlayers of the GR_{SO₄} and the possible existence of a Green Rust phosphate (GR_{PO₄}) type compound. The compound transformed to vivianite (Fe^{II}₃(PO₄)₂) within 60 days. Parmar et al. (2001) reported that during bacterial reduction of hydrous ferric oxides (HFO), GR_{PO₄} may be precipitated. The presence of GR intercalated with phosphate was shown using Energy Dispersive

Spectroscopy (EDS) (Parmar et al., 2001). Benali et al. (2001) observed with TMS and XRD that when orthophosphate (HPO_4^{2-}) was added to a mixture of GR_{CO_3} , goethite and ferrihydrite in solution, no transformation took place either to GR_{PO_4} or to vivianite.

4.1.2.5 Green Rust perchlorate

Vinš et al. (1987) attempted to make Green Rust perchlorate (GR_{ClO_4}) but it transformed rapidly to magnetite, so they were unable to give any data of its crystallographic or chemical properties. In the study by Lewis (1997), the unstable character of GR_{ClO_4} was also noted, but it was possible to obtain X-ray data for the compound. Based on a hexagonal unit cell it was found that $001=11.02 \text{ \AA}$, $002=5.52 \text{ \AA}$ and $003=3.69 \text{ \AA}$. From TMS data, Lewis (1997) formulated the anhydrous composition of GR_{ClO_4} to be:




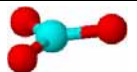



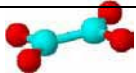

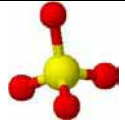
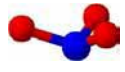
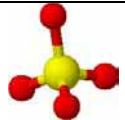
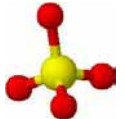

Thus GR_{ClO_4} is placed in the GR-2 group because of the tetrahedrally shaped ClO_4^- .

4.1.2.6 Other Green Rust compounds

Hansen (2001) reported on some his own previously unpublished data suggesting that linear alkylbenzene-sulphonates (LAS) could fit in the structure of GR, resulting in interlayer distances of 30 \AA and producing a hydrophobic interlayer. When Cornell and Schneider (1989) mixed Fe(III) (as ferrihydrite) and L-cysteine at a rate of 1:10, they observed a mixed valent iron compound with a characteristic X-ray diffraction line at 10 \AA . This compound was described by Hansen (2001) as a GR-type compound with cysteine as the possible interlayer anion.

In this literature review I have only focused on the Green Rust compounds that fulfil the rule that the metal hydroxide layer must consist of ferrous and ferric ions. There exist a vast number of compounds resembling GR but where divalent Fe is substituted with Ni^{2+} , Mg^{2+} or Mn^{2+} , and trivalent iron with Al^{3+} , Co^{3+} or Cr^{3+} . References for these compounds can be found in the book, "Layered Double Hydroxides: Present and Future" (Rives, 2001).

4.2 Overview of Green Rust parameters
Table 5

Abbreviation	Interlayer anion	Shape of Anion	Type	Ideal formula	Space group	Lattice parameters (Å)	Selected references
GR _{Cl}	Cl ⁻		1	$Fe_3^II Fe^III (OH)_8 Cl \cdot nH_2O$	$R\bar{3}m$	a=3.190, c=23.85	Refait et al. (1998a)
GR _{CO₃}	CO ₃ ²⁻		1	$Fe_4^II Fe_2^III (OH)_{12} CO_3 \cdot 2H_2O$		a=3.18, c=22.45	Drissi et al. (1995)
GR _{Br}	Br ⁻		1			a=3.18, c=24.2	Vinš et al. (1987)
GR _F	F ⁻		1				Bernal et al. (1959)
GR _I	I ⁻		1			a=3.19, c=24.8	Vinš et al. (1987)
GR _{C₂O₄}	C ₂ O ₄ ²⁻		1	$Fe_6^II Fe_2^III (OH)_{16} C_2O_4 \cdot 3H_2O$		a=3.195, c=23.4	Refait et al. (1998)
GR _{SO₃}	SO ₃ ²⁻		1	$Fe_6^II Fe_2^III (OH)_{16} SO_3 \cdot 4H_2O$		a=3.22 c=23.4	Simon et al. (1997)
GR _{SO₄}	SO ₄ ²⁻		2	$Fe_4^II Fe_2^III (OH)_{12} SO_4 \cdot 2H_2O$	$R\bar{3}m$	a=3.18 c=10.89	Refait et al. (1998)
				$Fe_4^II Fe_2^III (OH)_{12} SO_4 \cdot 8H_2O$	$P\bar{3}m1$	a=5.524 c=11.011	Simon et al. (2003)
GR _{NO₃}	NO ₃ ⁻		2				Gancedo et al. (1983) and Lewis (1997).
GR _{SeO₄}	SeO ₄ ²⁻		2	$Fe_4^II Fe_2^III (OH)_{12} SeO_4 \cdot 8H_2O$		a = ?, c = 10.9	Refait et al. (2000)
GR _{PO₄}	PO ₄ ²⁻		2			a = ?, c = 10.4	Hansen and Poulsen (1999) and Parmar et al. (2001)
GR _{ClO₄}	ClO ₄ ⁻		2	$Fe_{1.5}^II Fe^III (OH)_5 ClO_4$			Vinš et al. (1987) and Lewis (1997)

4.3 *The role of Green Rust in the transformation process of iron compounds*

Green Rusts (GR) and other layered double hydroxides are considered to have been important compounds in the Archean oceans both in the formation of the banded iron formations and also as catalysts for RNA precursor compounds (Arrhenius et al., 1989; Kolb et al., 1997; Arrhenius et al., 1997; and Pitsch et al., 2000). Layered double hydroxides have been shown to incorporate (ferro)cyanide (Arrhenius et al., 1989), phosphate (Arrhenius et al., 1997), simple aldehydes (Pitsch et al., 2000) and induce phosphorylations of glycolate ion (Kolb et al., 1997); all of the compounds could have played a role for biopoiesis[▲]. Layered double hydroxides might have acted as a medium for concentrating prebiogenic molecules from a dilute aqueous solution such as the primordial oceans (Arrhenius et al., 1993).

The role of GR in transformation reactions of iron compounds is important to understand because it can provide an idea of what happens to contaminants that are adsorbed to or incorporated in the iron compound. In all reaction processes of GR, there is always, eventually, transformation to a more or less stable Fe-oxide or -oxyhydroxide. The type of (hydr)oxide depends on a number of parameters, such as temperature, pH, redox potential, oxidation rate, concentration, the possibility of biogenic reduction, anions and other compounds in solution. Because GR is stable at conditions normally found in nature, is it very likely that GR plays a role in the reactions controlling iron-containing compound transformation. To interpret the relationship between GR and other Fe-(oxy)hydroxides, a comparison of crystal lattice parameters and stability and formation conditions is presented. Some of the Fe-(oxy)hydroxides may form directly from Fe³⁺, but the following section focuses on their formation during Fe²⁺ oxidation.

4.3.1 *Fe(OH)₂*

Fe(OH)₂ has not been found in nature in pure form. It is based on hexagonal close packed (hcp) anions. A mineral phase, where some of the Fe(II) is substituted with Mn(II), Mg(II) or both, known as amakinite, is found in nature (Anthony et al., 1997). The pure phase is important to mention in the context of GR, because both groups of GR are built of sheets with the same structure as Fe(OH)₂; they simply contain some Fe(III) and the layers are held together by anions. The structure of Fe(OH)₂ resembles that of brucite (Mg(OH)₂). It is hexagonal, with crystal axes $a = 3.258 \text{ \AA}$ and

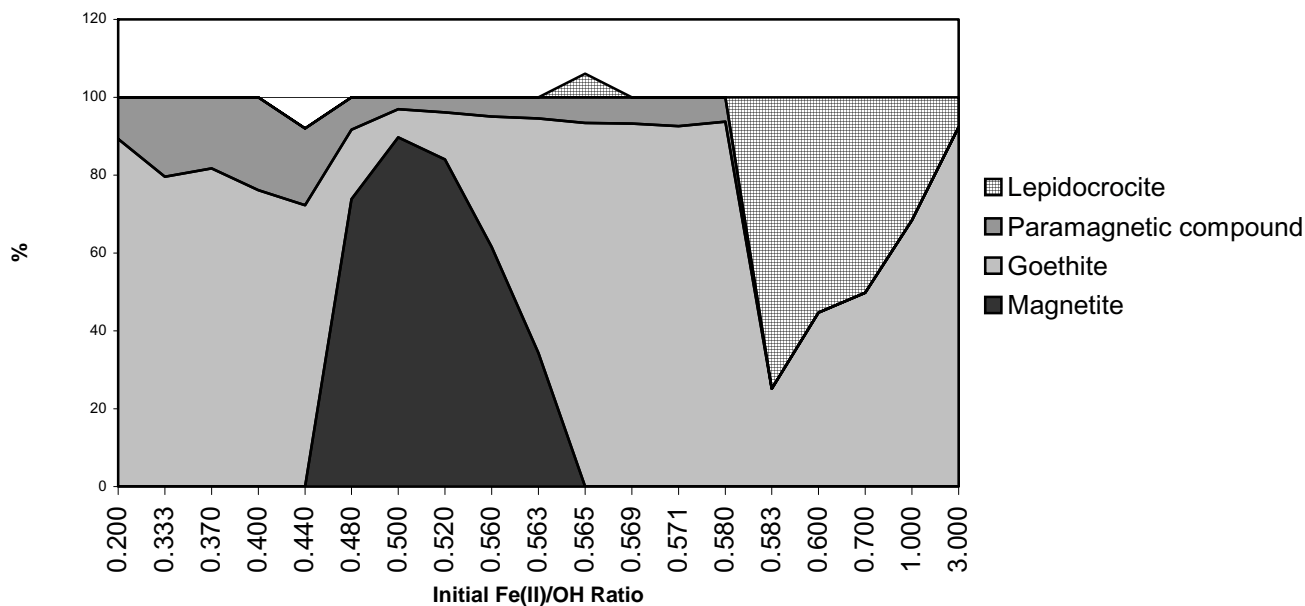
[▲] a process by which living organisms are thought to develop from nonliving matter, and the basis of a theory on the origin of life on Earth. (<http://www.britannica.com/eb/article?eu=81416&tocid=0&query=biopoiesis&ct=eb>)

$c = 4.605 \text{ \AA}$ (Bernal et al., 1959). $\text{Fe}(\text{OH})_2$ can hold up to 10% $\text{Fe}(\text{III})$ before it becomes unstable (Feitknecht and Keller, 1950). It can be formed by mixing a ferrous solution with excess alkali and strict exclusion of oxygen (Bernal et al., 1959). Because of the structural resemblance between GR and $\text{Fe}(\text{OH})_2$, it is a common perception that the transformation from $\text{Fe}(\text{OH})_2$ to GR is topotactic (Bernal et al., 1959; and Génin et al., 1998a).

4.3.2 Goethite

Goethite ($\alpha\text{-FeOOH}$) is an orthorhombic mineral with hcp arrays of anions stacked along the [100] direction (Cornell and Schwertmann, 1996). It belongs to the $Pnma$ space group with $a = 4.608$, $b = 9.956$ and $c = 3.021 \text{ \AA}$. It is one of the thermodynamically most stable iron oxides at ambient temperature (Cornell and Schwertmann, 1996). Olowe et al. (1991) examined the influence of the initial ratio between reactants (Fe/OH , SO_4/OH) on the final oxidation product from ferrous hydroxide in a sulphate system. They found goethite formation in varying degrees for several sets of conditions (Figure 2). Olowe et al. (1991) concluded that the controlling mechanism for the oxidation product was the excess of either Fe^{2+} or OH^- because an excess of either after GR_{SO_4} formation was complete, led to only goethite production.

Figure 2. Oxidation products as a function of Fe/OH initial ratio. The two ratios ($R=0.4$ and 0.5625) exhibit a total sum of products different than 100%, which is not explained in the original. Notice the ordinance is not equidistant. Plotted from original data presented by Olowe et al. (1991).



Olowe et al. (1991) did not discuss the influence of oxidation rate on the final product. Because they did not describe their experiment with respect to oxidation rate nor concentration of reactants, it is difficult to compare their results with other publications.

Formation of goethite from GR seems to be dependent on the type of anion incorporated in the GR. Research has shown that for experiments with GR_{Cl} as the precursor, lepidocrocite is the primary product with trace amounts of goethite (Schwertmann and Fechter, 1994). When the precursor is GR_{CO_3} , the final product consists of goethite (Drissi et al., 1994; Abdelmoula et al., 1996) and magnetite (Drissi et al., 1994). When GR_{SO_4} is the precursor, however, no clear tendency of final oxidation product is presented. Lepidocrocite (Schwertmann and Fechter, 1994; Génin et al., 1996; Lin, et al., 1996; and Srinivasan et al., 1996), goethite (Detournay et al., 1975; and Olowe et al., 1991) and magnetite (Tamaura et al., 1984a, b; and Domingo et al., 1993) are all observed as final products. These observations are consistent with results showing that an increase in the CO_2/O_2 ratio of the gas used for oxidation, causes the goethite/lepidocrocite ratio to rise (Carlson and Schwertmann, 1990). The preference for goethite formation to lepidocrocite formation when CO_2 is present is believed to be a result of an inhibition for lepidocrocite to nucleate (Carlson and Schwertmann, 1990) or to goethite containing some perturbed and tightly bound carbonate anions (Cornell and Schwertmann, 1996). It is not well understood why goethite forms as the sole product from GR_{SO_4} in some experiments (Detournay et al., 1975; and Olowe et al., 1991) and only as trace amounts in others (Tamaura et al., 1984a; Schwertmann and Fechter, 1994; Lin et al., 1996; and Srinivasan et al., 1996). More work needs to be made with careful characterisation of the conditions of formation, including oxidation rate, absolute concentration, temperature, pH, Eh, relative concentration ratios and other solution descriptions if the precise fields of formation conditions are to be defined.

Goethite is used as a precursor of the iron oxides made for the production of recording materials such as magnetic tapes (Tochihara et al., 1970 as cited by Kurokawa and Senna, 1999). The best iron oxides for recording materials, are those formed from a precursor mineral with a high aspect ratio (length/width) i.e. long thin crystals. Kurokawa and Senna (1999) found that coexistence of GR_{SO_4} and goethite favours goethite growth in the axial direction, increasing the aspect ratio. The authors observed that GR_{SO_4} adsorbed $\text{Fe}^{2+}_{(\text{aq})}$ during oxidation and thereby stabilising the structure.

The higher aspect ratio was related to the self-stabilising nature of GR because the longer GR_{SO_4} could exist in solution during oxidation the better the Fe^{3+}O_6 chains of goethite could form.

4.3.3 *Lepidocrocite*

Lepidocrocite ($\gamma\text{-FeOOH}$) has an orthorhombic unit cell with cubic close packed (ccp) arrays of anions stacked along the [051] direction (Cornell and Schwertmann, 1996).

In studies (Schwertmann and Fechter, 1994; Génin et al., 1996; Lin et al., 1996; and Srinivasan et al., 1996) made with GR_{SO_4} where no compounds other than GR and O_2 were introduced to the system, the final oxidation product found was lepidocrocite. In some studies (Kounde et al., 1989; and Schwertmann and Fechter, 1994), it has been observed that GR_{Cl} exhibits a tendency to lead to lepidocrocite as the main oxidation product.

Tamura (1985) observed that GR_{Cl} occurred in the transformation process of lepidocrocite to ferrites in aqueous suspension, when the temperature of the process was kept under 25°C , pH over 6 and there was free Fe(II) present in the suspension. Tamura (1985) assumed that the transformation is a dissolution-precipitation process because of the crystallographic differences between the rod-like lepidocrocite and the hexagonal GR-2.

4.3.4 *Feroxyhyte and $\delta\text{-FeOOH}$*

Two types of hexagonal FeOOH exist: the synthetically produced $\delta\text{-FeOOH}$, with $a = 2.94 \text{ \AA}$ and $c = 4.49 \text{ \AA}$ and the mineral feroxyhyte ($\delta'\text{-FeOOH}$), with $a = 2.93 \text{ \AA}$ and $c = 4.53 \text{ \AA}$ (Cornell and Schwertmann, 1996). They are both made up of disordered hcp arrays of anions, but feroxyhyte requires two formula units per unit cell, whereas $\delta\text{-FeOOH}$ contains only one (Cornell and Schwertmann, 1996). $\delta\text{-FeOOH}$ forms when $\text{Fe}(\text{OH})_2$ is oxidised rapidly, e.g. with H_2O_2 .

Feroxyhyte is found in oceanic, iron-manganese nodules (Chukhrov et al., 1977) and in gley soils under cold oxidising conditions (Chukrov et al., 1977; and Carlson and Schwertmann, 1980).

Taylor (1980) observed with XRD that freeze-dried GR_{CO_3} broke down on exposure to air to either ferrihydrite or feroxyhyte, but because a sharper line profile of the {110} diffraction peak it is more likely feroxyhyte than ferrihydrite. Preliminary experiments, conducted in our group, produced either feroxyhyte or $\delta\text{-FeOOH}$ when a solution containing $\text{Fe}(\text{OH})_2$ and GR_{SO_4} was oxidised during freeze-drying.

The observation made by Taylor (1980), of GR_{CO_3} transforming to ferrosiderite, is interesting because it is hypothesized (Burns, 1980a and b) that the red surface of Mars consists of ferrosiderite. Mars, having a CO_2 -rich atmosphere, could form carbonate rich ferrous compounds, but not siderite though. It would be essential, however, that there be water present to form a reactive solution. Ferrosiderite formation and its dependence on the activity of water are beyond the scope of this study and are not discussed further.

4.3.5 Magnetite and Maghemite

Magnetite (Fe_3O_4) is a cubic mineral with a ccp unit cell where $a = 8.39 \text{ \AA}$. Oxygen anions are stacked along the [111] direction (Cornell and Schwertmann, 1996). Maghemite ($\gamma\text{-Fe}_2\text{O}_3$) is structurally similar to magnetite, with a cubic unit cell where $a = 8.34 \text{ \AA}$ (Cornell and Schwertmann, 1996). Cation vacancies in the maghemite structure compensate for the extra Fe^{3+} compared to magnetite structure.

Formation of magnetite from GR has been observed under various conditions (Tamura et al., 1984a, b; Hansen et al., 1994, 1996; and Hansen and Koch, 1998). Using XRD, Infrared spectroscopy (IR) and electron microscopy, Tamura et al. (1984a) observed that GR_{SO_4} transformed to magnetite at temperatures between 30 and 75°C. Whether it is a result of temperature or dilution of the GR_{SO_4} solution is not evident, because GR_{SO_4} have been observed to be metastable towards magnetite (Arrhenius et al., 1993) and especially in diluted solution (Christiansen, Sonne Larsen, Skovbjerg and Stipp, unpublished). Hansen et al. (1994 and 1996) and Hansen and Koch (1998) observed formation of magnetite from GR_{SO_4} when it reduced nitrate or nitrite to nitrogen or nitrous gasses.

Taylor and Schwertmann (1974) observed that at low oxidation rate, GR_{Cl} becomes maghemite.

4.3.6 Hematite

Hematite ($\alpha\text{-Fe}_2\text{O}_3$) has been indexed based on both a hexagonal and a rhombohedral unit cell. The dimensions for the hexagonal unit cell are $a = 5.034 \text{ \AA}$ and $c = 13.752 \text{ \AA}$, and for the rhombohedral cell, $a = 5.427 \text{ \AA}$ and $\alpha = 55.3^\circ$ (Cornell and Schwertmann, 1996). Hematite consists of hcp oxygen

ions stacked along the [001] direction (Cornell and Schwertmann, 1996). No connection between GR and hematite has been found in the literature.

4.3.7 *Ferrihydrite*

Ferrihydrite is a poorly ordered compound that is believed to consist of hcp arrays of anions (Cornell and Schwertmann, 1996). It can be recognised with XRD based on the degree of ordering where it exhibits between 2 and 6 very broad diffraction peaks. The number of diffraction lines is used for ferrihydrite characterisation. Schwertmann and Fechter (1994) precipitated GR_{Cl} by adding fresh Fe(Cl)₂ solution dropwise to a solution containing 2-line-ferrihydrite. Hansen et al. (1994) also used ferrihydrite as the ferric source, added to a solution containing ferrous hydroxide to precipitate GR_{SO₄}. Schwertmann and Fechter (1994) suggested that ferrihydrite acts as a precursor of GR under reducing conditions. They suggested the same pattern of their titration experiment as presented by Hansen et al. (1994). The experiments were conducted at pH=7.0 so why Schwertmann and Fechter (1994) did not consider Fe(OH)₂ as the precursor is not clear.

Karim (1986) observed that oxidation of Fe(OH)_{2(s)} in the presence of silicon inhibited the formation of GR, and favoured formation of ferrihydrite.

4.3.8 *Siderite*

Siderite (FeCO₃) is a hexagonal mineral belonging to the $\bar{3}2/m$ system, the same group as calcite, CaCO₃. Its crystallographic axes are: $a = 4.72$ and $c = 15.45 \text{ \AA}$ in a hexagonal cell, or $a = 5.83 \text{ \AA}$ and $\alpha = 47^\circ 45'$ in the rhombohedral cell. Siderite is often found in banded iron formations (BIF), and is often associated with clay minerals. Benali et al. (2001) observed that GR_{CO₃} in solution with ferrihydrite and goethite is metastable under anoxic conditions and, the assemblage transforms to siderite and magnetite within hours. They observed that when orthophosphate was added, no siderite formation took place. We have observed similar metastability of GR_{CO₃}, favouring siderite and goethite in our group's research (Sonne Larsen, Skovbjerg, Christiansen and Stipp, not yet published).

4.3.9 *Summary*

The literature review of transformation process of GR to other Fe-(oxy)hydroxides and oxides has presented a difficult task of explaining the processes behind them. The difficulties are in some cases

a result of insufficient or missing details in the reported experimental details. It is still possible, though, to extract some of the overall parameters for the transformation process.

4.4 Biogenically formed Green Rust

Génin et al. (1991 and 1994) observed GR_{SO_4} on steel sheet piles in a harbour using XRD and TMS. They found GR_{SO_4} and sulphate reducing bacteria (SRB) present simultaneously and concluded the presence of SRB on the steel sheet piles induced a low oxidation zone supporting formation of GR_{SO_4} . Cooper et al. (2000) observed that *Shewanella putrefaciens* could reduce lepidocrocite to magnetite and hypothesised that GR could act as an intermediate compound but no evidence was supplied any to support the hypothesis. Using XRD and TMS, Ona-Nguema et al. (2002) observed that *Shewanella putrefaciens* could reduce lepidocrocite to magnetite and siderite, and also produced GR_{CO_3} . The GR_{CO_3} produced was unlike the stoichiometric material generally described (section 4.1.1.2). Chaduri et al. (2001) observed, using XRD, that *Dechlorosoma suillum* formed GR_{CO_3} from $\text{Fe}^{2+}_{(\text{aq})}$ in nitrate containing media.

4.5 The role of Green Rust in immobilising toxic compounds

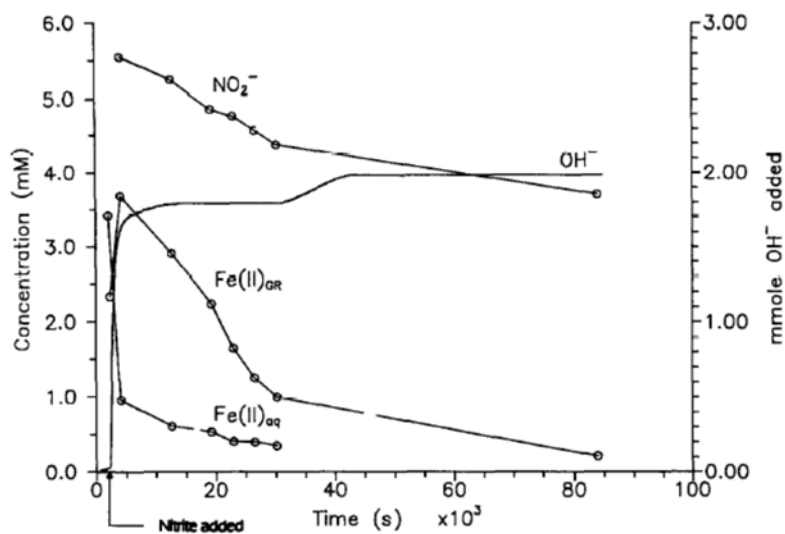
4.5.1 Inorganic compounds

A number of inorganic compounds constitute a threat to the environment and to health when they are present in a certain valence state, such as e.g. Chromium(VI), Arsenium(V) and Selenium(VI). It has been shown that GR has the possibility to react with some of the environmentally problematic or dangerous compounds. The reaction could involve a change in redox state to one that is less toxic such as Cr(VI) to Cr(III) and NO_2^- to N_2O , or an immobile state, such as As(V) to As(III) or to final transformation into non-toxic compounds such as TCE to CO_2 , Cl^- and H_2O .

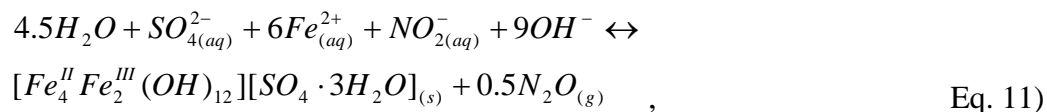
4.5.1.1 Nitrite

Nitrite (NO_2^-) has been shown to be reduced by $\text{Fe}^{2+}_{\text{aq}}$ to either NO or N_2O (Chalamet, 1973 as cited by Hansen et al., 1994; and Moraghan and Buresh, 1977). By introducing NO_2^- to a solution containing ferrihydrite and FeSO_4 , the concentration of NO_2^- decreased along with a decrease in concentration of Fe^{2+} (Hansen et al., 1994). The presence of both ferrihydrite and FeSO_4 induced formation of GR_{SO_4} . Without NO_2^- , GR formed only slowly. After addition of NO_2^- , first a rapid increase of GR precipitation and decrease of NO_2^- was followed by a constant decrease in NO_2^- (Fig. 3). Control experiments with only Fe^{2+} and SO_4^{2-} present did not show any significant reduction of nitrite.

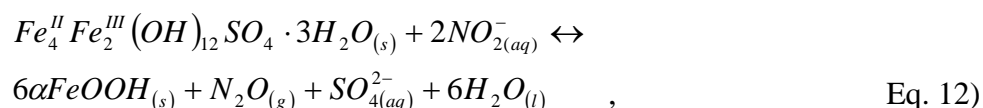
Figure 3. Changes in concentrations of dissolved Fe(II) ($\text{Fe(II)}_{\text{aq}}$), Fe(II) in GR_{SO_4} ($\text{Fe(II)}_{\text{Gr}}$) and NO_2^- and consumption of base on addition of NaNO_2 to system containing ferrihydrite, GR_{SO_4} and excess Fe^{2+} in solution (Hansen et al., 1994).



The controlling reactions were interpreted to describe the system (Hansen et al., 1994):



which was responsible for the first rapid decrease in nitrite concentration, and



which was responsible for the constant decrease of nitrite concentration that followed.

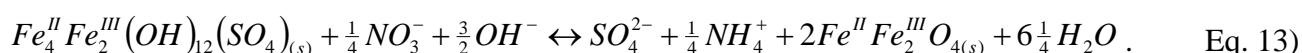
It appears that equation 11 is not consistent with the conclusion that $Fe_{(aq)}^{2+}$ had no role in the reduction of NO_2^- in notable amounts. Thus, because GR is already present in the solution with ferrihydrite and there is a dramatic decrease of NO_2^- in this solution, GR must act as a catalyst for the reduction of nitrite and therefore be part of the chemical equation (Eq. 12).

4.5.1.2 Nitrate

The ability of GR to reduce nitrate to ammonium has been investigated to establish a model for abiotic reduction rates in soils (Hansen et al., 1996; Bender Koch and Hansen, 1997; and Hansen and Koch, 1998). The reduction of NO_3^- only takes place when Fe(II) is present as solid GR and slowly as a dissolved species in solution. In a control experiment with only $Fe_{(aq)}^{2+}$ and SO_4^{2-} , NO_3^- reduction was so low that $Fe_{(aq)}^{2+}$ could be excluded as the reducing agent. To examine the reaction mechanism behind the reduction of nitrate (NO_3^-) to ammonium (NH_4^+), Hansen and Koch (1998) tested the effectiveness of both GR_{SO_4} and a sulphate-substituted pyroaurite (PY_{SO_4}) as well as two nitrate-salts, $NaNO_3$ and $Ba(NO_3)_2$. The PY_{SO_4} served as a redox inactive GR analogue. When nitrate was added as $Ba(NO_3)_2$, nitrate was converted to ammonium 40 times faster than when the same concentration was added as $NaNO_3$. Furthermore, XRD showed a decrease in both PY_{SO_4} and GR_{SO_4} c-axis length, when the nitrate was added as $Ba(NO_3)_2$ but no changes were observed with $NaNO_3$. Based on these results it was concluded that the barium forced the exchange of NO_3^- for SO_4^{2-} in the GR and PY structures by acting as a sink for the SO_4^{2-} . The NO_3^- substituted GR is not

stable because Fe(II) reduces NO_3^- , but it is stable enough that XRD patterns of the precipitate could be produced which correlated well with other GR_{NO_3} studies (Gancedo et al., 1983; and Lewis, 1997). No change in interplanar distance was observed in the presence of NaNO_3 , suggesting that the most likely interaction sites for NO_3^- with GR in natural systems are at the edges and surfaces of the GR crystal.

The reduction of NO_3^{2-} transformed GR_{SO_4} into magnetite (Hansen and Koch, 1998):



4.5.1.3 Selenium

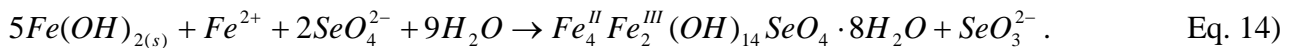
Selenium is an important nutrient, but it poses a health risk when present in too high concentrations. In some areas, the concentration of Se is 100 times higher in soils and stream waters than permitted by local authorities (Squires et al., 1989; and Thompson-Eagle and Frankenberger, 1992). As an element, selenium is geochemically quite complex, as is sulphur, because of its numerous valence states: (VI), (IV), (0) and (-II). It is therefore of interest to examine conditions that might change and control the mobility of Se-compounds.

Myneni et al. (1997) showed, using transmission X-ray microscopy, XRD, X-ray absorption near-edge spectroscopy (XANES) and extended X-ray absorption fine structure spectroscopy (EXAFS) that selenium (VI) was reduced in the presence of GR_{SO_4} . When SeO_4^{2-} was present during GR formation, there was a 48% decrease of aqueous Se within 36 seconds at $\text{pH} > 5.0$. After the initial drop, the reduction rate of aqueous Se decreased slowly at a linear to first order rate (average $k = 1.15 \pm 0.42 \times 10^{-2} \text{ hour}^{-1}$). Based on the results from EXAFS, Myneni et al. (1997) concluded that when SeO_4^{2-} was present during GR precipitation, it got incorporated into the GR structure and became reduced quickly to Se(IV) and then slowly to Se(0). The authors found similar reduction rates were observed when Se(VI) was introduced to a solution already containing GR. Se(VI) was reduced directly to Se(0) rather than *via* Se(IV) intermediates such as happened in the co-precipitation experiments. The thermodynamically most stable Se(-II) was only observed in small quantities when the adsorption experiment solutions were left to react for more than 60 hours (Table 6 summarises the reaction patterns).

Table 6. Conditions for Se reduction reactions in connection with GR_{SO₄} (after Myneni et al., 1997).

Reaction	Conditions
Se(VI) → Se(IV)	When GR precipitates during reduction (co-precipitation experiment).
Se(VI) → Se(0)	Directly when GR is already present in solution (adsorption experiment).
Se(VI) → Se(-II)	Only when GR is already present in solution and the solution is left to react for more than 60 hours.
Se(IV) → Se(0)	When GR precipitates during reduction (co-precipitation experiment).

In another study, Refait et al. (2000) examined SeO₄²⁻ in a solution containing Fe(OH)_{2(s)} and Cl⁻. By having a small amount of Fe²⁺, the study was limited to focus on the transformation of Se(VI) to Se(IV). When the solution was oxidised, SeO₄²⁻ concentration decreased rapidly for the first couple of minutes, then increased a bit and remained stable. TMS data suggested that the decrease in Se(VI) was a result of reduction by Fe(OH)₂, producing a compound incorporating SeO₄²⁻. It was shown to be GR-2 (details in section 4.1.2.3). Then, the combined results from EXAFS and electrophoresis showed that the selenate was reduced by both Fe(OH)₂ and the GR. In a control experiment with strict exclusion of oxygen, Se(VI) was reduced in the same way as in the experiment in an oxic environment. An overall reaction was presented:



Further oxidation of GR_{SeO₄} led to the formation of lepidocrocite and ferrihydrite. The produced selenite remained adsorbed to the produced iron(III) hydroxides.

Recently, Johnson and Bullen (2003), studied the isotope fractionation of selenium reduction by GR_{SO₄}. They examined reduction with GR_{SO₄} produced by two different methods. One solid was prepared by the titration method (Hansen et al., 1994) and the other, by the oxidation method (Refait et al., 1999). The produced GR_{SO₄} and reacting solution were then used as stock mixture for the experiments. The concentration of Se(VI) was observed to decrease by 50% within 2.9 – 4.3 h when fastest. In some experiments, there was a lag phase ranging from 2 h to 10 h before a decrease in Se(VI) was observed and it took between 11 h and 20 h to decrease the Se(VI) concentration by 50%. The lag phase was observed in all the experiments, except where 75% of the supernatant from the centrifuged GR_{SO₄} solution was removed prior to the experiments. In the experiment using the

stock solution prepared in accordance with Hansen et al. (1994), the 50% Se(VI) decrease was also observed to be quite long (7.9 h – 15 h). Johnson and Bullen (2003) concluded that the lag phase was a result of some alteration of the GR structure that eventually increased its reactivity. It is not clear, however, why they excluded the competition between SO_4^{2-} and SeO_4^{2-} as reason for the lag phase and decrease in reduction. It is consistent with behaviour in other GR systems that a higher concentration of SO_4^{2-} would inhibit exchange with SeO_4^{2-} . The slow reactivity observed in the experiments with the GR_{SO_4} prepared by titration is probably also a result of higher anion concentrations, in this case both Cl^- and SO_4^{2-} .

The reaction products had a fractionation for $^{80}\text{Se}/^{76}\text{Se}$ shifted to lighter Se isotopes by 7.36 ± 0.24 ‰ in both experiments. This fractionation is larger than that of microbial Se(VI) reduction which is -2.6 to -3.1 ‰ (Ellis et al., 2003 as cited by Johnson and Bullen, 2003). Johnson and Bullen intend to use this difference as a tool to establish whether Se reduction in soils is abiotic or biotic.

The rate of Se(VI) reduction by GR_{SO_4} in all experiments (Myneni et al., 1997; Refait et al., 2000; and Johnson and Bullen, 2003) was at least equal or higher than that of biogenic reduction. Therefore some of the reduction of Se species in soils may be abiotic reduction by green rust. Oremland et al. (1998) questioned this conclusion because all the experiments were made in the laboratory and not linked to measurements in a natural environment. Myneni et al. (1998) explained that their work was a proposal that Se(VI) reduction in nature is not necessarily biogenically derived.

4.5.1.4 Arsenium

Arsenium is known to be toxic to living organisms. As(III) is more mobile and therefore poses a greater risk than As(V), but both species are carcinogenic. Randall et al. (2001) examined how GR_{SO_4} influences the reduction of As(V) to As(III), by investigating behaviour of As(V) added before and after precipitation of GR_{SO_4} . They took samples during progressive oxidation with air, which could inhibit exchange of interlayer SO_4^{2-} with AsO_4^{3-} . Inhibition could also result from large SO_4^{2-} concentrations preventing exchange between SO_4^{2-} and AsO_4^{3-} . Furthermore oxygen was kept purging through the solution so GR might oxidise before exchange and reduction of As(V) to As(III) could take place. Randall et al. (2001) did not observe any reduction of As(V) to As(III) even though calculation using thermodynamic data suggest it should occur. They interpreted their

results as evidence of As(V) adsorption as AsO_4^{3-} to the GR_{SO_4} , which they documented using EXAFS. They found that AsO_4^{3-} remained adsorbed to GR throughout its oxidation and to the final oxidation product, lepidocrocite.

Recently, Lin and Puls (2003) studied arsenic adsorption, desorption, reduction and oxidation in solutions containing iron hydroxides: GR_{SO_4} , goethite or lepidocrocite. They found that 50 mg GR_{SO_4} could adsorb 99% of 1.0 mM As(V) on average, the highest adsorption percentage of the examined iron hydroxides. The authors did not, however, examine the influence of surface area. Desorption of As(V) from GR_{SO_4} was on average 7%; the lowest of the examined iron-(oxy)hydroxides (Table 7). Lin and Puls (2003) observed that when a solution containing GR_{SO_4} , As(V) and As(III) was left to settle for three months under anoxic conditions, GR_{SO_4} transformed to parasymphesite ($\text{Fe}^{\text{II}}_3(\text{AsO}_4)_2 \cdot 8\text{H}_2\text{O}$). They found that approximately 95% of the arsenic was removed from solution during the process. They also observed that GR_{SO_4} could reduce As(V) to As(III) and oxidise As(III) to As(V) (Table 8). These observations are interesting because they show that ferric hydroxides can oxidise As(III) to As(V) and that GR_{SO_4} can transform to parasymphesite in the presence of As(V). This combination is worth investigating, because ferric hydroxide reduction to a GR compound yields an attenuation mechanism for As(III) in soils containing ferric hydroxides.

Table 7. As(V) adsorption, desorption and reduction by iron hydroxides (data from Lin and Puls, 2003)

	As(V) adsorption (%)		As(V) desorption (%)		Reduction of As(V) on hydroxides (%) ^a	
	Range	Mean	Range	Mean	As(III)	As(V)
Green rust	99.1-99.6	99.4	5.2-10.1	6.7	4.3	95.8
Goethite	98.5-99.5	99.1	6.1-18.2	7.0	3.0	97.0
Lepidocrocite	97.1-99.3	98.0	13.0-18.1	15.3	1.2	98.8

^a Mean values

Table 8. As(III) adsorption, desorption and oxidation by iron hydroxides (data from Lin and Puls, 2003).

	As(III) adsorption (%)		As(III) desorption (%)		Oxidation of As(III) on hydroxides (%) ^a	
	Range	Mean	Range	Mean	As(III)	As(V)
Green rust	11.5-18.6	15.8	5.8-10.1	7.4	74.3	25.7
Goethite	19.2-24.8	21.5	3.9-8.8	5.7	79.1	20.9
Lepidocrocite	25.1-38.1	30.9	4.2-7.5	5.6	65.7	34.3

^a Mean values

The two studies (Randall et al., 2001; and Lin and Puls, 2003) cannot be compared directly because Randall et al. (2001) let the reaction between GR_{SO_4} and As(V) happen under aerobic conditions, whereas Lin and Puls (2003) made their experiments under anoxic conditions. Randall et al. (2001) concluded that no reduction of As(V) to As(III) took place during their study, whereas Lin and Puls (2003) showed that up to ~5% As(V) could be reduced to As(III) by GR_{SO_4} . The difference in results is probably caused by differences in experimental setup. Randall et al. (2001) did not let the reaction stabilise. They oxidised GR_{SO_4} with As(V) present, while Lin and Puls (2003) let the solutions equilibrate without any oxidants present other than GR_{SO_4} .

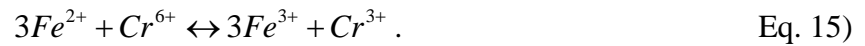
Nishimura and Robins (2000) observed that GR_{SO_4} can incorporate arsenic into its structure when $pH < 7$. They titrated a solution of Fe(II), Fe(III) and As(V) and observed that As(V) was associated with the solid between pH 4 and 7 and released to solution at pH higher than 7. They did not support their conclusion that AsO_4^{3-} incorporated in the structure of GR_{SO_4} with XRD patterns or any other bulk analytical analysis.

4.5.1.5 Chromium

Chromium is commonly used in leather tanning, wood treatment, metallurgy and stainless steel production and is becoming an increasing environmental problem because of its mutagenic and carcinogenic effects (Weckhuysen et al., 1996). Chromium can exist in valence states +II, +III and +VI. Cr(VI) is highly soluble and mobile and the most stable form of the metal under oxidising conditions, whereas Cr(III) forms moderately soluble solids is the most stable form under reducing conditions and. Cr(II) does not exist under Earth's surface conditions. Attenuation of chromium by

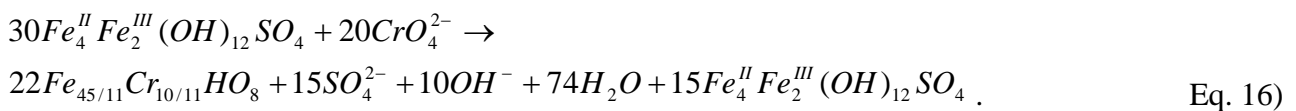
reduction has been investigated in combination with various reducing agents such as Fe^{2+}_{aq} , H_2S , FeS and also organic compounds (Bond and Fendorf, 2003 and references therein).

Removal of Cr(VI) from solutions containing GR_{SO_4} and GR_{Cl} was studied under oxidising conditions by Loyaux-Lawniczak et al. (2000). GR was able to reduce Cr(VI) to Cr(III) and immobilise it in a compound similar to 2-line-ferrihydrite. They suggested CrO_4^{2-} exchange with anions in the GR interlayer. Because CrO_4^{2-} reduces rapidly, the exchange results in a poorly ordered mineral. When the Fe(II)/Cr(VI) ratio was 3 or higher, all Cr(VI) was reduced and GR oxidised and the only resulting Cr-containing phase was the 2-line-ferrihydrite (Loyaux-Lawniczak et al., 2000). When Fe(II):Cr(VI) = 3, the electron balance is met:



There was no difference in the pattern of reduction for Cr(VI) to Cr(III), whether GR_{SO_4} or GR_{Cl} was the reductant. However, excess GR produced a difference oxidation product. With excess GR_{SO_4} , α -FeOOH (goethite) precipitated but with excess GR_{Cl} , the product was γ -FeOOH (lepidocrocite).

Loyaux-Lawniczak et al. (2000) proposed that a Fe(II)/Cr(VI) ratio of 6, lead to the reaction:



Williams and Scherer (2000 and 2001) observed Cr(VI) removed from solution in the presence of GR_{CO_3} . The rate of removal had a first order rate, with half of the Cr(VI) removed within approximately 4 min. Removal rate depended on GR_{CO_3} surface area. A surface area increase by two resulted in a four-fold increase in removal rate. Three possible pathways for chromate removal from solution are: 1) reduction of Cr(VI) to Cr(III) and precipitation as some solid, 2) adsorption of CrO_4^{2-} to the GR_{CO_3} surface, and 3) interlayer exchange of CrO_4^{2-} with the interlayer anion (CO_3^{2-}) in GR_{CO_3} . The authors also noticed that pH influenced the removal rate of CrO_4^{2-} from solution. When pH was decreased from 9.0 to 5.0, a five-fold decrease in the removal rate was observed.

They attributed this to protonation of the GR_{CO_3} surface, which increases the electrostatic attraction between the surface and the negatively charged CrO_4^{2-} . In the studies, the resulting end product of the reaction between Cr(VI) and GR_{CO_3} was not determined. They speculated that it probably resembled the 2-line-ferrihydrite reported by Loyaux-Lawniczak et al. (2000). Williams and Scherer (2000 and 2001) calculated a 4:1 ratio for Fe(II) oxidised to Fe(III) and Cr(VI) reduced to Cr(III), not the electron balance expected ratio of 3:1 (Eq. 15). They suggested that the higher ratio resulted from the presence of other oxidants, such as aqueous CO_2 and O_2 (aqueous carbonate suggested in Williams and Scherer, 2001). Because similar features had been observed in reactions between GR_{CO_3} and NO_3^- (Hansen and Koch, 1999 as cited by Williams and Scherer, 2001) but not in experiments involving GR_{SO_4} or GR_{Cl} , they suggested that CO_3^{2-} acted as the oxidant and assumed small-chain hydrocarbons or methane as products. Hardy and Gilham (1996) observed, using gas chromatography with a flame ionization detector or a photo ionization detector, that zero-valent iron converted aqueous CO_2 and H_2 to small-chain hydrocarbons and that the stability-field was above that of $\text{H}_2\text{O}/\text{H}_2$. It is interesting, however, that siderite was not observed. Experiments made in our own group (Sonne Larsen, Skovbjerg, Christiansen and Stipp, not yet published) show that GR_{CO_3} can very readily transform into siderite and goethite when left in solution under anoxic conditions for 12 to 24 hours.

Bond and Fendorf (2003) examined the interaction between Cr(VI) and GR_{CO_3} , GR_{SO_4} and GR_{Cl} . The experiments were carried out under anoxic conditions and with GR rinsed from salt used to form it. The authors observed that on a mass basis, GR_{Cl} was the most effective reductant of Cr(VI) to Cr(III); GR_{CO_3} was less effective and worst was GR_{SO_4} . However, normalised to relative surface area, the order of efficiency was changed and GR_{SO_4} became the most effective followed by GR_{Cl} and then GR_{CO_3} . Bond and Fendorf (2003) explained the higher reduction rate of mass-normalised GR_{Cl} by the higher Fe(II)/Fe(III) ratio 3:1 and thus more available phase Fe(II) per mole GR, whereas the Fe ratio for GR_{SO_4} and GR_{CO_3} is 2:1. The final oxidation product in all three experiments was magnetite and lepidocrocite. Based on X-ray absorption spectra, Bond and Fendorf (2003) reported Cr(III) to be incorporated within the structure of the oxidation products. The authors presented solubility products for the resulting Fe(III)-Cr(III) hydroxide (Table 9).

Table 9. Apparent solubility products of mixed Fe(III)-Cr(III) hydroxide end products.

GR	Cr(III) mole fraction	Solubility (Log Ks)
GR _{Cl}	0.829	4.14
GR _{CO₃}	0.481	3.67
GR _{SO₄}	0.324	3.23

The results of the various studies, Loyaux-Lawniczak et al., (2000), Williams and Scherer, (2000 and 2001), and Bond and Fendorf, (2003) are not directly comparable because of differences in experimental setup. Loyaux-Lawniczak et al. (2000) did not rinse the GR precipitate and kept oxidising the solution after addition of Cr(VI) so some of the produced Fe(III) undoubtedly resulted from oxidation by O₂. Williams and Scherer (2000 and 2001) and Bond and Fendorf (2003) are more similar in experimental conditions. Both studies use rinsed, freeze-dried GR precipitate, which they added to a fresh Cr(VI) solution. Both experiments were conducted at anoxic conditions. Rinsing GR precipitates results in an unstable compound that transforms readily (Hansen, 1989; and Christiansen, Sonne Larsen, Skovbjerg and Stipp, not yet unpublished) if not treated with a protective substance such as glycerol (Hansen, 1989). There is a difference, however, because Williams and Scherer (2000 and 2001) adjust pH with HCl and NaOH whereas Bond and Fendorf (2003) use a MOPS buffer (3-(N-morpholino)propanesulfonic acid, C₇H₁₅NO₄S). There is no information on how such an organic compound interacts with GR. It certainly could influence the transformation of GR and the formation of oxidation products. Because Williams and Scherer (2000 and 2001) did not supply data on what end product they produced in their experiments, it is not possible to compare the reduction pathways for the three studies.

4.5.1.6 Other inorganic compounds

O'Loughlin et al. (2003b) examined with XRD, TEM and XAFS the influence of GR_{SO₄} on Ag(I), Au(III), Cu(II) and Hg(II). They observed that GR_{SO₄} could reduce the four components to zero-valent state. For Ag, Au and Cu, the reduction makes them less mobile. Hg is, however, more mobile as Hg(0), partly because of its low vapour pressure (O'Loughlin et al., 2003b).

4.5.2 Radioactive compounds

Recently the search for methods to sequester radioactive compounds has begun to include GR.

There are an increasing number of studies published on the interaction of radioactive compounds and GR. The motivation comes from the need to insure safe disposal for radioactive material that is left over from power generation, use in hospitals and for scientific research. Radioactive waste can be stored in iron or copper canisters under reducing conditions. If the redox conditions surrounding the canisters change, corrosion would begin and leakage would result. Understanding of the uptake potential and behaviour of GR is required for establishing contamination scenarios and assessing safety risk.

4.5.2.1 Technetium

Nuclear fission reactions produce up to 6% of the long-lived radioactive isotope ^{99}Tc , which has a half-life of 2.13×10^5 years (Pepper et al., 2003). Roh et al. (2000b) investigated an electrochemical remediation method. They used a commercial “Fe(0) foam” composed of 92% Fe(0) and 8% aluminosilicate particles in electrochemical contact with solutions containing $^{95\text{m}}\text{Tc}$, present as pertechnetate (TcO_4^-), uraniumcarbonate ($\text{UO}_2(\text{CO}_3)_2^{2-}$), sodium and nitrate. $^{95\text{m}}\text{Tc}$ was used to resemble the long-lived isotope ^{99}Tc . $^{95\text{m}}\text{Tc}$ is an excited isotope with a half-life time of 60 days; it is often used as tracer in groundwater experiments. Roh et al. (2000b) observed that ~87% of the technetium was removed from solution and incorporated in the precipitates produced during the electrochemical treatment. The precipitates were initially X-ray amorphous but after approximately 2 weeks storage in the treated solution a GR-1 type compound had evolved. The XRD pattern exhibited parameters resembling GR_{CO_3} . Gamma activity showed that the $^{95\text{m}}\text{Tc}$ was incorporated in the precipitates. Fourier transformed infrared spectroscopy (FTIR) showed that the technetium was associated with carbonate, suggesting CO_3^{2-} as the anion in the interlayers and supporting the identification of GR_{CO_3} .

Pepper et al. (2003) used XAS, XANES and EXAFS to show that >99.8% $[\text{}^{99}\text{TcO}_4]^-$ was removed by GR_{SO_4} and GR_{CO_3} . The Tc(VII) was shown to be reduced to Tc(IV) by oxidation of the GR and incorporated in a TcO_2 -like environment. There was, however, more dissolved Tc in solution than expected when compared to amorphous or crystalline TcO_2 . The authors concludes that this discrepancy is because a small portion of the TcO_4^- is not reduced (approximately 0.08%) and

because the Tc(VI) forms surface complexes that are more readily released back to solution. The surface complex persisted even by oxidation of the GR to goethite.

4.5.2.2 Uranium

Roh et al. (2000a) examined U(VI) reduction to U(IV) during passage through a reactive iron(0)-wall. They used electrochemical applications with and without direct current. They observed a decrease in aqueous uranium in both setups and based on EDS showed that uranium was incorporated in coatings on the Fe(0). XRD showed that the coatings in some of the experiments consisted of both GR-1 and 2, of the chloride and sulphate forms. It was concluded that this incorporation was of great importance to extend of uranium removal. Because the GR was crystalline, in comparison to an amorphous compound, it was thought to possess a long-term immobilisation possibility (Roh et al., 2000a). Electrochemical precipitation of GR type compounds was shown to remove 99% of ^{235}U from solution (Roh et al., 2000b). The capability of GR to take up uranium and the claim of long-term immobilisation needs further investigation, because GR is only stable in reducing and neutral to slightly alkaline environments. What happens when the system becomes oxidising? Does the uranium stay incorporated in the new product, or is it expelled back to solution?

In a study using X-ray Absorption Near Edge Structure (XANES) and X-ray photoelectron spectroscopy (XPS), Dodge et al. (2002) observed that uranium(VI) could be reduced to uranium(IV) in presence of GR_{SO_4} . The other iron oxides (goethite, lepidocrocite, 2-line-ferrihydrite, magnetite and maghemite) did not show any reducing capability for uranium; they all were associated with U(VI). In the final product, Dodge et al. (2002) were not able to detect GR_{SO_4} by XRD; they found only magnetite. They synthesised GR_{SO_4} by a method adapted from Srinivasan et al. (1996). However, Dodge et al. (2002) added uranyl nitrate initially together with the ferrous sulphate and only then, the oxidation was initiated. Whether they produced GR_{SO_4} is therefore uncertain. Nitrate is a known interlayer anion of GR and GR_{SO_4} is known to reduce nitrate, leading to magnetite as the end product. Thus, the U(VI) to U(IV) reaction pathway is impossible to determine from the study by Dodge et al. (2002).

O'Loughlin et al. (2003a) used XAFS, XRD and TEM to examine the reduction of U(VI) by GR_{SO_4} . They used uranium acetate as the U(VI) source and they used the formation solution of GR_{SO_4} as the reaction medium. The aqueous uranium concentration decreased by 4 orders of magnitude, from 4.4 mM to 420 nM within 48 hours. Furthermore, they showed that U(VI) was reduced to U(IV), accompanied by partial oxidation of the GR_{SO_4} to magnetite, producing UO_2 particles with a size of 2-9 nm observed with TEM. The particles were found in the interlayers at the edges of the hexagonal GR_{SO_4} . Although the production of a solid phase is normally considered ideal for treatment of contaminants because it is easier to immobilise, the size of the particles could pose another problem; they could move as colloids through fractures and pore spaces.

4.5.3 *Organic compounds*

Organic compounds are becoming an increasing health problem because of the extensive usage of pesticides, organic solvents and spillage of oil products. Some of the compounds have been used as solvents in the western world for several years to dry-clean cloths. The use of dry cleaning has decreased during the last couple of decades leaving buildings and grounds polluted with dry cleaning products or breakdown products thereof. Pesticides have likewise been used intensively in the western world and are still used in the development part of the world. A vast number of the pesticides are now banded in the western world but the problem is increasing because the pesticides and derivatives of them have polluted groundwater aquifers or moving downwards to such aquifers. Investigations to avoid contamination of groundwater sources have been intensified during the last decades. These investigations also included the role of GR in the immobilisation or breakdown of the organic compounds.

4.5.3.1 *Trichloroethene*

Roh et al. (2000a) observed trichloroethene (TCE) dechlorination during reaction with Fe(0)-reactive barriers. Using SEM on reacted Fe(0)-bearing material from a barrier at a dechlorination plant in Portsmouth, USA, they observed particles with a pseudo-hexagonal morphology which they believed were GR, but they could not confirm it by XRD. In a laboratory experiment with the same Fe(0)-bearing material and TCE, they produced samples that did show both GR_{Cl} by XRD and dechlorination of TCE by gas chromatography (GC) with a flame ionization detector (FID). Roh et al. (2000a) did not present any chemical properties, or make any comments on how the dechlorination took place, i.e. which dechlorination product was produced.

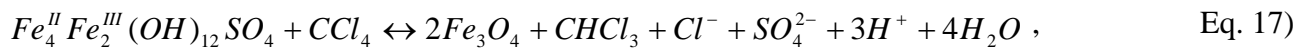
4.5.3.2 *1,1,1-Trichloroethane*

A recent study (Agrawal et al., 2002) on the effect of carbonate species on dechlorination of 1,1,1-Trichloroethane (TCA) by Fe(0) suggested that GR_{CO_3} was involved in the dechlorination process, but no evidence was provided to support the claim.

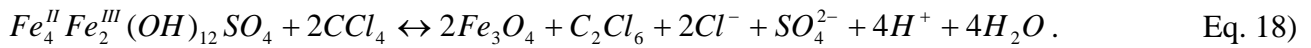
4.5.3.3 *Carbon tetrachloride*

Carbon tetrachloride (CCl_4) has been used in the cloth dyeing and cleaning industries for several decades. Now it is turning out to be an environmental problem because of its presence in soils

beneath these industrial buildings. Erbs et al. (1999) found that GR_{SO_4} could dechlorinate carbon tetrachloride (CCl_4) to either chloroform ($CHCl_3$) or to lesser degree to hexachloroethane (C_2Cl_6). The dechlorination was considered to occur in association with the phase Fe(II), in this case GR_{SO_4} . Evidence was that no dechlorination of CCl_4 took place in control solutions containing only CCl_4 and dissolved Fe(II). Because the dechlorination rates are similar to nitrate reduction rates, which is assumed to take place at surfaces, it was concluded that the dechlorination must only happen at the surface and not in the interlayers. CCl_4 dechlorination to chloroform and hexachloroethane leads to GR_{SO_4} oxidation and formation of magnetite according to the following reactions, where crystal water is excluded (Erbs et al., 1999):



and:



From the equations, it is apparent that only half of the Fe(II) in the GR is oxidised to Fe(III) in the magnetite. According to Erbs et al. (1999), researchers agree that the first step in the CCl_4 transformation is a one-electron reduction, yielding a trichloromethyl radical. Reaction of two such radicals forms C_2Cl_6 . Erbs et al. (1999) compared their results with those from experiments on Fe(0). Although direct comparison was not possible, they assumed GR to be responsible for CCl_4 dechlorination based on observation of GR as a common intermediate phase when Fe(0) oxidises. They concluded that the polar-layered GR and the non-polar CCl_4 somehow interact, but only at the outer surface of the GR and not in the interlayer, where a larger reducing capability exists. If CCl_4 had access to the GR interlayer, there would probably be a greater dechlorination rate.

5 Experimental details

5.1 Glove Box

The glove box supplied by Coy Laboratories Product Inc.® is made of two main parts: a slightly overpressurised anaerobic chamber and a fast entry chamber. The anaerobic chamber, approximately 180 cm long, 120 cm high and 80 cm wide, is made of a PVC membrane. In order to avoid venting the entire chamber to air each time equipment and materials are transported into and out of the anaerobic chamber, they go through the fast entry chamber. The fast entry chamber is a steel box with Plexiglas doors that withstand low vacuum (10^{-3} to 10^{-4} bar) conditions. To ensure that a minimum of oxygen enters the anaerobic chamber, the entry chamber is evacuated to approximately 2.5×10^{-3} bar three times and refilled the first two times with nitrogen of 99.9990 % purity and finally with a gas mixture composed of 4% hydrogen and 96% nitrogen both of 99.9990% purity.

Even with this purging procedure, a small amount of oxygen, approximately 7,500 ppm enters the anaerobic chamber every time the entry chamber is used. In addition, the permeability of the PVC membrane allows entry of about 0.5-1.0 ppm $O_2 \text{ min}^{-1}$. To remove O_2 that enters and to ensure an oxygen depleted atmosphere, two fan boxes are equipped with packs of palladium pellets, which act as a catalyst for reacting hydrogen from the gas mixture with oxygen, to create water. To keep the moisture at low levels, the fan boxes are also equipped with plates containing aluminium pellets that adsorb the water vapour. A gas analyser monitors the oxygen (± 20 ppm) and hydrogen (± 1 %) levels in the chamber. When pressure sensitive equipment needs to be placed in the chamber, larger amounts of oxygen enter because the airlock cycle cannot be carried out. When this is necessary, such as for transferring the Atomic Force Microscope, redox sensitive samples are stored in gas-tight bottles, and the whole chamber is evacuated and backfilled with gas mix. Total time for oxygen levels to reach 0 ppm after entry of pressure-sensitive equipment is about 15 minutes.

5.2 Synthesis

All glass and plastic ware were washed by standard laboratory procedure. They were first soaked in 20% HCl for 24 hours to remove iron(oxy)hydroxides, then left overnight in 10% HNO_3 to remove remaining adsorbed Cl^- and finally rinsed 5 times in doubly deionised water. For the synthesis of the Green Rust in the main experiments, I used doubly deionised (MilliQ) water ($< 0.1 \mu S/cm$) that

was sterilised in polypropylene bottles in an autoclave at 125°C for 15 min. and then transferred to the glove box. The water was stirred with a Teflon coated magnetic stirrer for approximately 2 hours in the glove box to remove dissolved oxygen. No special care was taken to remove dissolved carbon dioxide at this stage.

Green Rust sulphate (GR_{SO_4}) can be synthesised by three methods: 1) appropriate amounts of a Fe(II) and a Fe(III) salt are mixed with hydroxide and sulphate to precipitate GR_{SO_4} , 2) ferrous sulphate is titrated with hydroxide to maintain constant pH while oxidising the solution and 3) ferrous sulphate is reacted with an appropriate concentration of base and the solution is then oxidised. I used the third method. The GR_{SO_4} was synthesised without specific control of pH according to the method of Lin et al. (1996). In the two main experiments, about 66.7 g of analytical grade $\text{FeSO}_4 \cdot 7\text{H}_2\text{O}_{(\text{s})}$, (purchased from Applichem®, and containing a maximum of 0.0005% Cl and 0.02% Fe(III)) was added to 2 litres of the deoxygenated water. Approximately 16.0 g (0.2 mol/l) of $\text{NaOH}_{(\text{s})}$ (Baker analytical grade) was added to the solution, yielding a Fe/OH ratio of 0.6. The $\text{NaOH}_{(\text{s})}$ had a maximum content of 0.4% CO_3^{2-} (as Na_2CO_3). The synthesis solution was left for approximately 2 hours under constant stirring to allow pH to stabilise. To start the experiment, oxidation was initiated by bubbling compressed air through a fritted glass tube into the solution. The air was purged of CO_2 by passing it over surface enhanced NaOH pellets and then through two vessels containing doubly deionised water. Phenolphthalein was added to the first vessel to monitor the transport of base in the vapour phase; the solution stayed colourless throughout the whole oxidation indicating $\text{pH} < 8.5$. Using adjustable Cole Parmer® flow meters, the air flow rate was set at 143 ± 5 ml/min for the slow oxidation experiment and at 286 ± 10 ml/min for the fast one. Total Fe was measured using an Atomic Absorbance Spectrometer. Fe(II) was measured using the 1,10-phenantroline method and spectrophotometry.

In the three experiments where the effect of different cations (Li^+ , K^+ and Na^+) was examined, a slightly different synthesis method was applied. The relative ratio Fe/OH was still 0.6, but because of stirring difficulties in the two main experiments a lower absolute concentration was chosen. Instead of 0.12 mol/l Fe^{2+} a concentration of 0.05 mol/l Fe^{2+} was used. The concentration of base was then 0.83 mol/l. All of the chemicals were of *pro analysis* quality or better. To examine the influence of Li^+ , I used $\text{LiOH} \cdot \text{H}_2\text{O}$ with a maximum content of 0.71% CO_3^{2-} as Li_2CO_3 . KOH was used to examine K^+ influence, but because of the KOH hygroscopic ability, I determined K^+

concentration of the solution using Atomic Absorption Spectroscopy. I used NaOH to examine the influence of Na⁺ and I used the same reagent that was used in the main experiments. The salts were dissolved in 0.200 L doubly distilled water. All solutions and materials were prepared in the same way as in the transformation experiment. Air was introduced to the solution with a peristaltic pump set at a speed of 25 rpm.

5.3 *Sampling*

Samples were extracted from the solution during the experiments. Table 10 presents sampling times and analytical methods applied. All the extraction and sample preparation were done in the glove box. With a plastic syringe, 100 ml of solution was extracted and put into a 100 ml Pyrex bottle with polypropylene screw cap (Blue Cap bottles). For CT-XRD and TMS, material was collected on a cellulose nitrate filter (0.2 µm) placed in a plastic holder attached to the syringe. When the filter was clogged, meaning enough material had accumulated, it was placed on top of the fan boxes and left to dry. After about 30 minutes, the dry filter cake was taken off the filter paper and crushed in a piece of paper. The crushed material was filled in a Markrörchen® “Special Glass” capillary tube (ø=0.3 mm, thickness = 0.01 mm). The tube was sealed with liquid paraffin to avoid oxidation of the material during transport and analysis outside the glove box. Prior to CT-XRD, the tubes were placed in an ultrasonic bath to compact the powder, ensuring a maximum amount of material in the diffraction area of the tube. More details of the analytical parameters are presented in the next section.

Table 10. Sample time and analysis method; numbers correspond to arrows on Figures 9 and 10.

Experiment 1					Experiment 2				
Sample time	Sample notation	AFM	CT-XRD	TMS	Sample time	Sample notation	AFM	CT-XRD	TMS
-9 ^a	1-01	+			-38 ^a	2-01	+	+	
27	1-02	+	+		21	2-02	+	+	
79	1-03	+			89	2-03	+	+	
172	1-04	+	+		129	2-04	+	+	+
234	1-05	+			190	2-05	+	+	
364	1-06	+	+	+	256	2-06	+	+	
427	1-07	+			342	2-07	+	+	
500	1-08	+	+		401	2-08	+	+	
556	1-09	+			423	2-09	+	+	
621	1-10	+	+						
682	1-11	+							
847	1-12	+	+						
973	1-13	+							
994	1-14	+	+						

^a Sample taken when solution composition became stable (as indicated by pH stability) before oxidation began, at t=0.

Crushed material for TMS (about 20 mg) was placed in Plexiglass holders covered with a Plexiglass lid. They were wrapped in Para-film and placed in a Pyrex bottle with a tight sealed polypropylene cap, all inside the glove box.

AFM samples were prepared from a few millilitres of unfiltered solution removed from the reaction vessel with a plastic pipette. A drop of sample was placed on the sample substrate and left to settle for approximately 30 sec. to allow particles time to sorb to the substrate. The sample was squirted with a jet of double deionised water for a few seconds to remove excess material. Excess water was sucked away with a tissue to avoid precipitation of salts and the sample was left to dry on top of the fan box for minimum 30 minutes. The substrate was attached to an iron disc with double-sided tape. All AFM samples were examined in the glove box.

6 Techniques

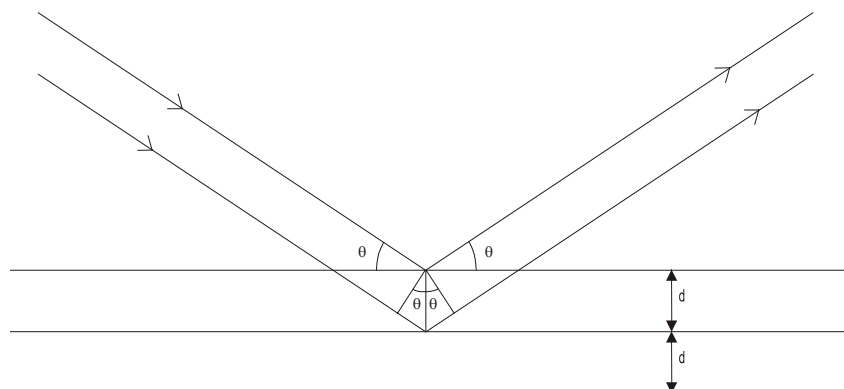
6.1 X-Ray Diffraction

X-ray diffraction (XRD) is a bulk analysis method based on the interaction of the ordered array of atoms in a solid using X-rays. Wilhelm Conrad Roentgen discovered X-rays in 1895 and on a design proposed by Max von Laue in 1912, X-rays were used to study crystals (Klein and Hurlbut, 1993). XRD is based on wave interference as X-rays pass through a crystal. Electrons are energised and begin to vibrate at the frequency of the incoming X-rays. They absorb some of the original energy and emit new waves with the same frequency and energy as the incoming X-rays. The new waves interfere with each other, most of them in a destructive way. When there is constructive interference, however, Bragg's law is fulfilled:

$$n\lambda = 2d \sin\theta, \quad \text{Eq. 19)}$$

where n represents the integral number of planes, λ represents the wavelength of the X-rays, d denotes the interplanar spacing and θ is the diffraction angle (Fig. 4).

Figure 4. Principle of X-ray diffraction.



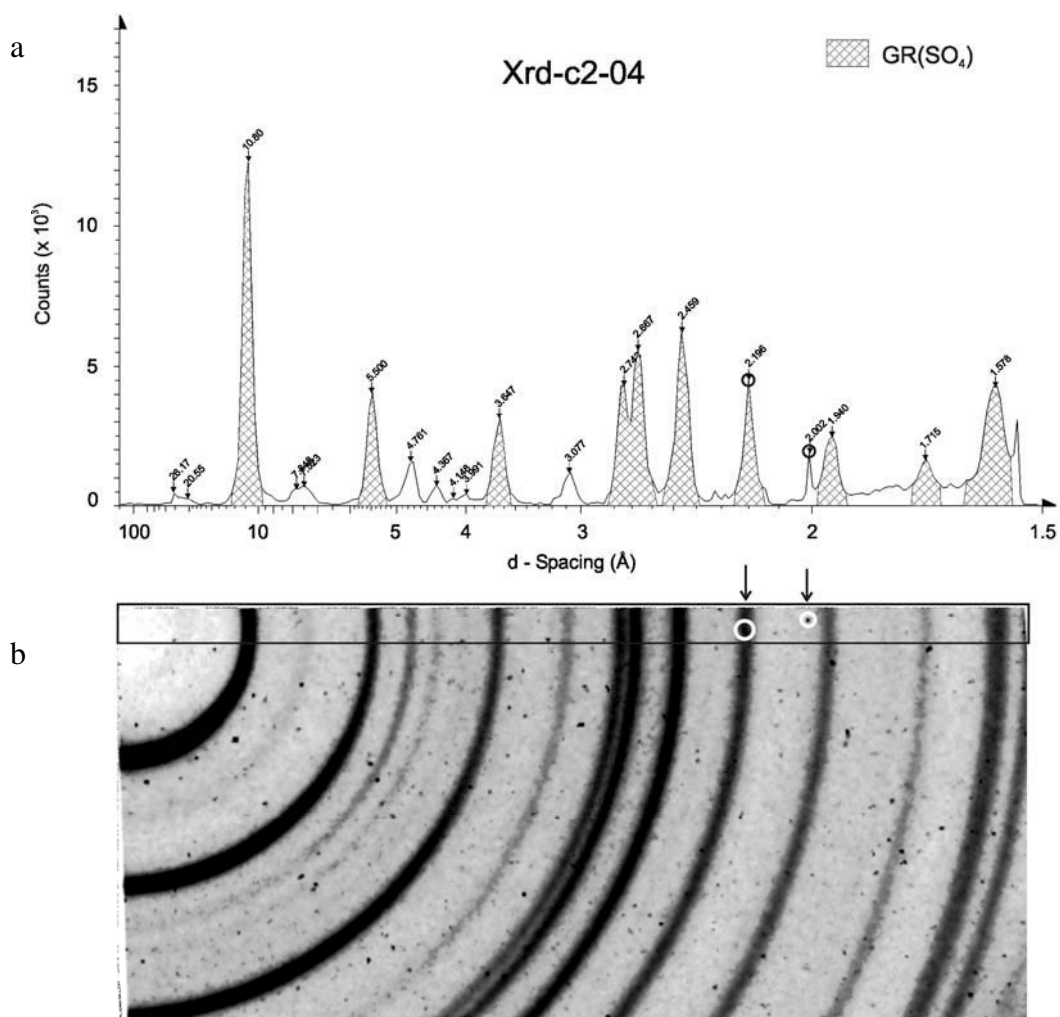
I used a Philips PW1730 equipped with $\text{Cu}_{K\alpha}$ source, which has a wavelength $\lambda = 1.5418 \text{ \AA}$. Energy was 40 kV and current was 40 mA. The instrument uses a graphite monochromator and a collimator slit width that changes as a function of 2θ .

6.2 Capillary Tube X-Ray Diffraction

Because of problems with oxidation of the samples, I choose another approach for analysing the samples with XRD. Methods to examine GR using normal powder XRD exist, such as stabilisation with glycerol (Hansen, 1989) but they result in preferred orientation of the sample so the data do not exhibit all details of the crystallographic pattern. For this study, X-ray diffraction of the samples was made on a BrukerAXS four-circle diffractometer equipped with $\text{MoK}\alpha$ ($\lambda=7.093 \text{ \AA}$) source, which runs at 40 kV and 37 mA. The instrument is equipped with a graphite monochromator and a 0.5 mm collimator slit. The detector was placed 12 cm from the sample at an angle of $2\theta = -13^\circ$. The pattern was obtained using rotation diffraction with exposure time of 900 sec. Data were calibrated against a quartz standard analysed before the sample. The diffraction trace (an example is shown in Figure 5b) was obtained by integrating a strip of the diffraction pattern (Fig. 5a). Unfortunately, random spikes of high intensities, resulting from noise in the diffractometer, are common on the diffraction pattern. These are visible as black spots on Figure 5b and where intersected by the strip for integration, they produce recognisable artefacts, such as that observed on Figure 5a at d-spacing 2.002 \AA . Sometimes they only add incorrect intensity to a genuine peak such as d-spacing 2.196 \AA . In order to minimise the effect of artefacts the original patterns were always consulted, together with the diffraction trace, during data interpretation. Background intensity originating from the capillary tube was removed using a simple curve subtraction.

To examine the evolution of the phases in solution, an experiment similar to Exp-1 was conducted. I doped the samples produced with a known amount of pure goethite. This was done 3 times, adding a different amount of goethite to each sample. The goethite and sample were mixed and poured in capillary tubes. The tubes were sealed with paraffin and treated in an ultrasonic bath to concentrate the material in the bottom. The samples were then analysed by CT-XRD.

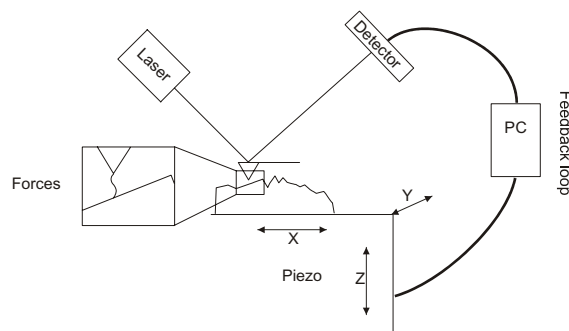
Figure 5. Conversion of a Capillary Tube X-Ray Diffractogram to XRD-trace. The trace (a) results from integrating the area in the box in the upper part of (b). Only peaks that can be linked to actual diffraction rings are presented with d-spacings. In part (b), there are two spikes (white circles) and their effect can be seen on the trace (a) as well (black circles). The spikes were removed from the CT-XRD traces for the data used and presented in this work.



6.3 Atomic Force Microscopy

Atomic Force Microscopy (AFM) belongs to the family of Scanning Probe Microscopes (SPM). SPM is based mostly on the physical interaction between a local area of a surface and a sharp tip. AFM uses the attractive and repulsive forces interacting between the surface and the tip to create an image of the investigated material (Eggleston, 1994). An outline of the principles of an AFM is presented in Figure 6.

Figure 6. Principles of Atomic Force Microscopy.



The piezo electric scanner is the adjustable part of AFM. It moves by voltage impulses both in horizontal and vertical directions. The range and precision of movements are dependent on the type and size of piezo and can be as small as fractions of an Ångström. The uppermost part of the scanner has a magnet embedded, so it is possible to attach a steel sample holder to it. Above the sample is placed a flexible cantilever that has a small tip integrated into silicon nitride. When the cantilever and tip are brought close to the sample, forces begin to interact between them and the cantilever bends. A laser beam is focused on the back of the cantilever, reflected by a mirror and shines on a photosensitive diode. The diode is sensitive to where the laser beam hits it and sends a signal to the feedback loop based on position. The signal passes through a processor that generates feedback to the piezo, controlling its vertical movement. Two types of imaging are possible: 1) The forces between tip and sample are held constant, by feedback mechanisms, producing height images or 2) the distance between the tip and sample are held constant, so no feedback signal is used, producing deflection images.

A height image is generated when the tip is held at constant force above the surface. Thus, the piezo is moved vertically to adjust the force back to that set at the beginning of imaging. It is this information, movement in the z-direction, that generates an image where the z-coordinates are true

for height measurement. The deflection image is generated when the sample is held at a constant distance to the tip with respect to the tip at time=0, so the tip is bent by the forces of the surface. The reflected laser beam shifts position on the photosensitive diode because of changed reflection on the back of the cantilever; hence the name “deflection image”. This type of image is particularly useful for studying morphological changes.

6.4 *Transmission Mössbauer Spectroscopy*

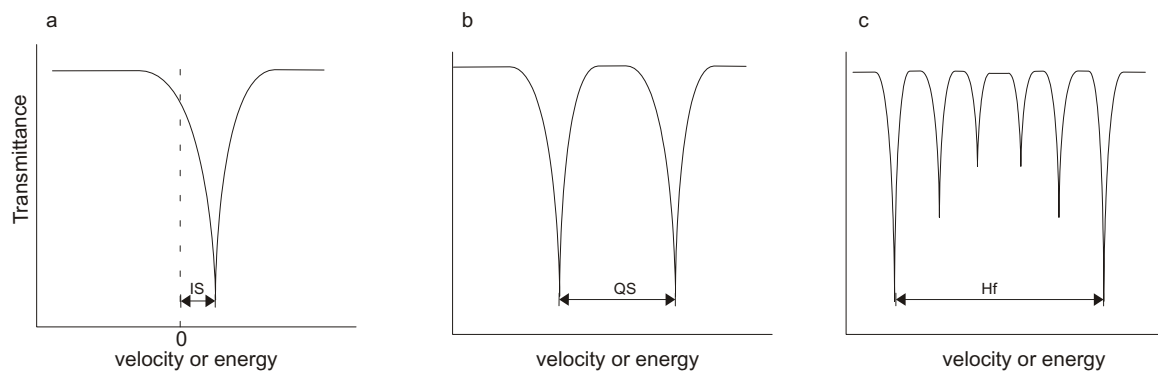
Mössbauer spectroscopy is a bulk analytical method that only works on materials containing a Mössbauer sensitive element. A Mössbauer sensitive element is an isotope that is stable or long-lived in its ground state but that can exist in an excited state, decaying by a gamma transition at appreciable gamma-ray energies. More information is available at http://www.britannica.com/nobel/micro/406_43.html.

The method was made possible by a discovery of Rudolf L. Mössbauer in 1957. He observed that γ -radiation could be emitted and resonantly absorbed without recoil in solids. Mössbauer Spectroscopy can be applied to any materials containing a Mössbauer sensitive element. There exist approximately 35 isotopes that possess the properties required to be a Mössbauer sensitive element. A few examples include: ^{57}Fe , ^{119}Sn and ^{151}Eu . 90% of all papers on Mössbauer spectroscopy analysis represent ^{57}Fe . The spectroscopy yields information about the valence state, coordination chemistry and magnetic properties (hyperfine interactions) of a Mössbauer sensitive element in the material. The absorption of energy in the sample is related to the energy distribution around the nucleus of the atom.

An isomer shift (IS) (Fig. 7a) results from an interaction between s-electrons and the nucleus of the atom. Because the atomic nuclei have different radii in the excited and ground states, the energy distribution at the nucleus is different for the two states (Mørup, 1997). This results in a shift in energy between the source and the sample. Normally, however, a shift is presented relative to a reference material. Because of the quantised properties of atoms, spin quantum numbers are used to describe the nucleus in ground and excited state. When the spin quantum number, $I > \frac{1}{2}$, the atom possesses a non-spherical charge distribution. The deviation from spherical distribution is referred to as the electric quadrupole moment. The interaction between a non-homogenous electric field gradient (EFG) at the nucleus and the electric quadrupole moment results in a charge distribution

called the electric quadrupole interaction, or quadrupole split (QS) in Mössbauer spectra (Fig. 7b). The EFG and thus also the quadrupole split, can be considered to have two contributions: 1) the lattice contribution arising from neighbouring ions surrounding the Mössbauer element and 2) a valence electron contribution arising from the anisotropic electron distribution in the valence shell of the Mössbauer element (Mørup, 1997). When a nucleus possesses a spin quantum number, $I > 0$, it has a non-zero magnetic dipole moment, so it interacts with any magnetic field at the nucleus (Mørup, 1997). The magnetic interaction splits the energy levels of the atom into a number of sublevels. The energy between these sublevels defines the magnetic hyperfine interaction. For ^{57}Fe Mössbauer spectroscopy such a magnetic hyperfine split (Hf) results in six absorption lines (Fig 7c).

Figure 7. Types of interactions presented in Mössbauer spectra. a) isomer shift, b) quadrupole split and c) hyperfine splitting



In addition to the three types of interaction, there is also the effect of temperature that can be seen on Mössbauer spectra. Because the frequency of the vibrations in the lattice is in the order of 10^{13} s^{-1} , it implies that when temperature changes, the energy shifts. Furthermore the magnetic orientation of a particle may fluctuate when the particles are very small. In such case, the magnetic moment may shift direction so fast, that it appears as a single absorption line in the spectra. When the temperature becomes very low, the speed of fluctuation decreases and at some point, the energy of the lattice becomes large enough to maintain the magnetization direction. This results in hyperfine splitting. The combination of the interactions exhibits details of the investigated material in such detail that the spectroscopy may provide valuable insight into the fundamental chemistry of unknown materials.

The valence state, coordination chemistry and magnetic properties of an element are often unique for a given phase. Thus, Mössbauer spectroscopy may be used to determine phase assemblages by comparison of spectra for unknown materials with that of well-characterised material. Mössbauer spectroscopy can be done in two ways, by reflection or transmission. Transmission Mössbauer spectroscopy (TMS) is now a commonly used analytical tool in a range of scientific disciplines, such as material sciences and mineralogy. Mössbauer spectroscopy complements other techniques well, such as X-ray diffraction, but should not be used alone to identify separate phases in a mixed sample. Amorphous phases, which are difficult or impossible to identify with X-ray diffraction, may be studied with ease using Mössbauer spectroscopy.

For the study here, two samples were examined with Transmission Mössbauer Spectroscopy (TMS) using a constant accelerating Mössbauer spectrometer with ^{57}Co in a Rh matrix as the source. Calibration of the spectrometer was made with $\alpha\text{-Fe}$ foil. The spectra were obtained at 295 K, 80 K and 20 K without application of an external magnetic field. The samples for TMS were prepared in the glove box. The material was crushed and placed in the Plexiglass holder and closed with a Plexiglass lid. The samples were then placed in a 250 ml glass jar with a tight fitting lid before transportation from the glove box at Geological Institute to the Mössbauer Lab at the Technical University of Denmark. The sample chamber was held under vacuum during analysis. The samples were analysed at various amounts of time until reasonable spectra were obtained, usually ranging from 10 to 30 hours.

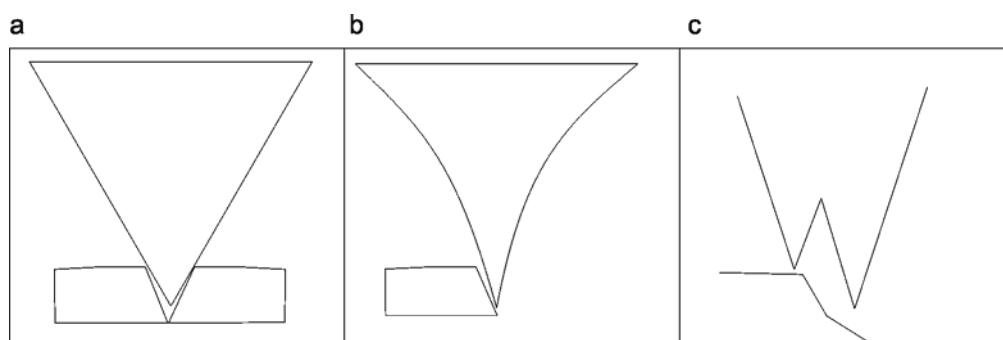
6.5 Reproducibility and Uncertainty

6.5.1 Atomic Force Microscopy

The sources of uncertainties in AFM imaging result mainly from image distortion. Distortion has two components: drift and scaling (Henriksen and Stipp, 2002). Both components are dependent on the stabilisation of the electronic impulses in the piezo electric scanner. Scaling also depends on scan speed variations. It is linear and can thus be accounted for quite easily, whereas drift is nonlinear and thus influences the angles of the image. I expect the uncertainties related to distortion to be on the order of $\pm 10\%$ in this study.

The shape and size of the tip also influences sharpness of the edges and the width of features in AFM images. The shape of the tip is pyramidal and if the edges of a particle have a steeper angle than the slope of the pyramid it results in an image of the tip instead of the particle edge (Fig. 8a). The problem can to some extent be avoided using a sharper tip with steeper pyramid sides (Fig. 8b). The size of the tip can also influence the images obtained because of limitations for the tip to penetrate holes in the particle (Fig. 8a) producing an image with false depth information. Furthermore it is possible that the tip breaks so it gets a double tip, which results in images with particles represented twice oriented in exactly the same direction (Fig. 8c).

Figure 8. Examples of tip artefacts. a) the sample has steeper slopes than the tip and the obtained image will represent the slope of the tip and not the sample. The tip is too big to penetrate the gap fully and produces thus an image with wrong depth information. b) Sharper tip than in (a) that can record the edge slope correctly. c) zoom of the front of a tip with a double tip.



6.5.2 X-ray diffraction

Uncertainties arise in X-ray diffraction from sample preparation methods and from the instrument, such as preferred orientation, energy absorption and incorrect calibration. Because I used Capillary-

Tube X-ray diffraction (CT-XRD), the effect of preferred orientation is limited and if present it would be possible to see on the diffraction rings as incongruous areas of increased intensity, thus only affecting the relative intensities. Atoms with wavelength in the range of the incoming X-rays, can induce energy absorption and thereby affect the intensities of the diffraction lines. I used in this study a $\text{Mo}_{\text{K}\alpha}$ source for CT-XRD. The source has a wavelength that is lower than Fe, so there is, no energy absorption in the sample. Using the CT-XRD method involves calibrating the samples manually, based on a visual estimate of diffraction ring correlation. Because calibration has a large influence on the d-spacing of the diffraction lines. It is the one that probably has greatest effect in this study. Uncertainties of d-spacings are normally approximately 0.1%. In this study, I have estimated the uncertainties resulting from calibration to be <0.5%.

6.5.3 Mössbauer spectroscopy

The widths of absorption lines in Mössbauer spectroscopy are dependent of the sample thickness. An extremely thin sample produces absorption lines with area that are proportional to the thickness of the sample. When γ -radiation passes through the sample, the intensity is decreased exponentially (Mørup, 1997). For thicker samples, there is a saturation effect on the spectra, which is usually observed when absorption >85%. This implies that if absorption is close to saturation the relative area distribution cannot be used to quantify the Fe phases or states present.

7 Results and Discussion

7.1 Transformation study

Lin et al. (1996) and Srinivasan et al. (1996) presented a detailed work of the transformation of GR_{SO_4} involving XRD, SEM, EDS and TEM analysis and chemical considerations. This work forms the base for my transformation study of the oxidation of $\text{Fe}(\text{OH})_2$ in solution containing sulphate and sodium. With access to a glove box and AFM it is possible to examine the evolution of GR_{SO_4} morphology during oxidation from formation from $\text{Fe}(\text{OH})_2$ to its decomposition to iron (oxy)hydroxide. Placing the AFM inside the glove box made it possible to examine the transformations without oxidation of the sample. Furthermore I developed the CT-XRD method where it is possible to examine the sample material without further preparation than filtering and (oxygen free) air-drying.

Plots of Eh and pH as a function of time for the two experiments are presented in Figures 9 and 10. Figure 9 presents the 17 hour long, slow oxidation experiment (airflow rate = $143 \pm 5 \text{ ml min}^{-1}$) and Figure 10 presents the 10 hour long, faster oxidation experiment (airflow rate = $286 \pm 10 \text{ ml min}^{-1}$). Notice that the plots only show development from the time oxidation began, i.e. when airflow began. The numbers along the arrows refer to samples analysed by CT-XRD, AFM or TMS extracted at that particular time. The notation y-xx refer to sample xx from experiment y. Table 10 summarises sample extraction time and analytical method applied.

The Eh and pH plots for Exp-1 (Fig. 9) can be divided into several characteristic regions for the oxidation period. From the Eh pattern (lower curve), there are three regions where the curve is relatively flat: Plateau 1 (0 – 320 min.), 2 (490 – 780 min.) and 3 (800 – 1000 min.) and there are two regions where Eh changes distinctly: Step 1 (323 – 490 min.) with an increase from –500 to –80 mV and Step 2 (776 – 800 min.) with a smaller increase from –200 to –50 mV. These divisions can also be made in the same time intervals for pH but the pattern is less marked. Step 2 is almost hidden in the noise of the pH curve. The spike during Step 1 (at 370 min) in both pH and Eh is the result of the sudden release, during a sampling event, of some starting material that was stuck in a stirring shadow in one of the bottlenecks.

Figure 9

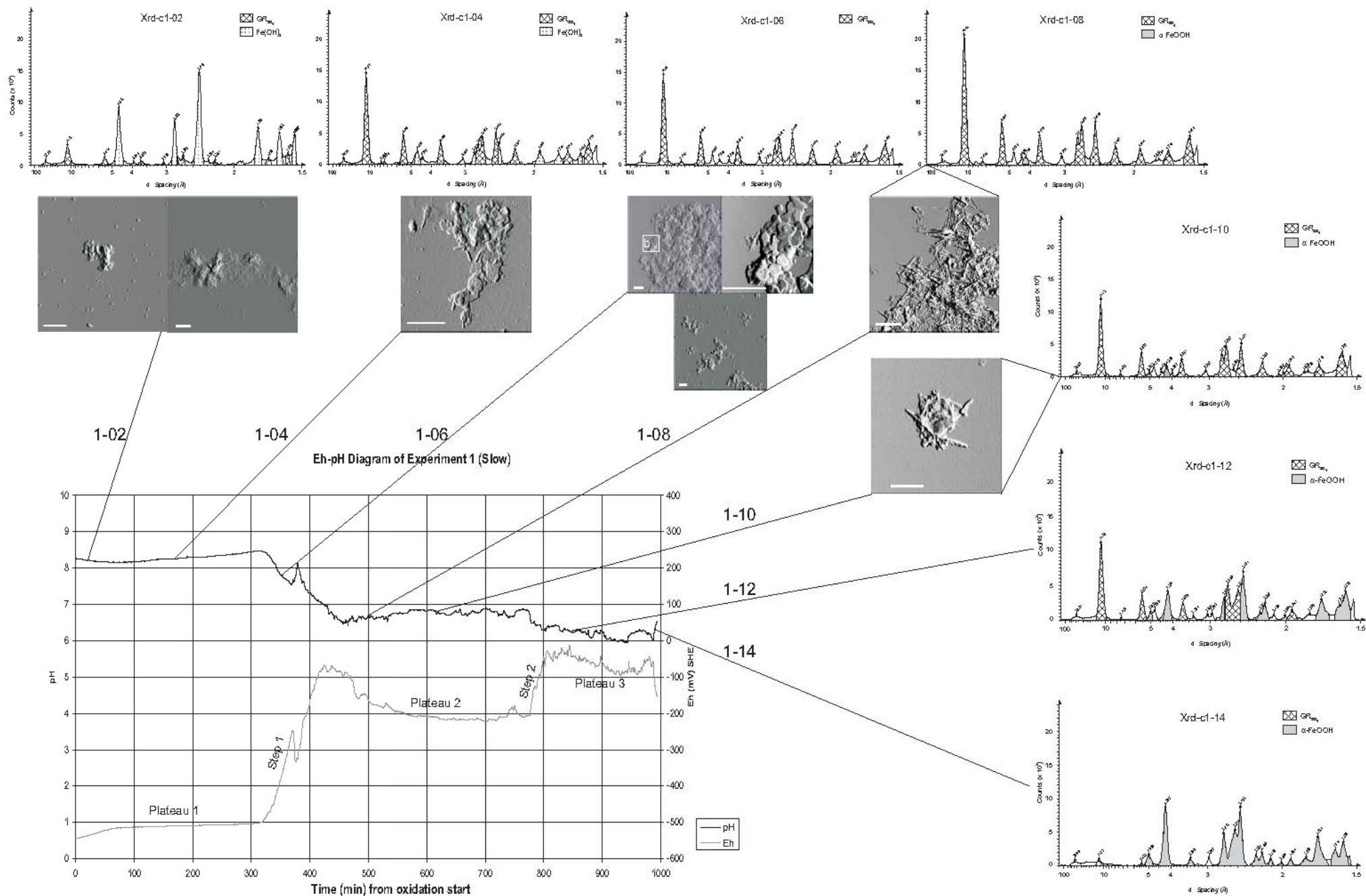
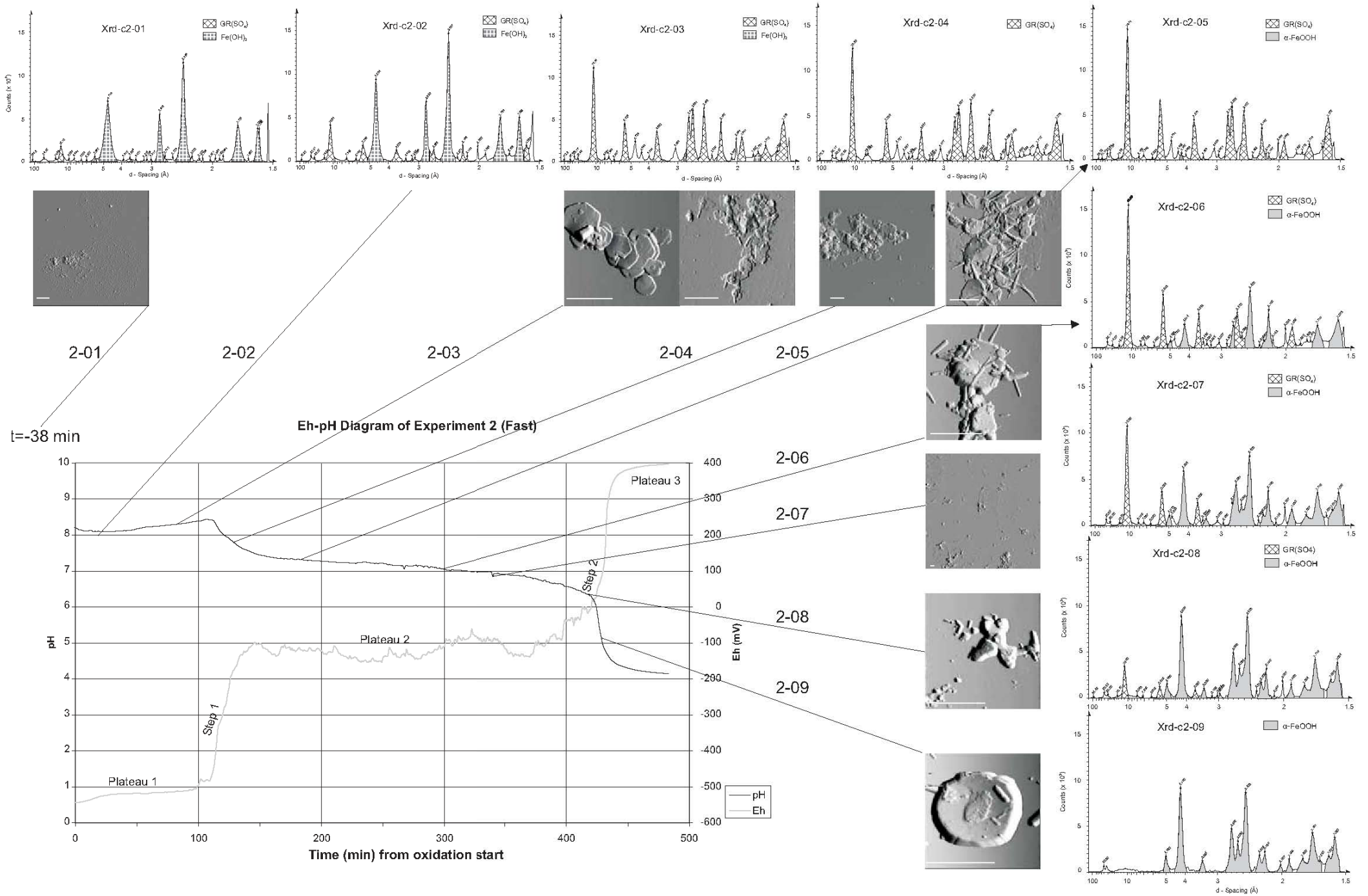


Figure 10



The curves for Exp-2 (Fig. 10) have the same overall look, but when the airflow is doubled the time reaching each step is halved and the plateaus are smoother and the Eh and pH steps are clear and large. Dividing Exp-2 according to the Eh pattern: makes Plateau 1 (from 0 – 113 min.), Plateau 2 (from 150 – 396 min.) and Plateau 3 (from 442 min. – end) and Step 1 with an increase from –500 to –100 mV (over 113 – 150 min.) and Step 2 with an increase from approximately –100 to 400 mV (over 396 – 442 min.).

7.1.1 Mineralogical and morphological changes

To identify the initial material, samples were taken before oxidation start, as well as in the very beginning of oxidation in each experiment (1-02, 2-01 and 2-02). The Capillary Tube - X-ray diffraction (CT-XRD) trace of 1-02 (Fig. 11) and 2-01 (Fig. 12) and 2-02 (Fig. 13) demonstrates that a majority of the peaks correspond to Fe(OH)₂; the d-spacings and peak intensities correspond well with data published by Bernal et al. (1959) (Table 11).

Table 11. Published X-ray diffraction data for Fe(OH)₂ and samples taken early in the experiments. Table include only peaks that are within detection range of this study.

Bernal et al. (1959)			This work			
			1-02 (Fig. 11)		2-01 (Fig. 12)	
hkl ¹	d _{hkl} (Å)	Intensity ²	d _{hkl} (Å)	% Intensity	d _{hkl} (Å)	% Intensity
0001	4.597	vs	4.612	61.8	4.708	44.1
10 $\bar{1}$ 0	2.817	s	2.822	45.6	2.817	47.0
10 $\bar{1}$ 1	2.403	vs	2.411	100	2.381	100
10 $\bar{1}$ 2	1.782	s	1.785	39.5	1.751	35.7
11 $\bar{2}$ 0	1.629	s	1.633	33.6	1.599	32.8
11 $\bar{2}$ 1, 0003	1.535	m	1.538	31.0	1.528	59.7

¹ Indices based on a hexagonal cell; a=3.258 Å and c=4.605 Å.

² vs = very strong, s= strong and m = medium.

Figure 11. CT-XRD trace of 1-02.

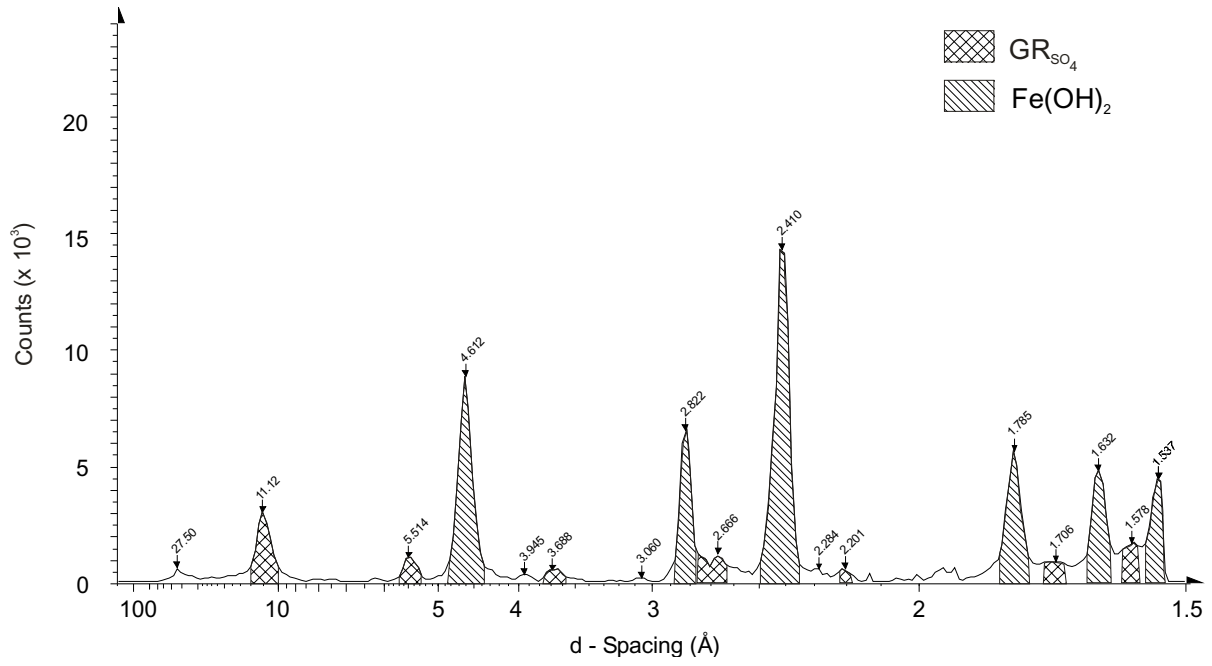


Figure 12. CT-XRD trace of sample 2-01

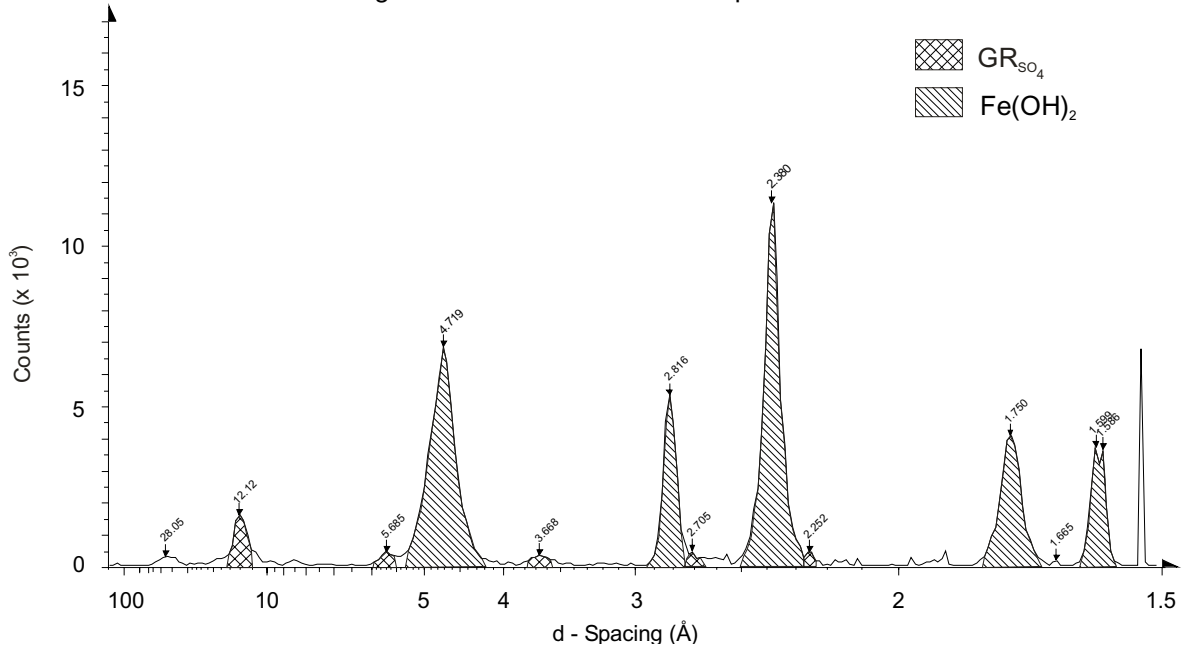
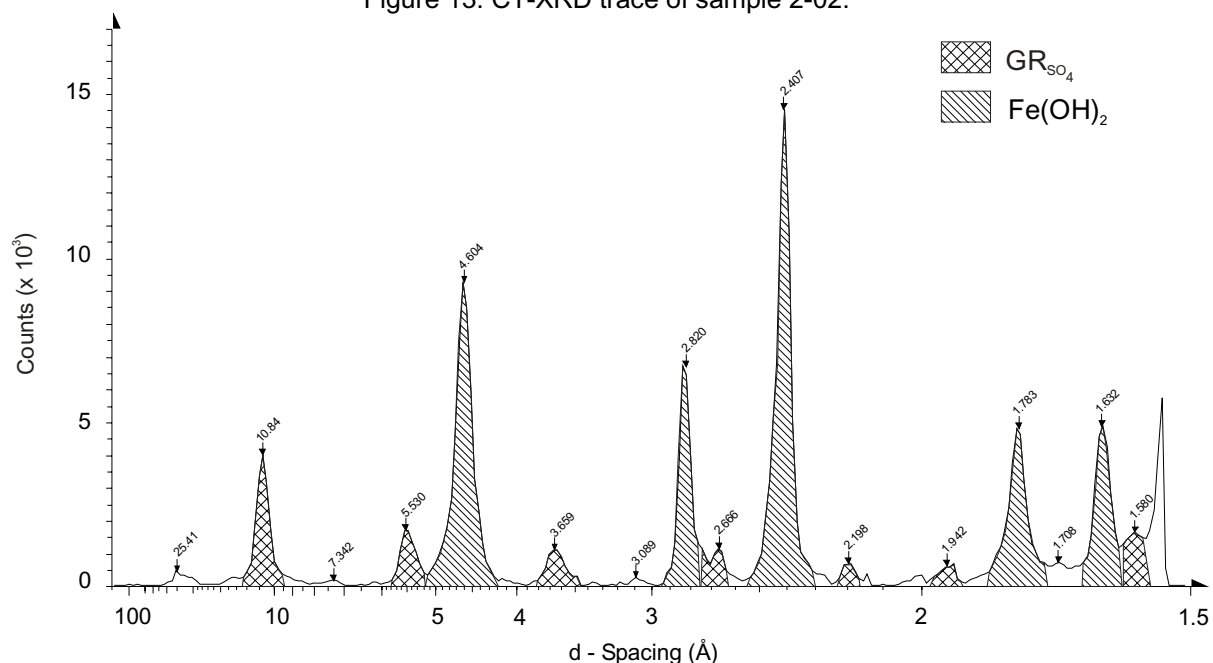


Figure 13. CT-XRD trace of sample 2-02.



Some minor peaks, however, do not fit the structure of this phase. Comparison of these intensities with XRD data published by Bernal et al. (1959), Hansen et al. (1994) and Simon et al. (2003) (Table 12) exhibits a match with GR_{SO₄}. Although the d-values of GR_{SO₄} in 2-01 are shifted to somewhat higher values (approximately by 1 Å), the overall d-spacing relationships and intensity between the three main peaks match well. Sample 2-01 (Fig. 11) was extracted before any air was added, so in principle it should not contain any GR_{SO₄}. However, oxidation of the surfaces of the FeSO₄ · 7 H₂O before dissolution would allow tiny amounts of Fe(III) to be present in the initial solution. Spectrophotometry and AAS analysis of the FeSO₄ · 7 H₂O exhibited, however, only Fe(II) present. The CT-XRD traces do not exhibit any evidence of any intermediate phase in the transformation of Fe(OH)₂ to GR_{SO₄}. Intermediate phases may be present in trace amounts that do not allow CT-XRD detection.

Table 12. X-ray diffraction data for GR_{SO₄}.

Bernal et al. (1959)			Hansen et al. (1998)		Simon et al. (2003) ⁽¹⁾		This work							
hkl ⁽²⁾	d _{hkl} (Å)	I ⁽³⁾	hkl ⁽⁴⁾	d _{hkl} (Å)	d (Å)	I/I _t ⁽⁵⁾	1-02 (Fig. 11)		2-01 (Fig. 12)		1-06 (Fig. 18)		2-04 (Fig. 19)	
							d (Å)	I/I _t ⁽⁶⁾	d (Å)	I/I _t ⁽⁶⁾	d (Å)	I/I _t ⁽⁶⁾	d (Å)	I/I _t ⁽⁶⁾
0001	10.92	vs	003	11.03	10.89	100	11.11	100	12.12	100	11.08	100.0	10.80	100.0
0002	5.48	s	006	5.49	5.442	40.9	5.514	34.6	5.685	28.8	5.534	30.3	5.500	32.7
	-			-	4.728	11.1	3.688	16.6	3.668	20.9	4.747	8.8	4.761	12.5
	-			-	4.326	7.0	-	-	-	-	4.390	4.0	4.367	5.5
	-			-	3.953	4.1	-	-	-	-	3.986	3.3	3.991	3.0
0003	3.65	s	009	3.657	3.610	33.3	-	-	-	-	3.675	19.5	3.647	25.2
	-			-	3.084	9.4	3.060	6.2	-	-	3.074	6.3	3.077	9.3
0004, 10 $\bar{1}$ 0	2.747	m	101	2.751	2.759	31.0	-	-	-	-	2.750	20.0	2.743	34.7
10 $\bar{1}$ 1	2.660	ms	013	2.668	2.640	36.3	2.652	37.4	-	-	2.671	27.2	2.667	45.2
10 $\bar{1}$ 2	2.459	ms		-	2.455	32.7	-	-	-	-	2.461	33.9	2.459	50.3
0005, 10 $\bar{1}$ 3	2.195	ms	019	2.200	2.201	21.1	2.201	52.1	-	-	2.198	27.8	2.196	36.4
10 $\bar{1}$ 4	1.938	ms	10 $\bar{1}$ 2	1.958	1.945	15.5	1.948	20.4	-	-	1.946	15.0	1.940	19.7
	-		00 $\bar{1}$ 8	1.829	1.793	5.0	1.912	19.9	-	-	1.779	4.0	1.776	6.2
10 $\bar{1}$ 5	1.712	w	10 $\bar{1}$ 5	1.716	1.719	9.4	-	-	-	-	1.717	11.0	1.715	13.0
11 $\bar{2}$ 0	1.587	w	110	1.589	1.592	23.4	-	-	-	-	⁽⁷⁾		⁽⁷⁾	
11 $\bar{2}$ 1	1.570	w	113	1.573	1.575	25.7	-	-	-	-	1.575	21.5	1.578	34.4

¹ d-spacing and intensities are determined from Figure 2 in Simon et al. (2003).

² Indices based on a hexagonal cell; a=3.18 Å and c=32.92 Å.

³ v:very; s:strong; m:medium; w:weak.

⁴ Indices based on a hexagonal cell; a=3.174 Å and c=10.94 Å.

⁵ Intensities relative in %.

⁶ Intensities recalculated for only GR_{SO₄} intensities.

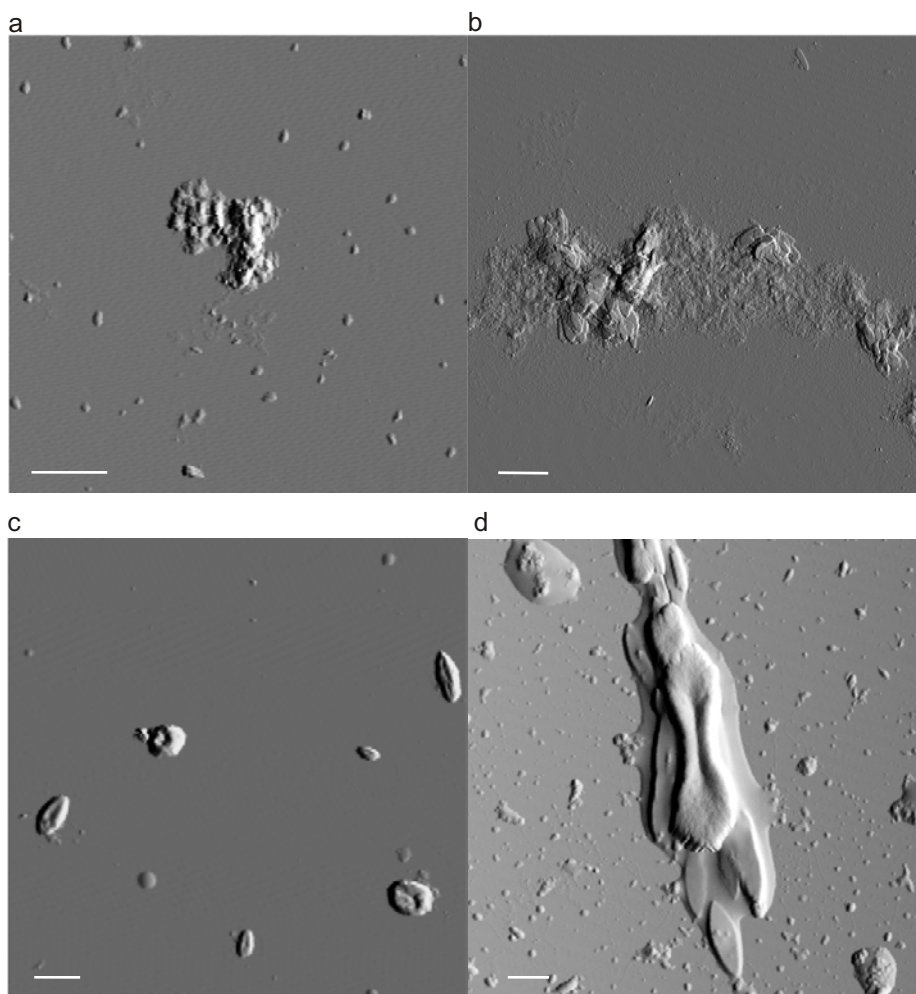
⁷ This peak is probably the shoulder on the 1.575 peak.

To compare crystallographic data with morphological changes, AFM images were obtained. For sample 1-02 and 1-03 (Fig. 14) the images show small-grained particles and ellipsoidal crystals attached to the mica surface. Because the CT-XRD patterns show essentially all Fe(OH)₂ I interpret these particles to be Fe(OH)₂ probably with the beginning of GR_{SO₄} formation. Srinivasan et al. (1996) observed with scanning electron microscopy (SEM) that Fe(OH)₂ forms both thin, shapeless material and spherical particles and they confirmed the crystallinity of the material using transmission electron microscopy (TEM).

On some particles, expansion was observed during the early stage of the oxidation process (Fig. 14c and d). The crystallographic properties of Fe(OH)₂ are quite similar to GR_{SO₄} the only major difference is the missing intercalation of anions in Fe(OH)₂. The brucite-like layer of Fe(OH)₂ is becoming oxidised and begin to intercalate sulphate to satisfy the positive charge from Fe³⁺ in the

layer. Such a transformation is consistent with topotatic transformation of $\text{Fe}(\text{OH})_2$ to GR_{SO_4} (Bernal et al., 1959) where the $\text{Fe}(\text{OH})_2$ expands in the c-axis direction as SO_4^{2-} and H_2O are incorporated.

Figure 14. AFM deflection images. a) sample 1-02, particles are 10 to 40 nm high, b) sample 1-02, ellipsoidal particles are approximately 12 nm high c) sample 1-03 particles approximately 120 nm high at the edges and 23 nm in the suppression and d) sample from preliminary experiment, particle approximately 475 nm high at the edges and 90 nm in the suppression. Scale bar 1 μm .



The CT-XRD trace of the more matured 1-04 (Fig. 15) reveals that GR_{SO_4} is becoming dominant and that only a small amount of $\text{Fe}(\text{OH})_2$ is left. The same is observed in Exp-2 (2-03, Fig. 16). AFM images of these samples show clearly hexagonal particles with width of 0.7 to 1.1 μm and height distribution from 3 to 20 nm (Fig. 17). Measurement of the diameter of GR_{SO_4} particles on several images reveals size distribution ranging from approximately 0.1 to 1.1 μm . Height variation

of GR_{SO_4} measured on single oriented particles ranged from approximately 3 to 30 nm. AFM images produced from other experiments conducted in our group (Sonne Larsen, Skovbjerg and Christiansen, unpublished data) reveals the formation of terraces on the surface of the GR_{SO_4} particles. The height difference between terraces can be as low as 1.1 nm, which is expected from a single molecular layer of GR_{SO_4} , indicating the growth of GR layers on existing GR_{SO_4} . The AFM image of sample 1-04 (Fig. 17b) reveals also some elongated particles approximately 250 nm long. The CT-XRD trace (Fig. 15) exhibits, however, no evidence of other phases present than GR_{SO_4} and trace amounts of $\text{Fe}(\text{OH})_2$.

Figure 15. CT-XRD trace of sample 1-04.

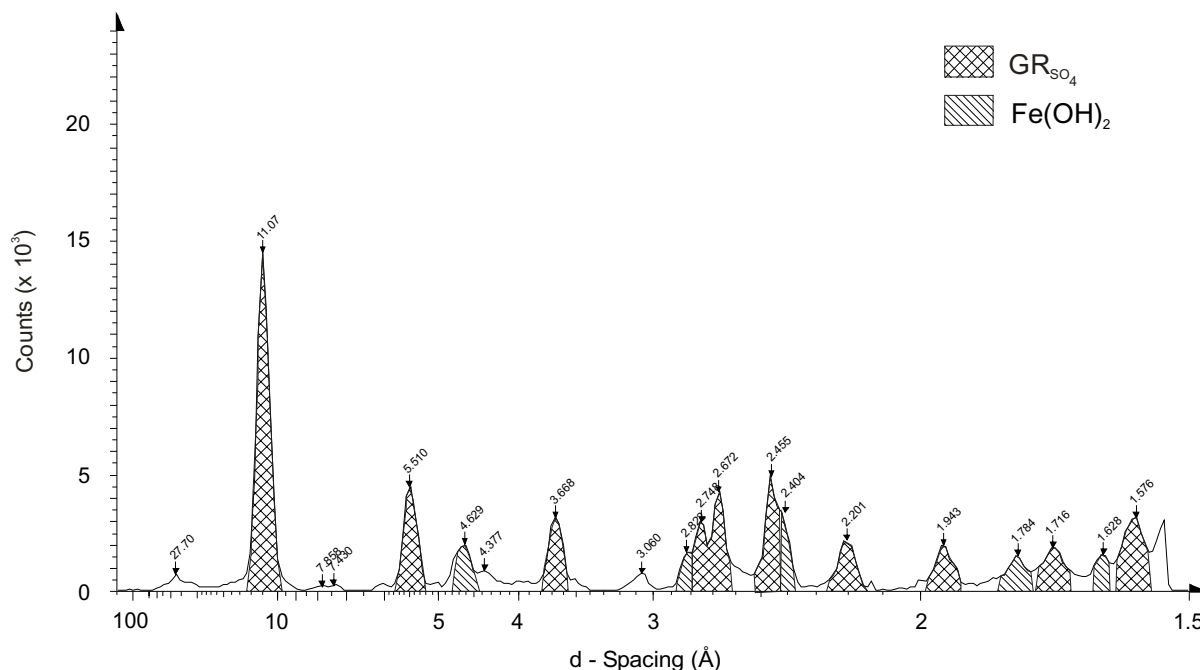


Figure 16. CT-XRD trace of sample 2-03.

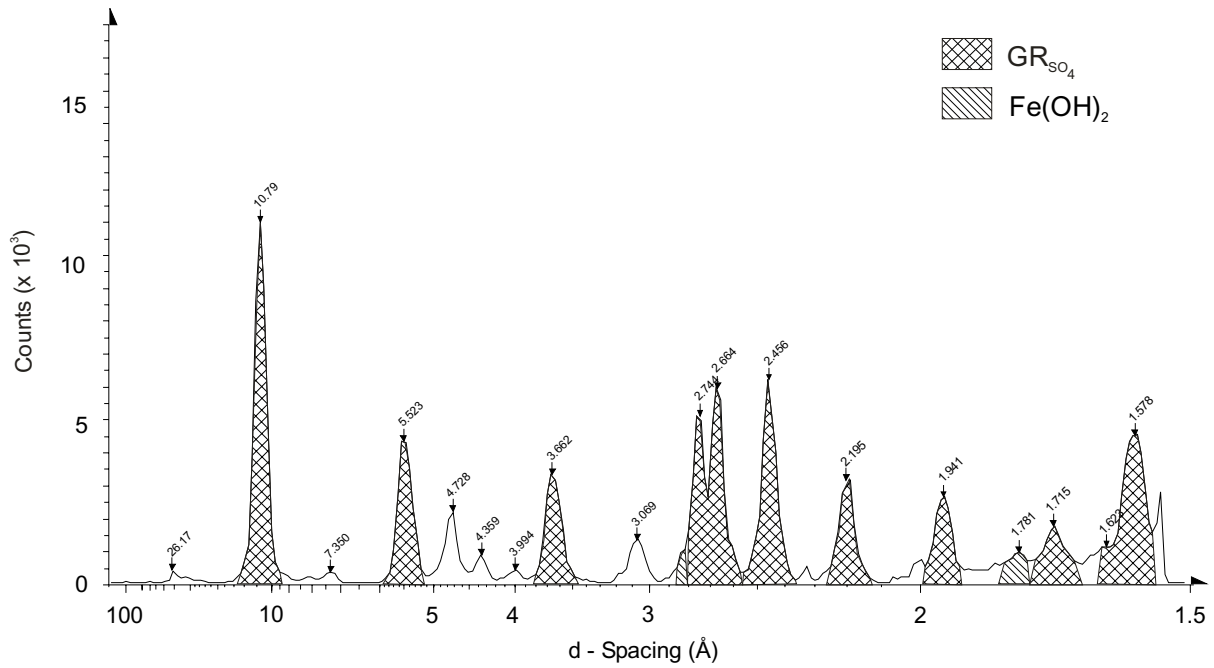
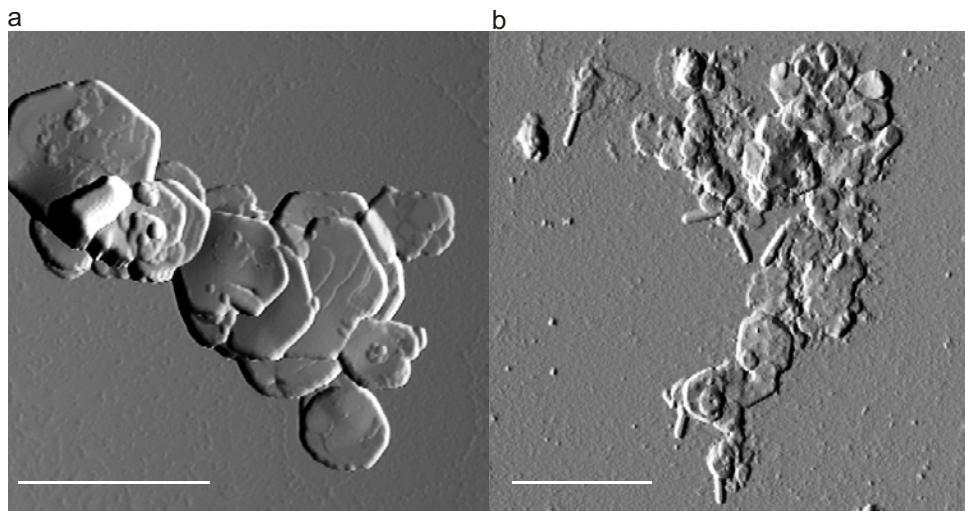


Figure 17. AFM deflection images. a) sample 2-03, height of particles are 17 to 30 nm and b) sample 1-04, height of hexagonal particles are between 3 and 12 nm. Scale bar 1 μ m.



The CT-XRD traces of the two samples extracted midway during step 1, 1-06 (Fig. 18) and 2-04 (Fig. 19), show peaks with d-spacings and intensities that correlate with published data for GR_{SO4} (Table 12).

Figure 18. CT-XRD trace of sample 1-06.

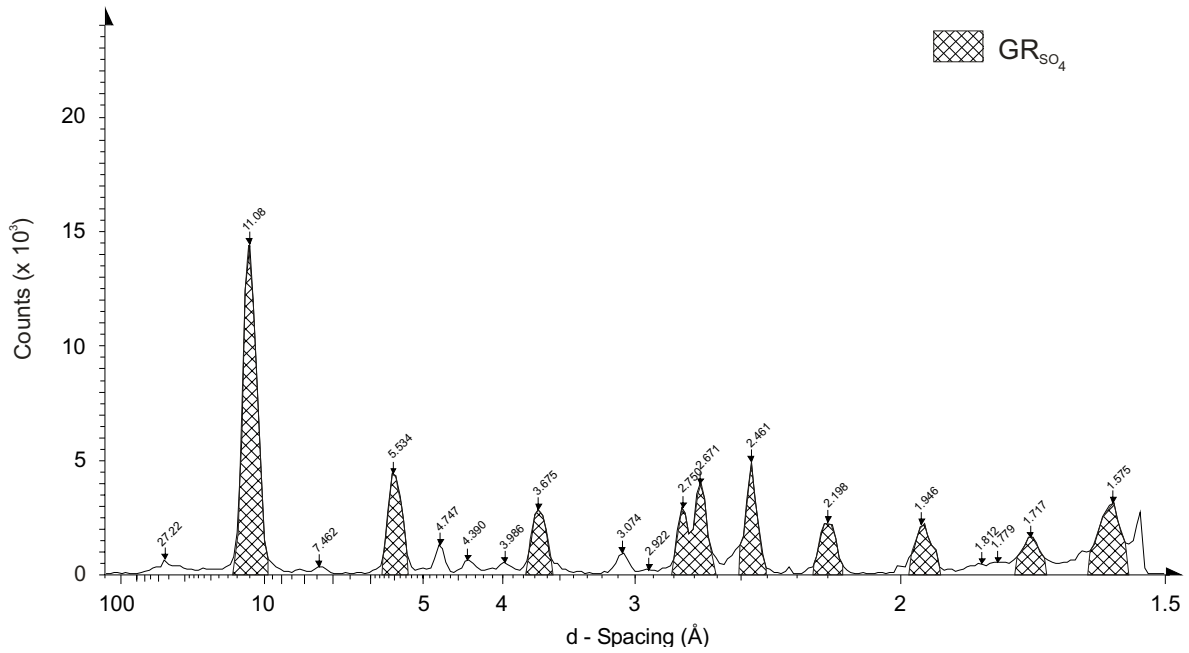
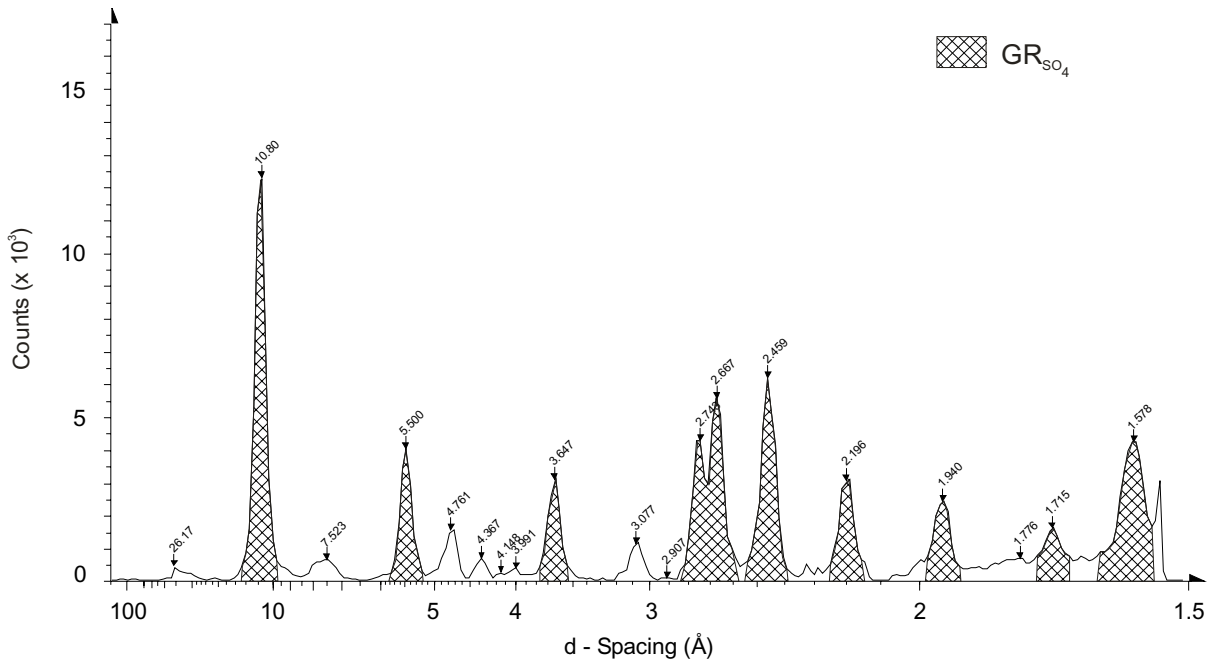


Figure 19. CT-XRD trace of sample 2-04.

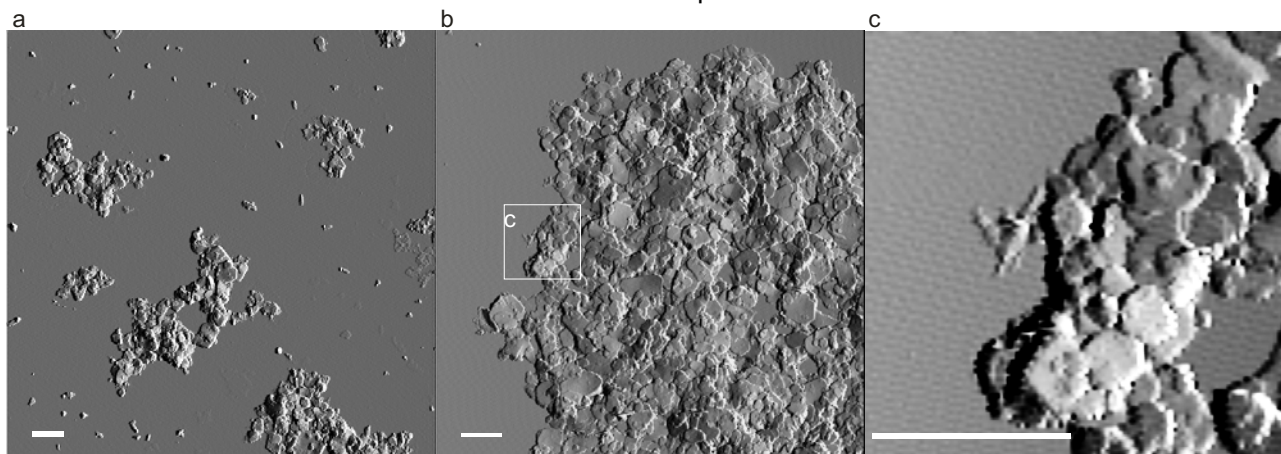


Some of the extra peaks not identified (no texture applied on the plots, at $d \sim 7.46, 4.75, 4.40, 3.99$ and 3.07 \AA) are also found in the work of Simon et al. (2003), but are not described. The new results does not correlate entirely with data from the study of Hansen et al. (1994), presumably because their glycerol preparation method orients the GR_{SO_4} particles so the intensities cannot be

used to determine the structure of GR_{SO_4} . The preferred orientation of the GR particles makes the basal plane intensities extreme and the other crystal faces become hidden in the background noise. Because of the preparation method, the peak expected at $\sim 2.46 \text{ \AA}$ is absent and therefore has not been incorporated in the crystallographic calculations by Hansen et al. (1994).

The AFM images of 1-05 and 1-06 show that the hexagonal material dominates and is always found as large agglomerates (Fig 20). Based on morphology and CT-XRD, there is no doubt about its identity as GR_{SO_4} . There are, however, also found some approximately $0.5 \mu\text{m}$ long needle shaped particles on the same images (Fig. 20c). These resemble goethite, $\alpha\text{-FeOOH}$, seen in abundance later in the experiment, but there is not enough material to be visible with CT-XRD.

Figure 20. AFM deflection images. a) sample 1-05, b) sample 1-06 and c) close-up of area in square on b. Scale bar $1 \mu\text{m}$.



To determine the Fe(II)/Fe(III) ratio of the GR_{SO_4} , transmission Mössbauer Spectroscopy (TMS) was also applied to sample 1-06 and 2-04. Spectra obtained at 80 K (Fig. 21) could be fitted with two Lorentzian-shaped doublets. Doublet 1 (D1) correlates well with Fe(II) and Doublet 2 (D2) with Fe(III) (Table 13). The parameters fit with previously published TMS parameters of GR (Cutler et al., 1990; Génin et al., 1996). In sample 1-06 there is also a sextet (S1), which accounts for 11% of the absorption. The Mössbauer parameters of the sextet are consistent with goethite and this phase accounts for approximately 1.6% by total mass. The presence of goethite is consistent with the needle-like particles observed in Fig. 20b. However the TMS sample 1-06 was taken from the original 1-06 solution sample approximately 2 months after the experiment ended so it is most likely that some of the GR_{SO_4} had transformed to goethite by this time. The presence of

approximately 1.6% goethite in the sample would not be observable in the CT-XRD pattern. Comparing the relative area of the two doublets for Fe(II) and Fe(III) correlates well with stoichiometric GR_{SO_4} for a Fe(II)/Fe(III) ratio of 2/1. The ratio is not exactly 2/1 because absorption by the TMS sample is so high (28%) that can influence the interpretation of the spectra. No other iron phases were observed by TMS.

Figure 21. TMS of sample 1-06 (a) and 2-04 (b) obtained at 295, 80 and 20 K.

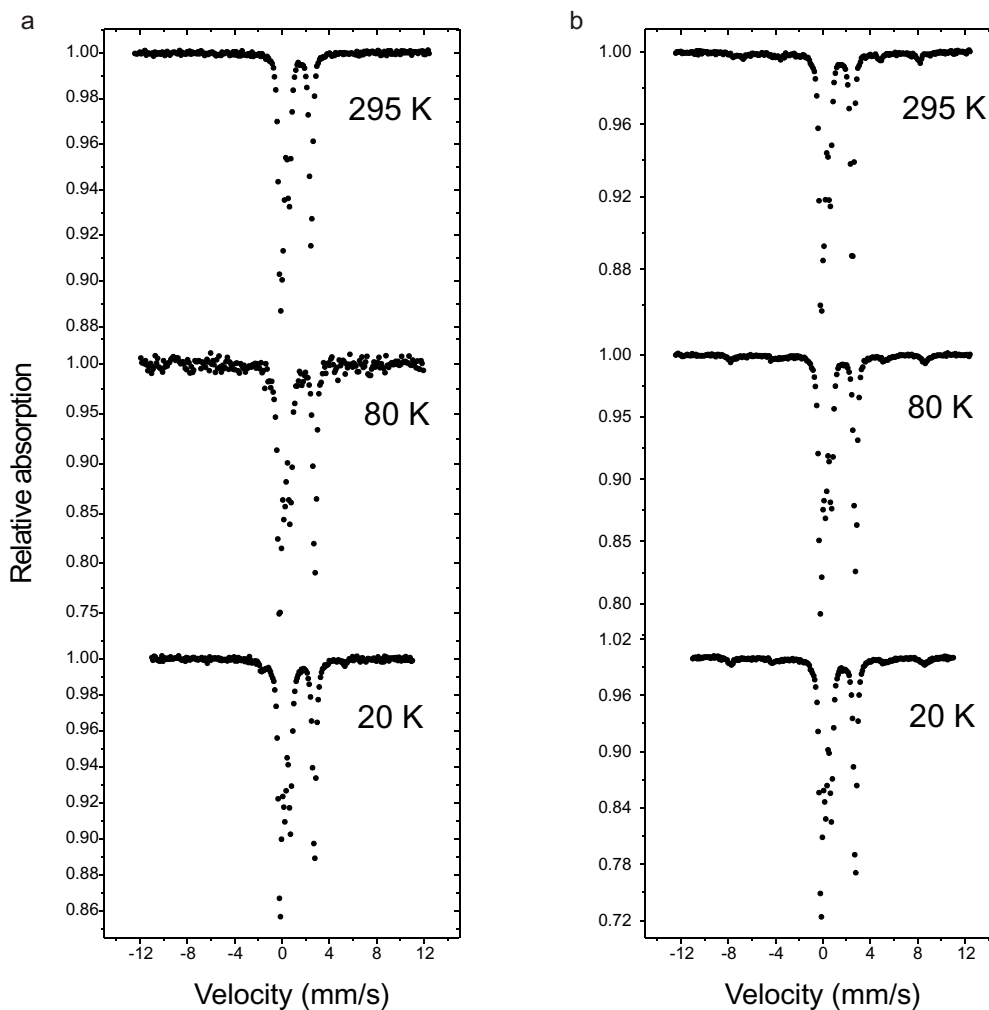


Table 13. Mössbauer parameters of fitted lines for spectra shown in Fig. 21.

	1-06, 80 K				2-04, 80 K		
	Hf (Ts)	IS (mm s ⁻¹)	QS (mm s ⁻¹)	RA (%) ⁽¹⁾	IS (mm s ⁻¹)	QS (mm s ⁻¹)	RA (%)
D1	-	1.28	2.95	57 (64)	1.29	2.97	64
D2	-	0.47	0.48	32 (36)	0.46	0.48	36
S1	50.46	0.56	-0.07	11 (0)		-	

Hf=hyperfine field (Tesla), IS=Isomer shift relative to α -Fe foil centroid, QS=Quadrupole split and RA=relative area.

D1=Doublet 1

D2=Doublet 2

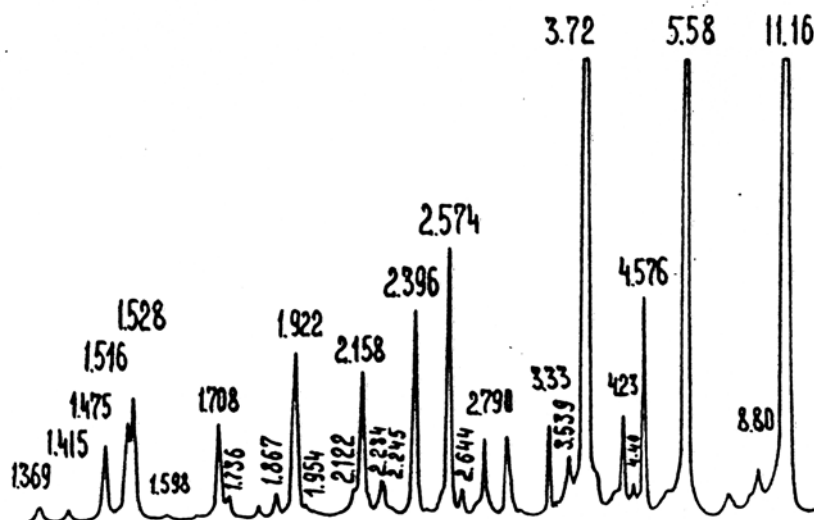
S=Sextet 1

¹ Numbers in brackets are the relative area of only the doublets.

Comparing the CT-XRD traces (Fig. 15, 16, 18 and 19) with data for 11-Å SO₄-hydrotalcite (Fig. 22) presented by Drits et al. (1987) reveals a structural similarity. Drits et al. (1987) hypothesised that Na could be part of the structure but did not follow it up with chemical analysis. Hansen et al. (1994) mentioned the possibility of Na in the structure of GR_{SO₄} but did not consider it in their structural model. I analysed the chemical composition of filter dried GR_{SO₄} with AAS and found 2.16 wt% Na in the filter sample. The filter sample was not washed before analysis, but to obtain 2.16 wt% of Na, there would need to be 0.2 l of solution to evaporate. I used only approximately 10 ml of solution to obtain material for CT-XRD and much of that was removed from the sample passing through the filter paper into the syringe. Na is, thus, most likely part of the GR_{SO₄} structure or adsorbed to the filter material. Later experiments with other cations indicate, however, that Na⁺ is part of the structure (these experiments will be explained and discussed further in chapter 7.3).

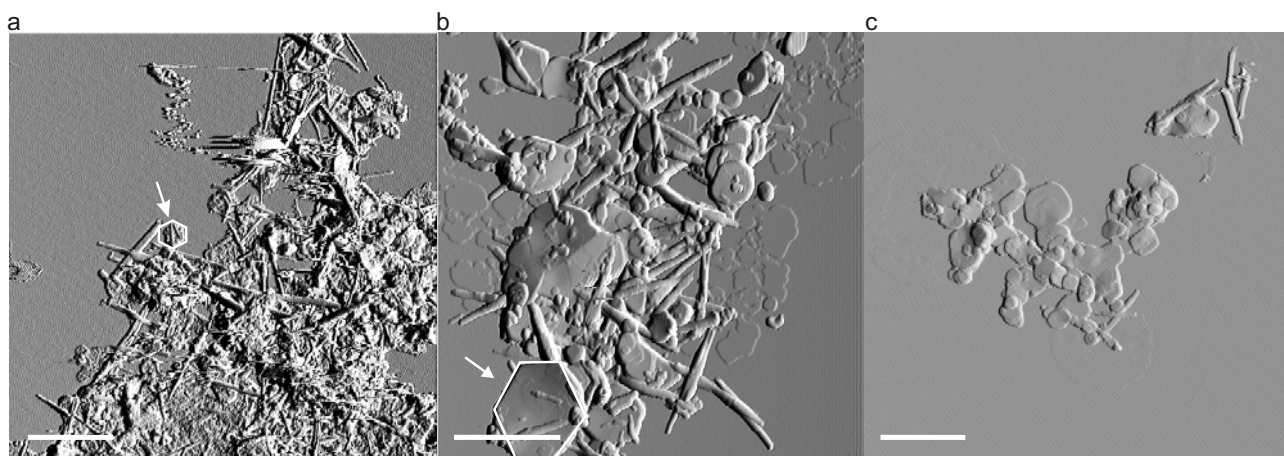
Figure 22. XRD trace of 11-Å SO_4 -hydrotalcite (from Drits et al., 1987).

It was presented originally with no axis and the d-spacings decrease from right to left.



AFM images of samples 1-08 and 2-05 (Fig. 23) demonstrate that the needle-shaped compound observed in sample 1-04 (Fig. 17b) is now present as larger particles and in larger amounts. The morphology of the particles correlates with AFM observations of goethite (Stipp et al., 2002; and Østergaard, 2003). The needle-like shape is in agreement with the orthorhombic nature of goethite. The AFM image of 2-05 (Fig. 23b and c) also shows that the edges of the GR_{SO_4} crystals are not as smooth and straight as on 2-03 (Fig. 17a) and 1-06 (Fig. 20b). There is no question of identifying the morphology as hexagonal. The AFM image of 1-08 (Fig. 23a) exhibits a large conglomerate of goethite particles arranged on top of material with hexagonal outlines.

Figure 23. AFM deflection images. a) sample 1-08, b) and c) sample 2-05. Arrows point to particles with a nearly hexagonal appearance. Scale bar 1 μm .



Because no other phase than GR_{SO_4} and goethite is observed on the AFM images it is reasonable to assume that the increased intensity d-spacing of $\sim 4.2 \text{ \AA}$ observed on the CT-XRD traces of 1-08 (Fig. 24) and 2-05 (Fig. 25) relates to goethite. The most intense reflections of goethite correlate also (Table 14).

Table 14. Comparison of experimental data and goethite data. Only peaks that are unique of goethite or primarily are composed of goethite is presented.

JCPDS card 29-713			This work											
hkl ¹	d _{hkl} (Å)	I/I _t	1-08 (Fig. 24)		1-10 (Fig. 26)		1-14 (Fig. 31)		2-05 (Fig. 25)		2-06 (Fig. 27)		2-09 (Fig. 32)	
			d _{hkl} (Å)	I/I _t ⁽²⁾	d _{hkl} (Å)	I/I _t ⁽²⁾	d _{hkl} (Å)	I/I _t	d _{hkl} (Å)	I/I _t ⁽²⁾	d _{hkl} (Å)	I/I _t ⁽²⁾	d _{hkl} (Å)	I/I _t
020	4.980	12			5.022	4.1	4.980	17.4			4.953	4.1	4.985	17.4
110	4.183	100	4.188	5.1	4.200	11.8	4.205	100.0	4.195	3.9	4.214	15.4	4.195	100.0
120	3.383	10					3.399	10.5			3.380	1.9	3.386	11.9
130	2.693	35					2.712	54.0					2.696	50.3
021	2.583	12									2.588	7.2	2.580	35.6
101	2.527	4					2.538 ⁽³⁾	59.5 ⁽³⁾						
040	2.489	10											2.453 ⁽⁴⁾	94.4 ⁽⁴⁾
111	2.450	50					2.462	99.6						
121	2.253	14					2.264	16.6					2.256	18.7
140	2.190	18					2.199	20.5					2.189	30.4
131	2.011	2											2.007	20.2
041	1.920	3											1.922	14.0
211	1.802	6					1.806	13.0					1.800	14.4
221	1.719	20					1.724	47.2			1.719	14.8	1.721	45.5
240	1.691	6											1.665	12.7
231	1.604	4					1.614	25.4					1.604	17.4
151	1.564	10					1.568	39.1					1.565	40.1

¹ Indices based on an orthorhombic unitcell with a = 4.608 Å, b = 9.956 Å and c = 3.0215 Å.

² Goethite intensities relative to the most intense GR_{SO_4} peak.

³ Peak probably a combination of {021} and {040}.

⁴ {040} shoulder on this.

Figure 24. CT-XRD trace of sample 1-08.

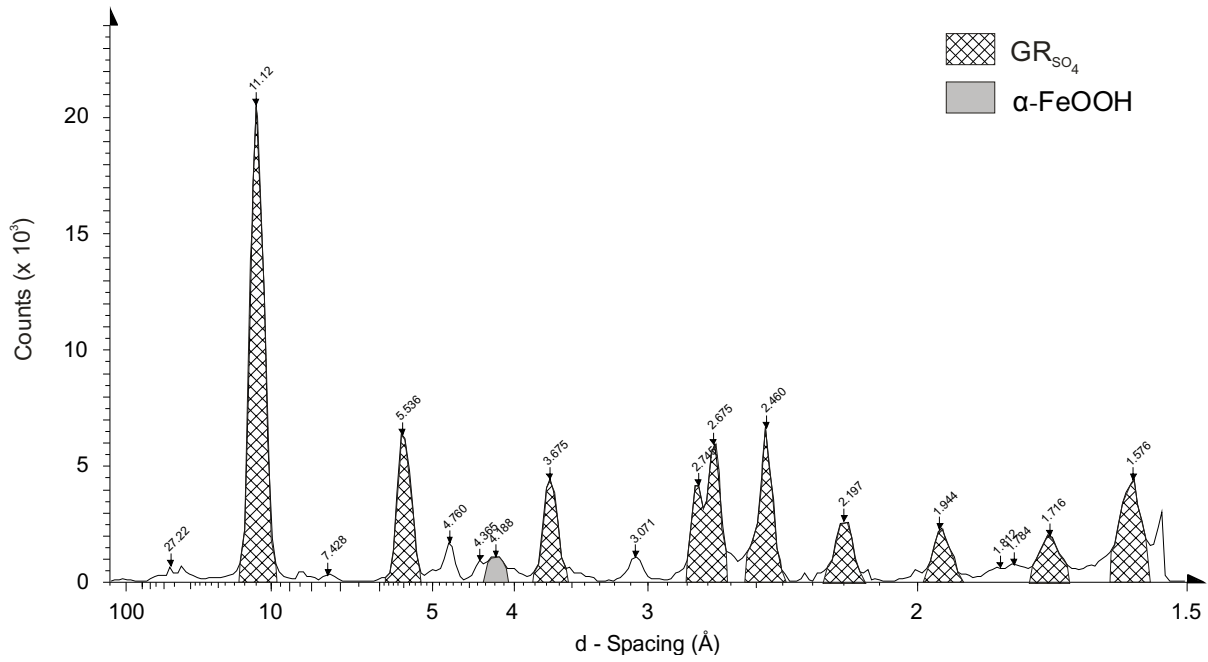
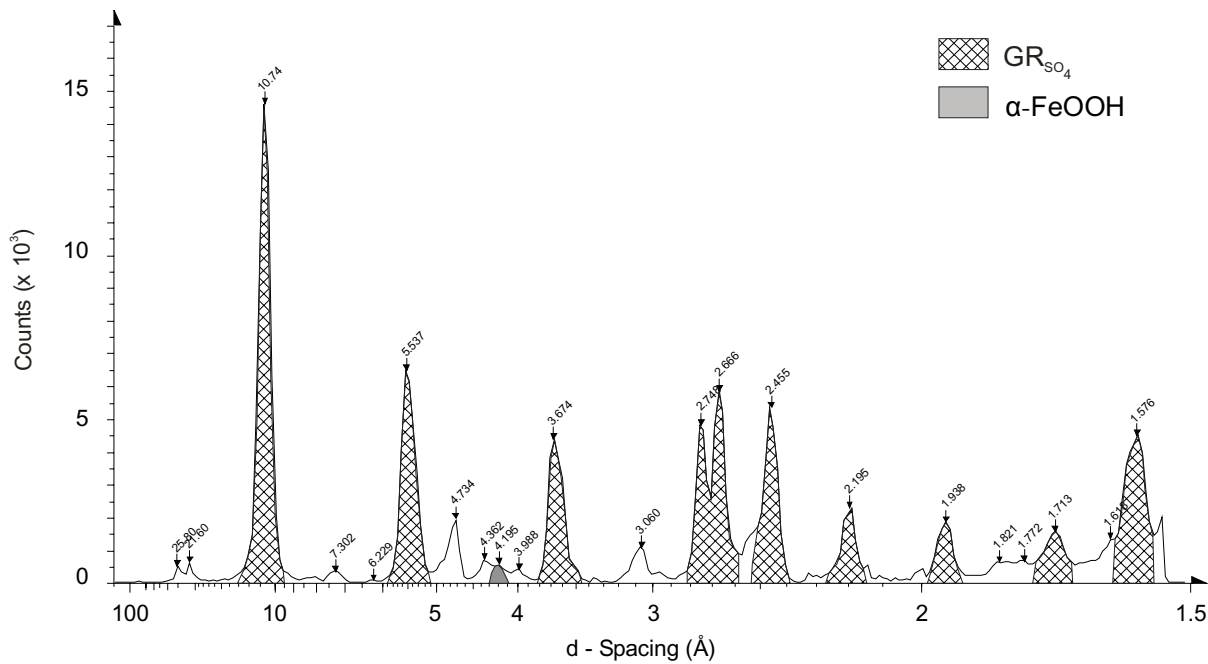


Figure 25. CT-XRD trace of sample 2-05.



As oxidation continues, the goethite peak at $d = 4.2 \text{ \AA}$ becomes more convincing on the CT-XRD traces of 1-10 (Fig. 26) and 2-06 (Fig. 27), and other peaks gradually make their appearance (Table 14). In the area between 2.75 and 2.45 \AA it is difficult to determine whether it is GR_{SO₄} or goethite that are responsible for the peaks there.

Figure 26. CT-XRD trace of sample 1-10.

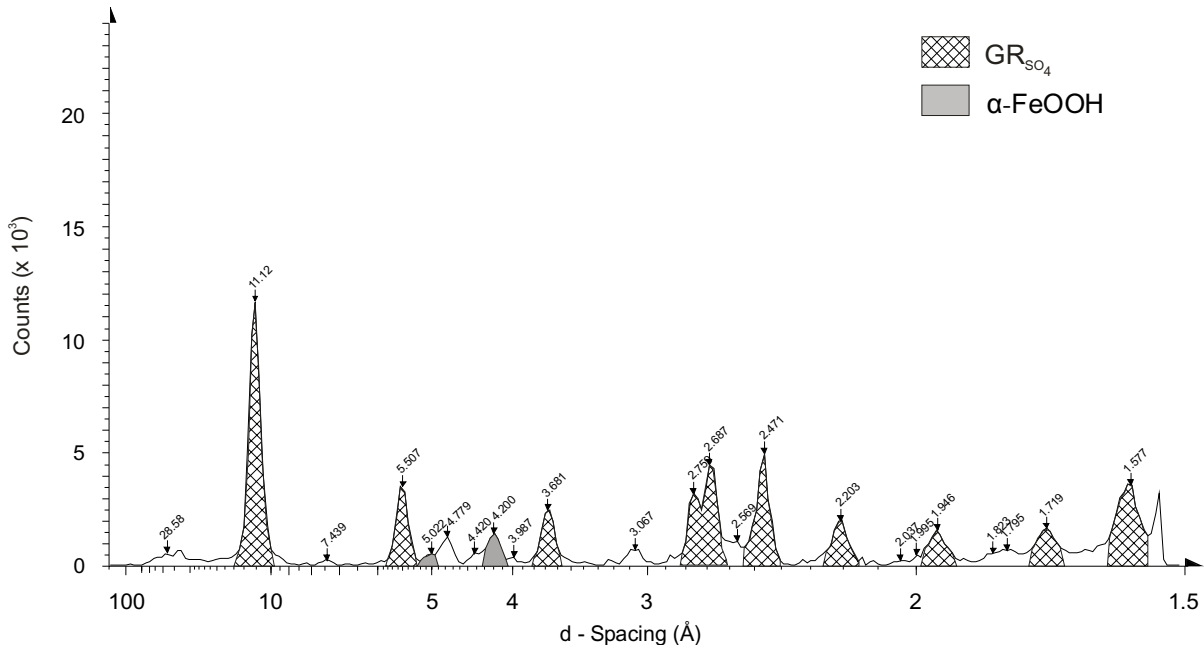
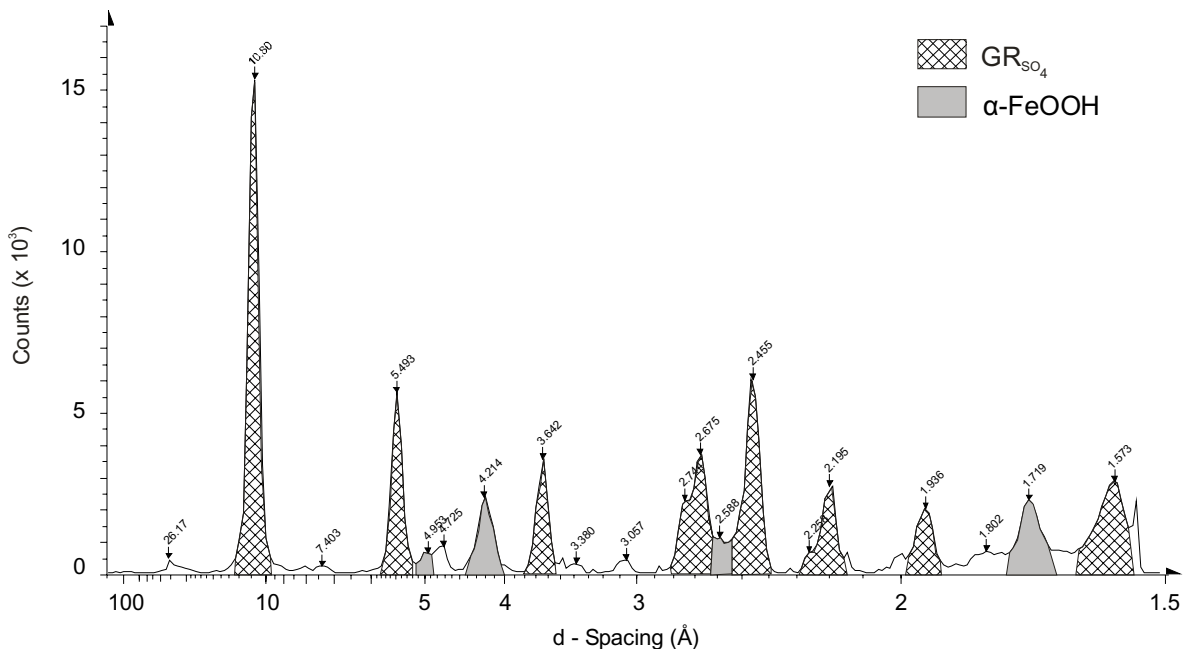


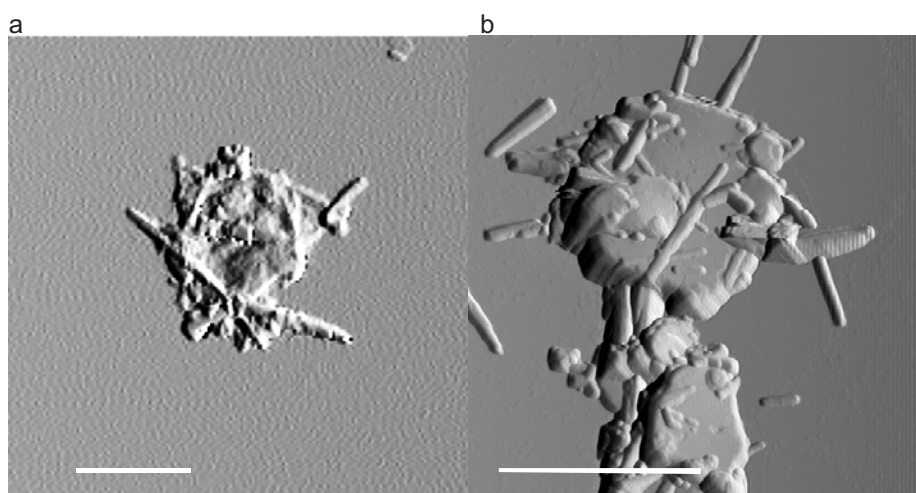
Figure 27. CT-XRD trace of sample 2-06. Peak at 1.719 \AA consist of both GR_{SO_4} and goethite, it is displayed as goethite because it is more intense compared to 2-05 (Fig. 24).



With AFM, increasing amounts of more goethite are observed, often as aggregates oriented on top of disintegrating GR hexagons (Fig. 28). GR has begun to lose its distinct form, suggesting local dissolution of GR, and precipitation of goethite very close by. On the AFM images some material does not exhibit the needle-like and the distinct hexagonal shape. The material has begun to lose the

distinct form, suggesting dissolution of GR to induce precipitation of goethite. The same pattern is seen on the AFM images of 1-08 (Fig. 23a and b). These semi-hexagonal compounds could be GR_{SO_4} changing into goethite. It is likely that as GR_{SO_4} becomes unstable, in the increasing oxic environment, the surface of the decomposing GR_{SO_4} particle might act as a template and source of Fe(III). They could be GR_{SO_4} particles changing topotactically, this is not evident, however, to determine based on the two sets of AFM images.

Figure 28. AFM deflection image of sample 1-10, scale bar 1 μm .



The CT-XRD trace of sample 2-08 exhibits increasing amounts of goethite (Fig. 29). On the AFM images of 2-08 (Fig. 30) there are mainly observed goethite particles.

Figure 29. CT-XRD trace of sample 2-08

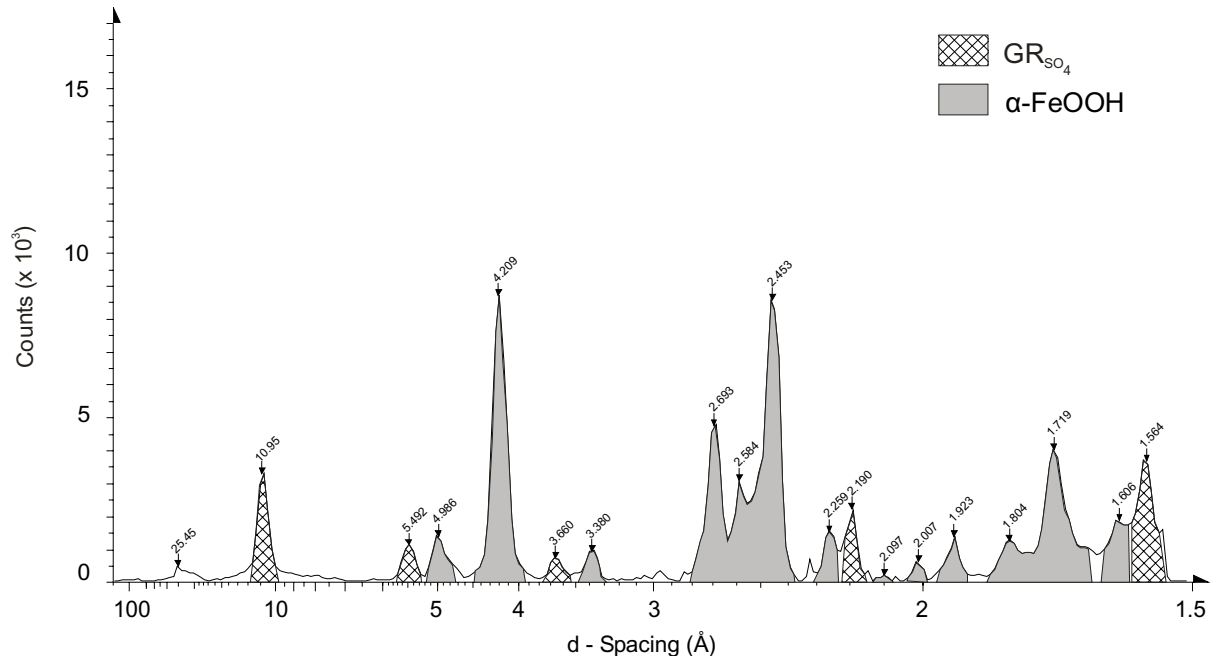
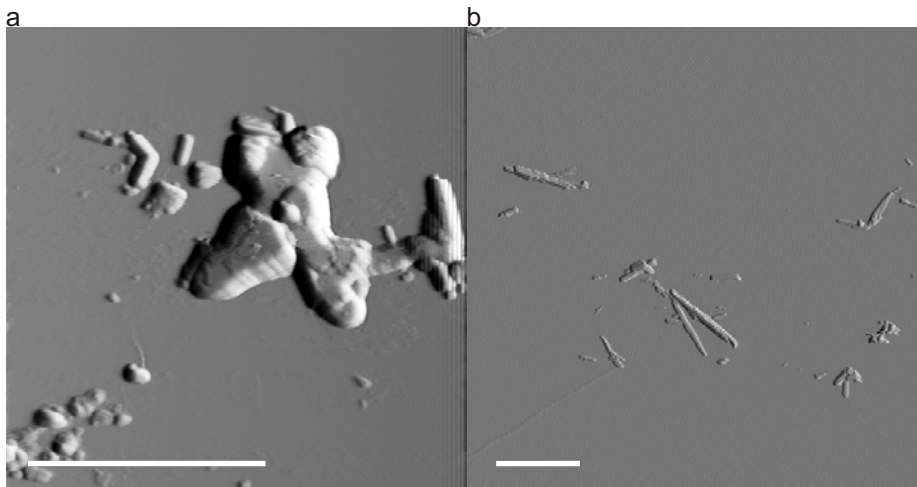


Figure 30. AFM deflection images of 2-08. Notice the goethite twin on (a). Scale bar 1 μm.



Samples 1-14 and 2-09, taken during the last stage of the experiments provide the CT-XRD traces (Figs. 31 and 32) proving goethite as the dominant phase only traces of GR_{SO₄} remain. On the last sample of experiment 2 (2-09), no patterns of GR_{SO₄} can be seen on the CT-XRD trace (Fig. 32).

Figure 31. CT-XRD trace of sample 1-14.

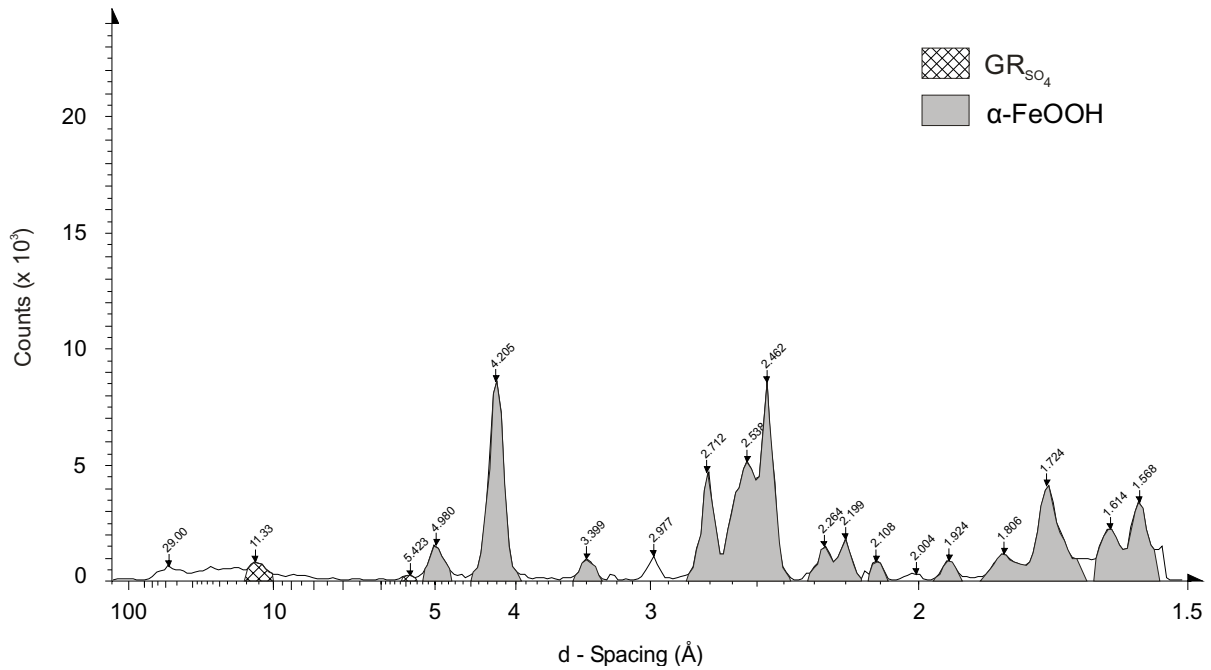
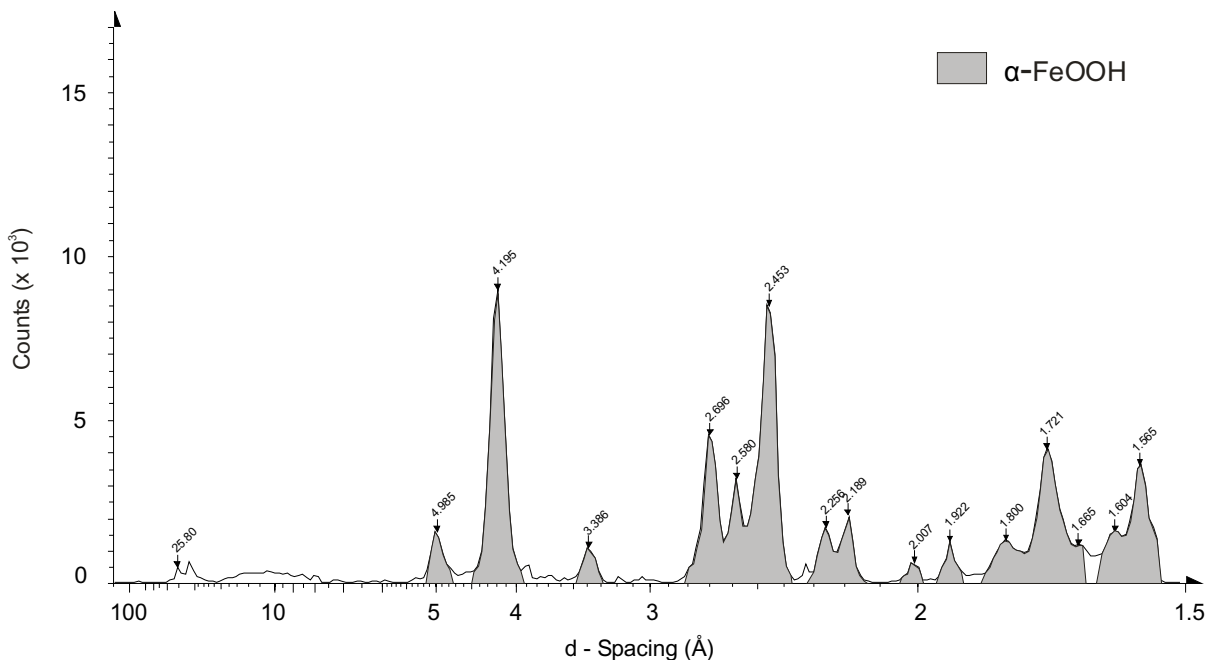


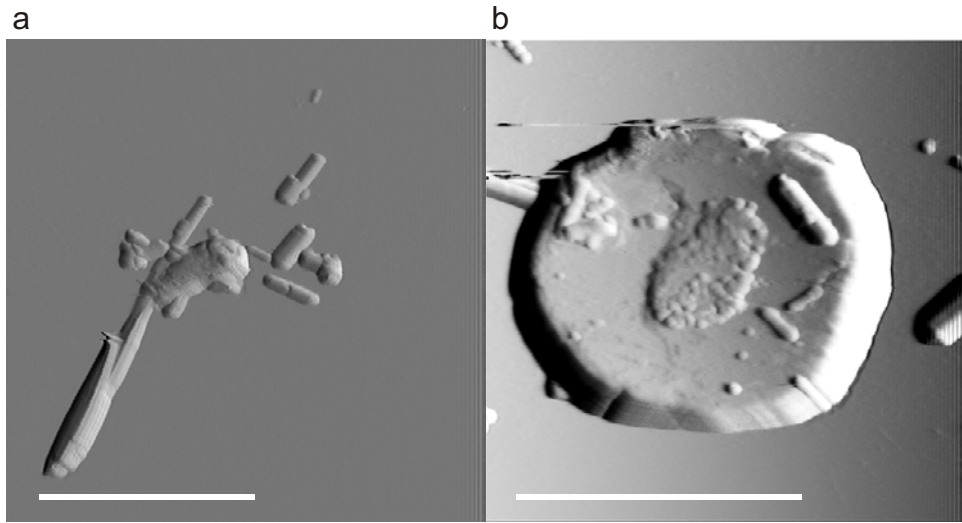
Figure 32. CT-XRD trace of sample 2-09



The AFM images of sample 2-09 show mainly particles with goethite morphology (Fig. 33a).

Because the last sample of experiment 2 (2-09) was not obtained at the very end of the experiment there is still some GR_{SO₄}-like material with rounded edges on the AFM images (Fig. 33b).

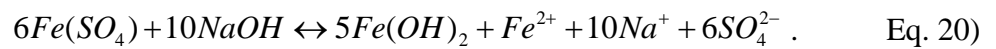
Figure 33. AFM deflection images of sample 2-09, scale bar 1 μm .



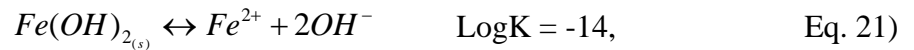
The d-spacing of Exp-1 was larger on most traces compared to those of Exp-2. This was especially observed on the basal planes. Because the only difference between the experiments were oxidation rate, it is not likely that this would result in structural differences. The CT-XRD of Exp-1 was the first series of CT-XRD to be produced and it is likely that the calibration and XRD fitting was not made with the appropriate accuracy.

7.1.2 Chemical changes

Based on data from AFM and CT-XRD, it is possible to interpret the changes in Eh and pH as a function of time and degree of oxidation, and to formulate a chemical and mineralogical progression. For plateau 1, pH in both experiments follow similar trends, starting at a pH of approximately 8.2 decreasing to 8.1 and then increasing slowly to approximately 8.4. Initially the phases present were $\text{FeSO}_4 \cdot 7\text{H}_2\text{O}$, NaOH and $\text{Fe}(\text{OH})_2$ but assuming complete dissolution of FeSO_4 and NaOH and using the initial ratio $\text{Fe}^{2+}/\text{OH}^- = 0.6$, the reaction before oxidation began can be written as:



This reaction represents the stable solution at $t < 0$. An equilibrium between $\text{Fe}(\text{OH})_2$ and solution is therefore present (Feitknecht and Schindler, 1963 as cited by Cornell and Schwertmann, 1996).



pH of the system is 8.2. From the XRD-traces, it is also seen that the most dominant phase is $\text{Fe}(\text{OH})_2$. When oxidation begins, there are two possible states where Fe(II) can be oxidised: 1) Fe^{2+} as a free ion or as an ion pair in the solution or 2) Fe(II) in $\text{Fe}(\text{OH})_{2(s)}$. The most energetically favoured oxidation of Fe(II) is believed to be in solid phase e.g. as $\text{Fe}(\text{OH})_{2(s)}$ (Stumm and Morgan, 1996). $\text{Fe}(\text{OH})_{2(s)}$ can tolerate as much as 10% Fe(III) in its structure before it starts to convert to GR_{SO_4} (Bernal et al., 1959). Based on AFM images (Fig. 14), the structural similarity of $\text{Fe}(\text{OH})_{2(s)}$ and GR_{SO_4} and that Fe(II) in solid phase is easiest oxidised, I interpret that the addition of oxygen lead to solid state transformation of $\text{Fe}(\text{OH})_{2(s)}$ to GR_{SO_4} .

As a result of oxygen addition to the reaction vessel, $\text{Fe}(\text{OH})_{2(s)}$ began to transform to GR_{SO_4} . Because the oxidation of $\text{Fe}(\text{OH})_{2(s)}$ to GR_{SO_4} produces Fe(III) and uses Fe(II), one might expect pH and Eh to change more than is seen during plateau 1, but measured Eh and pH only represent the solution composition, namely the proportions of the dissolved species, and not the oxidation state of the Fe tied up in the total mass of the system, which includes the precipitates. The $\text{Fe}(\text{OH})_{2(s)}$ acts as a buffer, providing e^- as the system is titrated with O_2 and soaking up oxidation effects. The

$\text{Fe}(\text{OH})_{2(s)}$ converts topotactically to the Fe(III)-bearing GR, thus both pH and Eh curves remain steady. The small decrease in pH during the first hour of the experiments is interpreted to be the result of the equilibrium between the partly oxidised $\text{Fe}(\text{OH})_2$ and the solution. Aqueous Fe^{3+} at pH around 8.2 is mainly in the form $\text{Fe}(\text{OH})_4^-$, whereas dissolved Fe^{2+} is present as $\text{Fe}^{2+}_{(aq)}$. H^+ is released when Fe^{3+} hydrolyses, explaining the slight pH decrease. Eh increases slightly as a result of a small increase of Fe^{3+} in solution. Some GR_{SO_4} is present at this stage but it is not yet the controlling phase.

I reproduced the experiments to quantify the phases (see chapter 7.2) and extracted samples of the supernatant to analyse the Fe(II) concentration and Fe(total). The Eh-pH diagram of the experiment resembling experiment 2 with plots of Fe^{2+} concentration is presented in Figure 34. The slope of the curves is not as expected from Figure 10, because the thickness of solution resulted in problems with the stirring.

Figure 34. Eh – pH plot of experiment similar to experiment 2 with $[\text{Fe}^{2+}]$ in supernatant plotted.

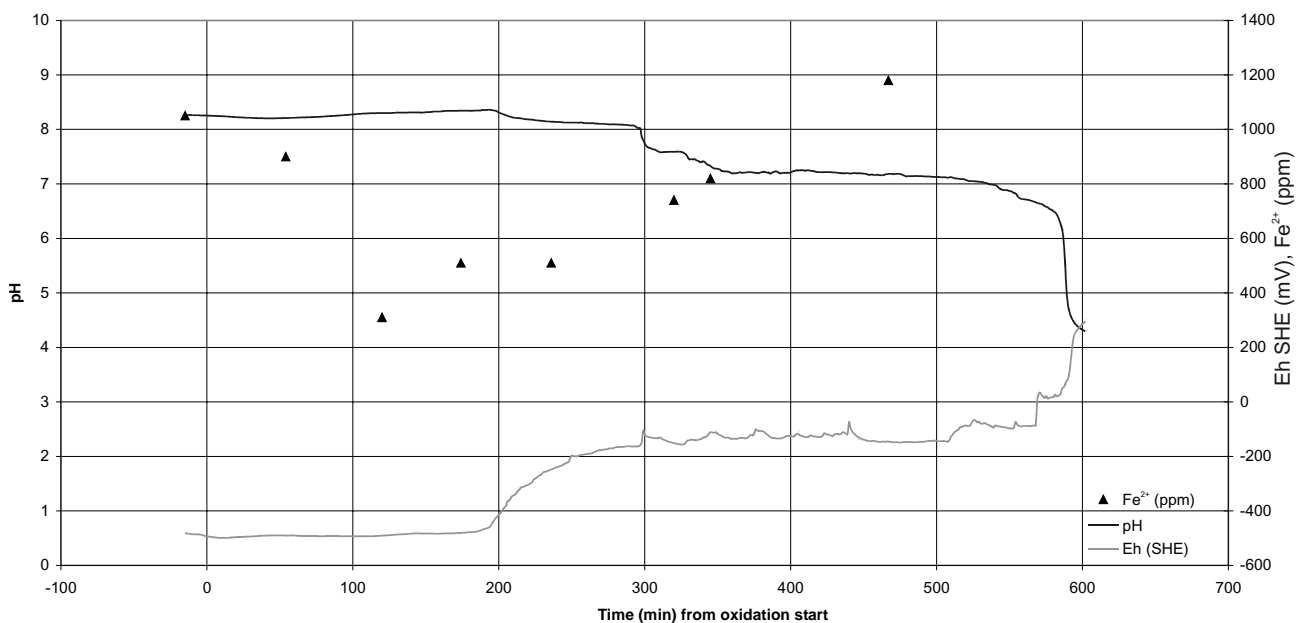
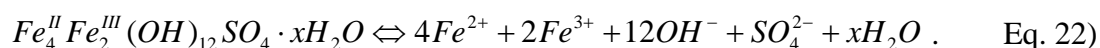


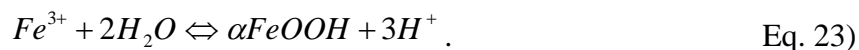
Figure 34 exhibit that Fe^{2+} is removed from solution during plateau 1. The rate of removal is low for the first third of plateau 1 but increases for the next third. The data points between 177 min. and 233 min. should be merged because in this time period there were problems ensuring a homogenous oxidation and mixing of the solution, resulting in regions of various degrees of oxidation.

Calculated from the Nernst equation, the $[\text{Fe}^{3+}]/[\text{Fe}^{2+}]$ ratio is approximately 4.8×10^{-10} . A decrease of $\text{Fe}^{2+}_{(\text{aq})}$ from 1200 ppm to 400 ppm would result in a $[\text{Fe}^{3+}]/[\text{Fe}^{2+}]$ ratio of 1.4×10^{-9} , assuming constant $[\text{Fe}^{3+}]$ and an increase of Eh by approximately 20 mV. Because there is Fe(III) present in the GR it is reasonable to assume that a small increase of $[\text{Fe}^{3+}]$ would take place and Eh would remain stable. The consumption of $\text{Fe}^{2+}_{(\text{aq})}$ results from the self-stabilising nature of GR_{SO_4} . As long as Fe(II) is available, it continues to form while maintaining the stoichiometric composition. At the point where pH begins a slow increase and Eh becomes constant, the system's mineralogical character begins to change. The CT-XRD traces and AFM images show more GR_{SO_4} present and equilibrium with GR controls the Fe(III)/Fe(II) ratio in solution, thus holding Eh stable. The concentration of Fe^{2+} decreases as a result of oxidation and more of the Fe^{3+} species become incorporated in the GR_{SO_4} structure, and all of this results in a pH increase. When Fe^{2+} and Fe^{3+} are removed from solution their hydrolysed species releases OH^- . During plateau 1, the solution became more and more thick with precipitate, as SO_4^{2-} , Fe^{2+} and Fe^{3+} that were present as ionic species earlier in the oxidation stage become incorporated in GR_{SO_4} . Just before Step 1 and the sudden decrease in pH and increase in Eh, samples showed only trace amounts of $\text{Fe}(\text{OH})_2$ left in the precipitate (Figs. 15 and 16) so transformation of $\text{Fe}(\text{OH})_2$ to GR_{SO_4} was essentially complete at the top point of the pH curve.

The abrupt change in pH and Eh at step 1 indicates that the chemical composition of the solution changes dramatically. Unlike GR_{Cl} , which can contain varying Fe(II)/Fe(III) ratios in its structure during progressive oxidation (Refait et al., 1998a), the GR_{SO_4} structure remains stoichiometric until the point where the stock of Fe^{2+} in solution is used up and, at that stage, the GR must decompose or transform. It is proposed that the maximum concentration of GR_{SO_4} occurs at the inflection point of the Eh curve. The rise in Eh results in a higher Fe(III)/Fe(II) ratio, which probably comes from the dissolution of GR_{SO_4} , meaning the relative concentration of GR_{SO_4} must be decreasing. Higher solution concentrations of Fe^{3+} remain until formation of a new phase. The transformation of GR_{SO_4} during step 1 releases Fe(II), Fe(III), OH^- and SO_4^{2-} to the solution (Eq. 22), and result in Eh increase and pH decrease:



The change in Eh comes from an increased proportion of Fe³⁺ in the solution. Because Fe³⁺ hydrolyses very easily at this pH, the reaction consumes OH⁻ and pH decreases. Further protons are generated as goethite, α -FeOOH forms:



The release of Fe²⁺ to solution while Eh increases, indicates a simultaneous release of Fe³⁺ to solution. I interpret this as evidence that the transformation of GR_{SO₄} to goethite is a dissolution/precipitation reaction. If it was a topotactic transformation, Fe³⁺ would not be released to solution because it would remain bound as solid phase Fe(III). Fe²⁺ becomes released back to solution because hydroxide is not in excess to precipitate the extra Fe²⁺ as Fe(OH)_{2(s)}.

At the change from step 1 to plateau 2 Eh drops from around -80 mV to -200 mV as can be seen from Exp-1 (Fig. 9) at approximately 475 minutes. I interpret this drop as the result from a larger formation rate of goethite than oxidation of GR_{SO₄} or there could be a delay in precipitation because a formation nucleus is lacking. The dropback effect is not seen in Exp-2 (Fig. 10), probably a result of the increased oxidation rate.

On the Eh and pH vs. time trace for Exp-2, the pH curve is very even during plateau 2, whereas Eh oscillates (Fig. 10). The oscillations are apparent, however, on both the Eh and pH curves of Exp-1. Why these oscillations occur is not clear. The controlling phase changes gradually from GR_{SO₄} (Eq. 23) to goethite (Eq. 24) because of the oxidation during plateau 2. When there is gradually more and more goethite present the equilibrium change, this can be seen on plateau 2. The plateau changes slowly and changes into step 2, most obvious in experiment 2.

The evolution from plateau 2 to step 2 is not as abrupt as plateau 1 to step 1. The solution equilibrium changes gradually because there is almost no more GR_{SO₄} present in the solution and finally the GR_{SO₄} does not act as a buffer anymore. A small amount of GR_{SO₄} is evident from the CT-XRD trace of sample 2-08 obtained right at the beginning of step 2 (Fig. 29). The solution comes into equilibrium with its final phase and the pH and Eh curves flatten into plateau 3, at this point there is no more GR_{SO₄} left in the solution. Experiment 1 exhibits only a change in Eh and not

in pH and the final Eh value is the same as the one obtained in experiment 2. The reason for this is not clear, but the slower oxidation rate of experiment 1 could be part of an explanation. Eh and pH reflect a new equilibrium for the solution and there is nothing left to oxidise.

7.1.3 Atomic resolution of GR_{SO_4}

Although getting atomic resolution on particles is difficult and on natural, non-cleaved samples nearly impossible, some of the GR_{SO_4} crystals were so smooth and perfect that it was tempting to try. There is no vibration isolation system in the glove box but with the use of silicon pads and turning off the O_2 consuming fan boxes, it was possible to obtain atomic scale images of a GR_{SO_4} surface (Figures 35 and 36).

Figure 35. AFM deflection images of GR_{SO_4} . a) Micrometer scale GR_{SO_4} particles; scale bar 1 μm ; white square is the area enlarged in the next image. b) Image is 13 x 13 nm; lower right insert is a 2 x 2 nm zoom. c) Fourier transform. The white circles indicate the most intense periods. Period 1 represents a row periodicity with spacing of 2.83 \AA , 2, spacing of 2.84 \AA , 3, of 2.97 \AA , 4, of 4.91 \AA and 5, of 5.05 \AA .

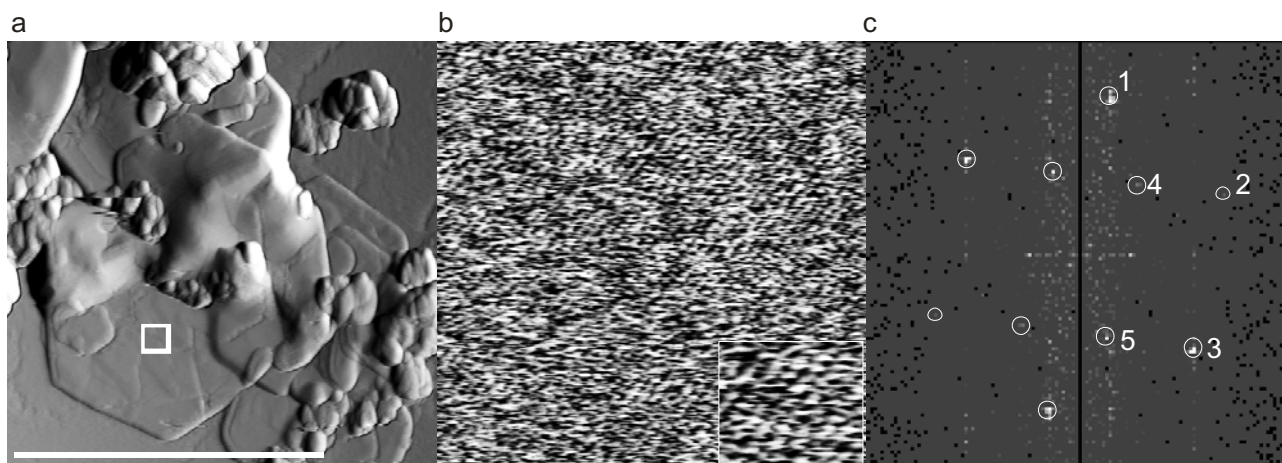


Figure 36. AFM deflection image. a) 5 x 5 nm image of Figure 35a. b) Fourier transformation image of a). White circles indicate the most intense periodicity. Period 1 represents a row spacing of 2.82 Å, 2, spacing of 2.89 Å and 3, of 2.81 Å.

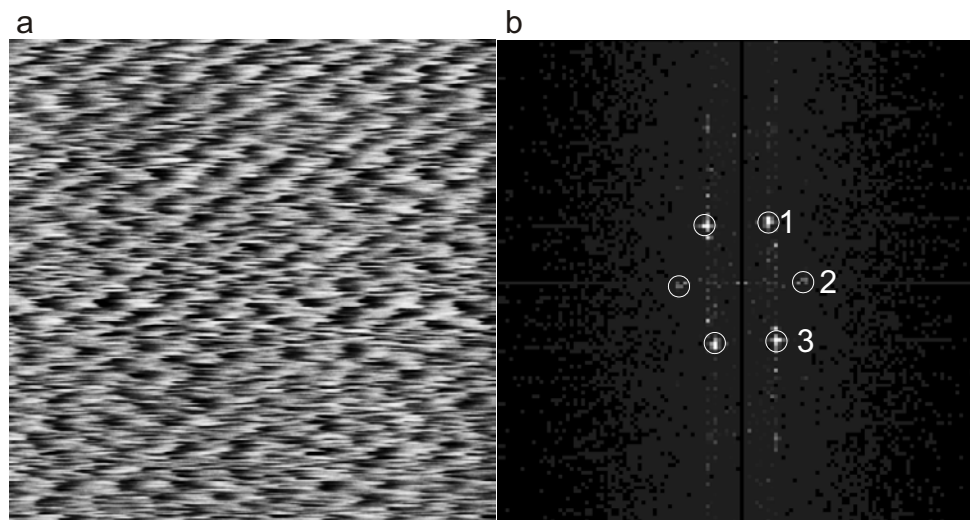
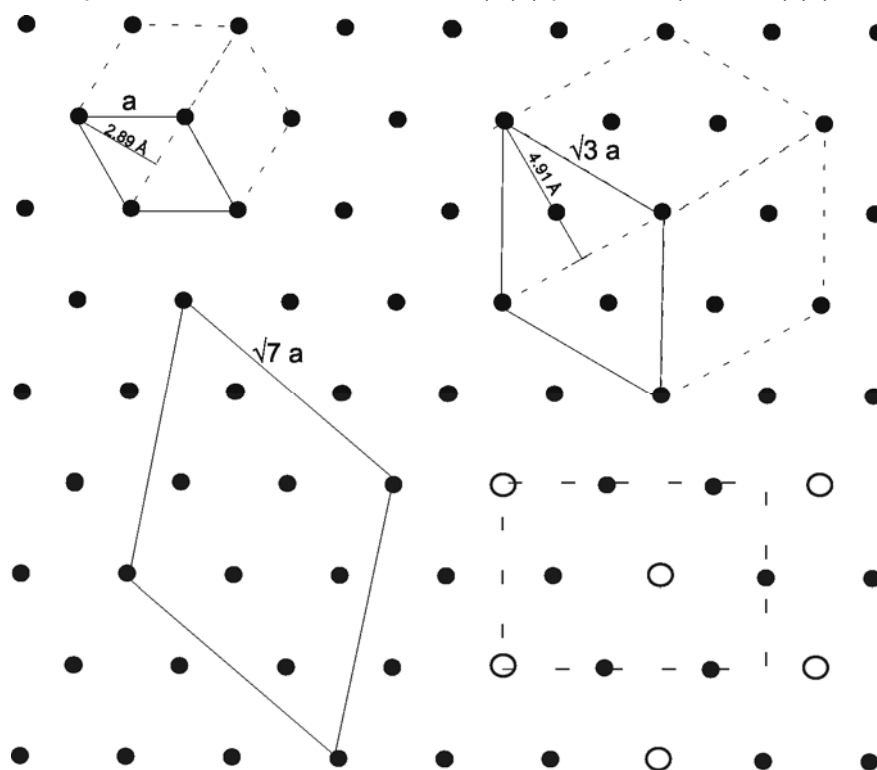


Figure 35b and 36a show a slightly distorted hexagonal pattern. Fourier analysis confirms the hexagonal pattern and demonstrates a row spacing of about 2.9 Å. Fourier analysis uses a mathematical function to determine periodicity based on frequency and amplitudes of a wave. When applying the analysis to Figure 35b and 36a it results in a periodicity image (Figs. 35c and 36b). The periods are represented twice because of the extension of the waves, and also because it is easier to visualise the symmetry of the repetition pattern. GR_{SO_4} is hexagonal so the a-axes are arranged in a triangular pattern (Fig. 37). The 2.9 Å distance is the height in this triangle, the distance between rows of atoms. The distance measured on several images ranged between 2.67 and 3.02 Å with a mean of 2.87 Å ($n=12$), equal to an uncertainty of $\pm 7\%$. Using the mean height of the triangle equals a triangle side length of 3.3 ± 0.12 Å. This is very close (well within 5% uncertainty) of published a-axis parameters for GR_{SO_4} of 3.18 Å.

Other periodicities observed are at 4.91 Å and 5.05 Å. These row spacings would give a length of 5.7 Å for a triangle side. These distances correspond to a superstructure of $\sqrt{3} \times \sqrt{3}$ relative to the unit cell distances in the hexagonal pattern (Fig. 37).

Figure 37. Trigonometric relationship between rows of atoms in a hexagonal system. The broken square indicates a superstructure area with ordered Fe(III) (open circles) and Fe(II) (black spots).



AFM interacts only with the topmost atom layer of the examined sample, but because of interactions between the topmost atoms and the interlayer, there are four possible explanations for the $\sqrt{3} \times \sqrt{3}$ superstructure. It could result from: 1) ordering of the interlayer anions; 2) ordering of interlayer water molecules; 3) distribution of Fe(II) and Fe(III) atoms, or 4) surface relaxation because of hydroxylation. The first explanation is also proposed by Simon et al. (2003) to explain their XRD observation of a $\sqrt{3} \times \sqrt{3}$ superstructure in GR_{SO_4} . The water molecules are smaller than the anions and they may arrange around the anions thus adding to the superstructure in some way. The size difference between Fe(II) and Fe(III) is approximately 0.13 \AA , so if the atoms are arranged in an ordered pattern as suggested by Figure 37, it is possible to explain the superstructure. Assuming a Fe(II)/Fe(III) ratio of 2:1, this explanation seems reasonable. Furthermore because the anions are bound to the Fe(III) it is possible that the combination of the two effects enhances each other enough to produce a superstructure. The fourth explanation, surface relaxation, might add to the superstructure because of surface charge difference resulting from the Fe(II)/Fe(III) distribution.

7.2 *Quantification*

I attempted to quantify the phase distribution during oxidation because this would help to describe the chemical and structural evolution. In order to do that, I reproduced Exp-2 and doped the dry samples before XRD analysis with goethite to determine peak intensity relationships. The efforts to quantify relative mineral proportions were not conclusive, however. The results showed no consistent patterns and were not consistent with amount of material added. The reason is almost certainly that the mixture of sample and standard goethite was not homogeneous. The ultrasonic treatment probably arranged the particles in an orderly way in the tubes. The particles were therefore not randomly ordered and the CT-XRD did not present the real distribution between added goethite and sample. These results will not be discussed further, but it is my intention to conduct new experiments to quantify the evolution of phases in transformation of $\text{Fe}(\text{OH})_2$ through GR and to the end-product. We shall test the use of wider capillary tubes to avoid ordered size distribution in the tubes and also drop the ultra sonic treatment in next experiments.

7.3 Structural study

In the literature, three models have been presented for the structure of GR_{SO_4} . They are listed in Table 15.

Table 15. Structural models proposed for GR_{SO_4} .

Reference	Spacegroup	a-axis	c-axis	XRD type
Bernal et al. (1959)	$\text{P}\bar{3}1\text{m}$	3.174 Å	10.94 Å	?
Hansen et al. (1994)	?	3.18 Å	32.92 Å	Glycerol treated, XRD
Simon et al. (2003)	$\text{P}\bar{3}1\text{m}$	5.524 Å	11.011 Å	CT-XRD

All have been determined on structural data that has either: 1) been treated with a protective substance that induces preferred orientation (Hansen et al., 1994) or 2) not all XRD peak intensities have been used (Bernal et al, 1959; and Simon et al., 2003). As a consequence of the discrepancy between X-ray data found during the literature review of GR_{SO_4} and the X-ray results from the morphology study new experiments were carried out. The similarity of my X-ray data and those presented by Drits et al. (1987) (Fig. 22) prompted a series of experiments where three types of alkali metal-hydroxides to precipitate GR_{SO_4} : Lithium hydroxide monohydrate, potassium hydroxide and sodium hydroxide were used. Concentrations of cation and hydroxide, as well as all other experimental conditions were identical in each case. Plots of Eh and pH as a function of time for the Li^+ , K^+ and Na^+ experiments are presented in Figures 38, 39 and 40 respectively. No chemical considerations of these experiments will be presented in this paper.

Figure 38. Eh – pH diagram of LiOH precipitated GR_{SO_4} . Arrow indicates sample point.

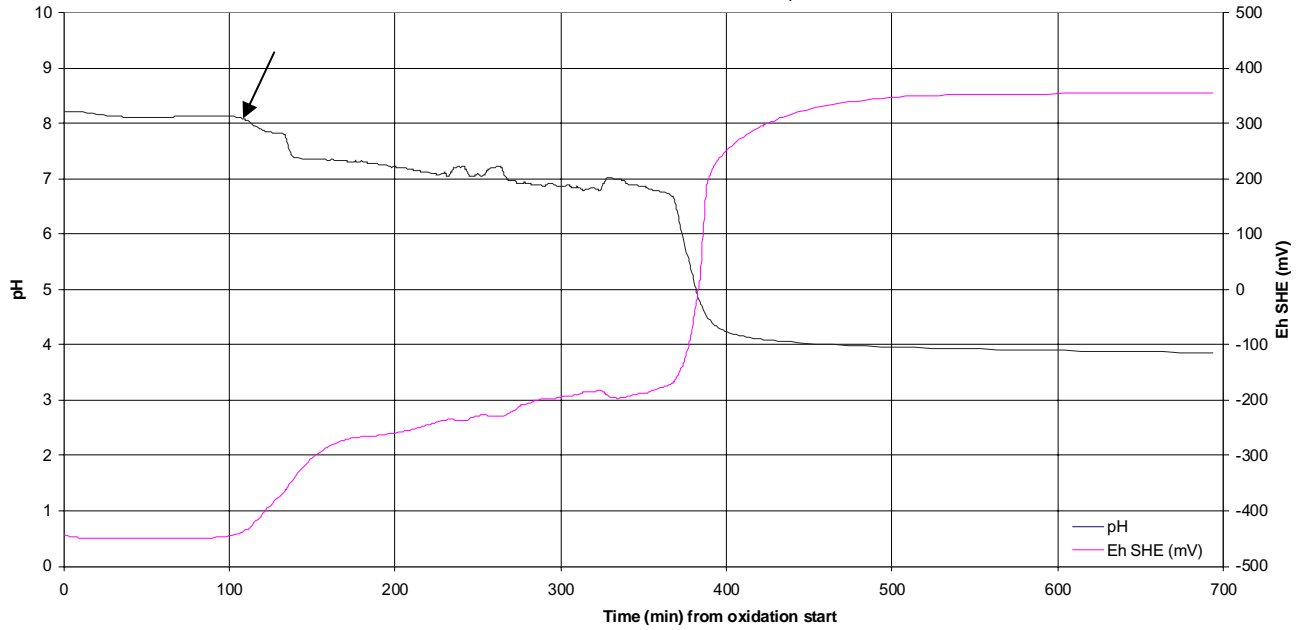


Figure 39. Eh – pH diagram of KOH precipitated GR_{SO_4} . Arrow indicates sample point.

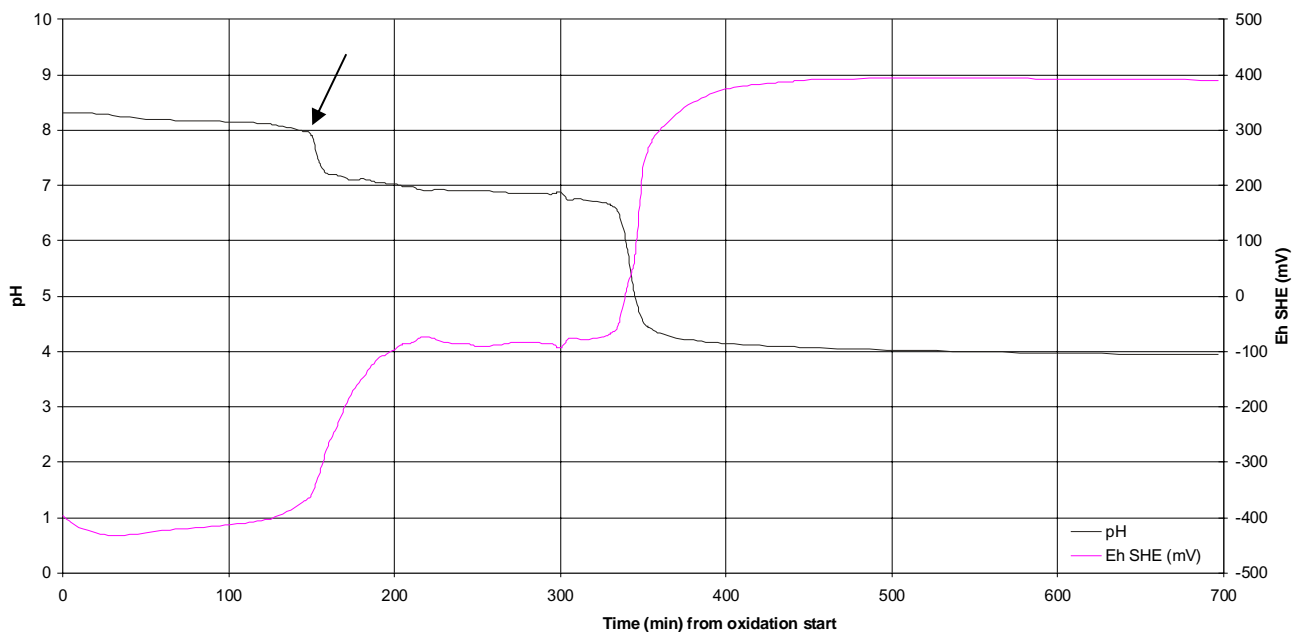
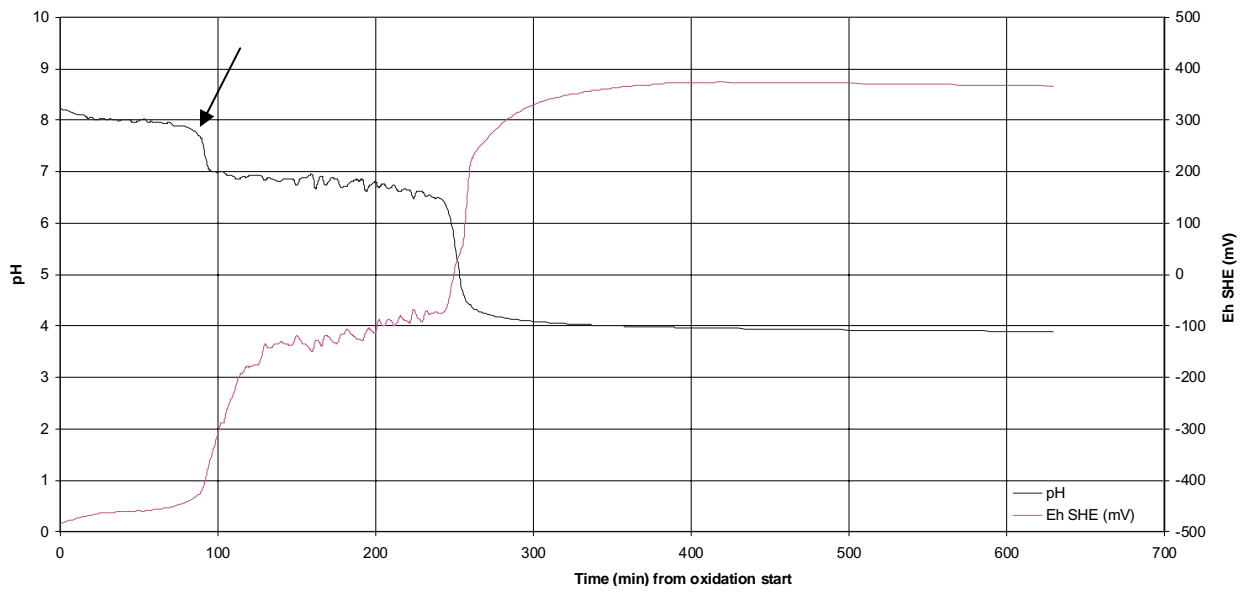


Figure 40. Eh – pH diagram of NaOH precipitated GR_{SO_4} . Arrow indicates sample point.



A comparison of the CT-XRD traces taken from material sampled at the point of maximum GR_{SO_4} mass % are presented in Figure 41 and in Table 16.

Figure 41. Comparison of CT-XRD traces and diffractograms of $\text{Li-GR}_{\text{SO}_4}$, $\text{K-GR}_{\text{SO}_4}$ and $\text{Na-GR}_{\text{SO}_4}$. Ordinate is d-spacing in Å.

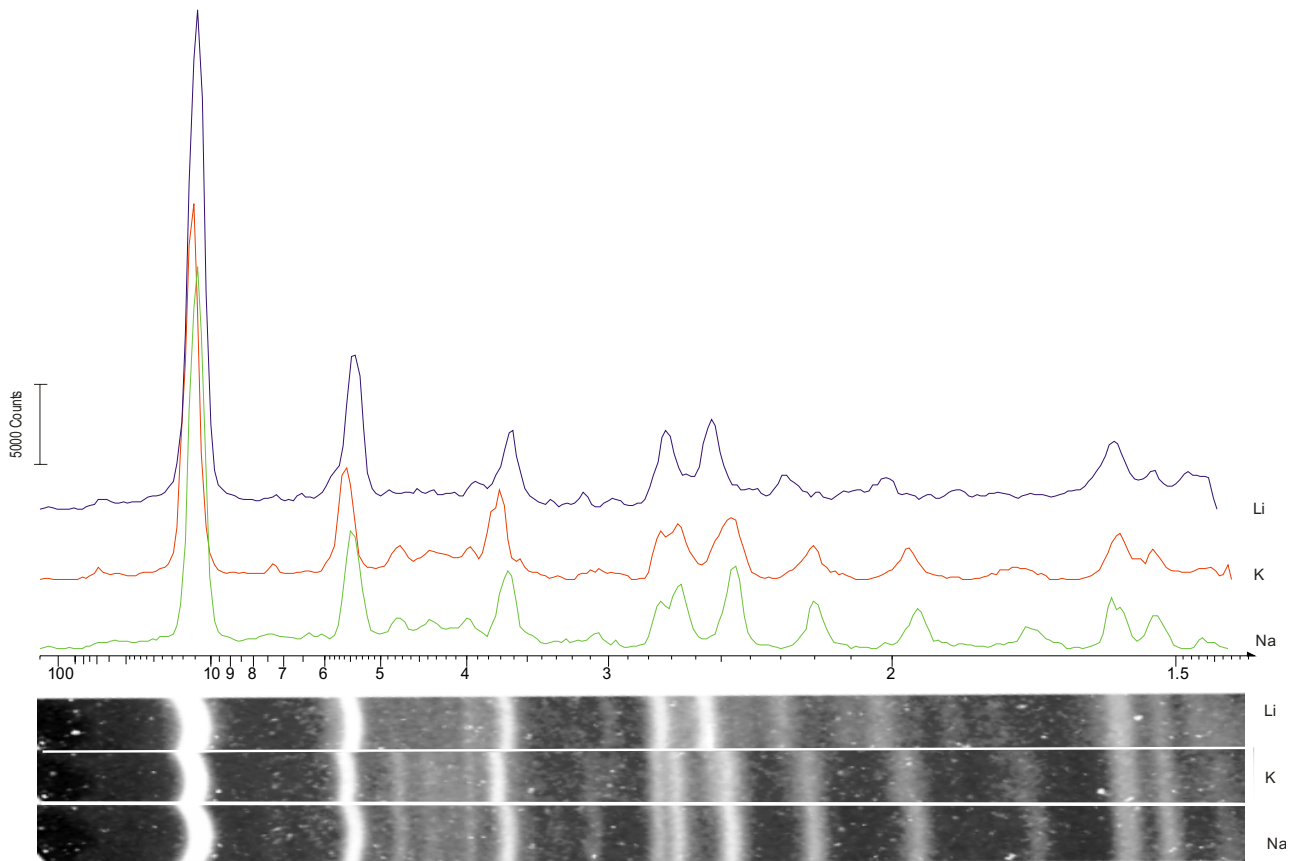


Table 16. Comparison of the d-spacings of NaOH precipitated GR_{SO₄} (Na-GR_{SO₄}), KOH precipitated (K-GR_{SO₄}) and LiOH·H₂O (Li-GR_{SO₄}). *Italics* indicate uncertain (very weak) peaks.

Na-GR _{SO₄}		K-GR _{SO₄}		Li-GR _{SO₄}	
d-spacing (Å)	Intensity	d-spacing (Å)	Intensity	d-spacing (Å)	Intensity
10.86	100.0	11.15	100.0	10.86	100.0
7.486	3.6	Not detected		Not detected	
5.455	30.9	5.579	29.7	5.436	30.8
4.756	7.9	4.750	8.8	4.519	4.0
4.342	7.5	4.351	7.8		
3.971	7.8	3.974	8.7	3.923	5.4
3.636	20.3	3.699	23.6	3.624	15.8
3.061	4.0	3.055	2.8	2.974	2.1
2.746	12.2	2.744	12.9	2.724	15.7
2.664	16.6	2.663	14.8		
2.452	21.4	2.464	16.4	2.537	17.9
2.198	12.2	2.203	9.0	2.295	6.8
				2.077	3.8
1.938	10.5	1.962	8.2	2.017	6.3
		<i>1.854</i>	<i>1.5</i>	1.854	3.8
<i>1.773</i>	<i>1.3</i>			1.780	3.5
1.726	5.5	1.747	3.2	<i>1.720</i>	3.0
1.591	13.1				
1.575	10.7	1.578	12.2	1.587	13.4
1.527	8.6	1.530	8.0	1.529	7.7
				1.487	7.4
1.466	2.7	Not detected		1.463	7.1

The CT-XRD traces and diffraction patterns exhibit similarities but also differences. Comparison of the diffraction pattern and trace of Na-GR_{SO₄} with that of K-GR_{SO₄} shows that some of the peaks are displaced. The first difference to be observed is the larger d-spacing of the primary basal-plane peak on the K-GR_{SO₄} trace. The peak is displaced by +0.29 Å. The displacement is also observed for the other two basal plane peaks by +0.124 Å and +0.063 Å. The larger basal plane distance of K-GR_{SO₄} is roughly what could be expected because of size variation in ionic radii of Na⁺ (1.02 Å) and K⁺ (1.38 Å). The basal plane distance seems to be identical whether it is Na-GR_{SO₄} or Li-GR_{SO₄}. Because the ionic radii of Li⁺ is 0.74 Å it is possible that the interaction between adjacent

sulphate anions could result in a minimum spacing of the GR_{SO₄} interlayer and thus explain the similar d-spacings of Na-GR_{SO₄} and Li-GR_{SO₄}. The larger c-axis distance of K-GR_{SO₄} compared to Na-GR_{SO₄} can explain why Lewis (1997) observed a {001} distance of 11.19 Å for precipitated GR_{SO₄}. He did not state, however, whether, he used NaOH or KOH to titrate, but because some of the presented XRD exhibits peaks are identified as KCl it is reasonable to assume that he used KOH. Vinš et al. (1987) used ammonia as titration medium and presented XRD data that is similar to K-GR_{SO₄} but different from results found of Na-GR_{SO₄}. Variations in d-spacings of GR_{SO₄} precipitated or analysed under various conditions are presented in Table 17.

Table 17. Comparison of XRD parameters of various GR_{SO₄} precipitates treated and precipitated under various conditions.

?		Glycerol		Na		K		NH ₄		This work				
Bernal et al. (1959)		Hansen et al. (1994)		Simon et al. (2003) ¹		Lewis (1997)		Vinš et al. (1987)		K		Li		
hkl ²	d _{hkl} (Å)	I ³	hkl ⁴	d _{hkl} (Å)	d _{hkl} (Å)	I/I ₁ ⁵	d _{hkl} (Å)	hkl	d _{hkl} (Å)	I/I ₁ ⁵	d (Å)	I/I ₁ ⁵	d (Å)	I/I ₁ ⁵
0001	10.92	vs	003	11.03	10.89	100	11.19	001	11.2	80	11.15	100.0	10.86	100.0
0002	5.48	s	006	5.49	5.442	40.9	5.60	002	5.58	40	5.579	29.7	5.436	30.8
	-			-	4.728	11.1					4.750	8.8	4.519	4.0
	-			-	4.326	7.0					4.351	7.8		
	-			-	3.953	4.1					3.974	8.7	3.923	5.4
0003	3.65	s	009	3.657	3.610	33.3	3.73	003	3.77	100	3.699	23.6	3.624	15.8
	-			-	3.084	9.4					3.055	2.8	2.974	2.1
0004, 10 $\bar{1}$ 0	2.747	m	101	2.751	2.759	31.0		100	2.76	20	2.744	12.9	2.724	15.7
10 $\bar{1}$ 1	2.660	ms	013	2.668	2.640	36.3		101	2.69	20	2.663	14.8		
10 $\bar{1}$ 2	2.459	ms		-	2.455	32.7		102	2.48	40	2.464	16.4	2.537	17.9
0005, 10 $\bar{1}$ 3	2.195	ms	019	2.200	2.201	21.1		103	2.22	5	2.203	9.0	2.295	6.8
10 $\bar{1}$ 4	1.938	ms	10 $\bar{1}$ 2	1.958	1.945	15.5		104	1.94	5	1.962	8.2	2.077	3.8
	-		00 $\bar{1}$ 8	1.829	1.793	5.0		105	1.74	5	1.747	3.2	2.017	6.3
											1.780		1.854	3.8
10 $\bar{1}$ 5	1.712	w	10 $\bar{1}$ 5	1.716	1.719	9.4		110	1.59	10	1.578	12.2	1.587	13.4
11 $\bar{2}$ 0	1.587	w	110	1.589	1.592	23.4		111	1.58	10				
11 $\bar{2}$ 1	1.570	w	113	1.573	1.575	25.7		112	1.53	5	1.530	8.0	1.529	7.7
11 $\bar{2}$ 2	1.525	w	116	1.525	1.530	21.9		113	1.46	5			1.487	7.4
	-		119	1.453	1.465	7.6							1.463	7.1

¹ d-spacing and intensities are determined from Figure 2 of article by Simon et al. (2003).

² Indices based on a hexagonal cell; a=3.174 Å and c=10.94 Å.

³ v:very; s:strong; m:medium; w:weak.

⁴ Indices based on a hexagonal cell; a=3.18 Å and c=32.92 Å.

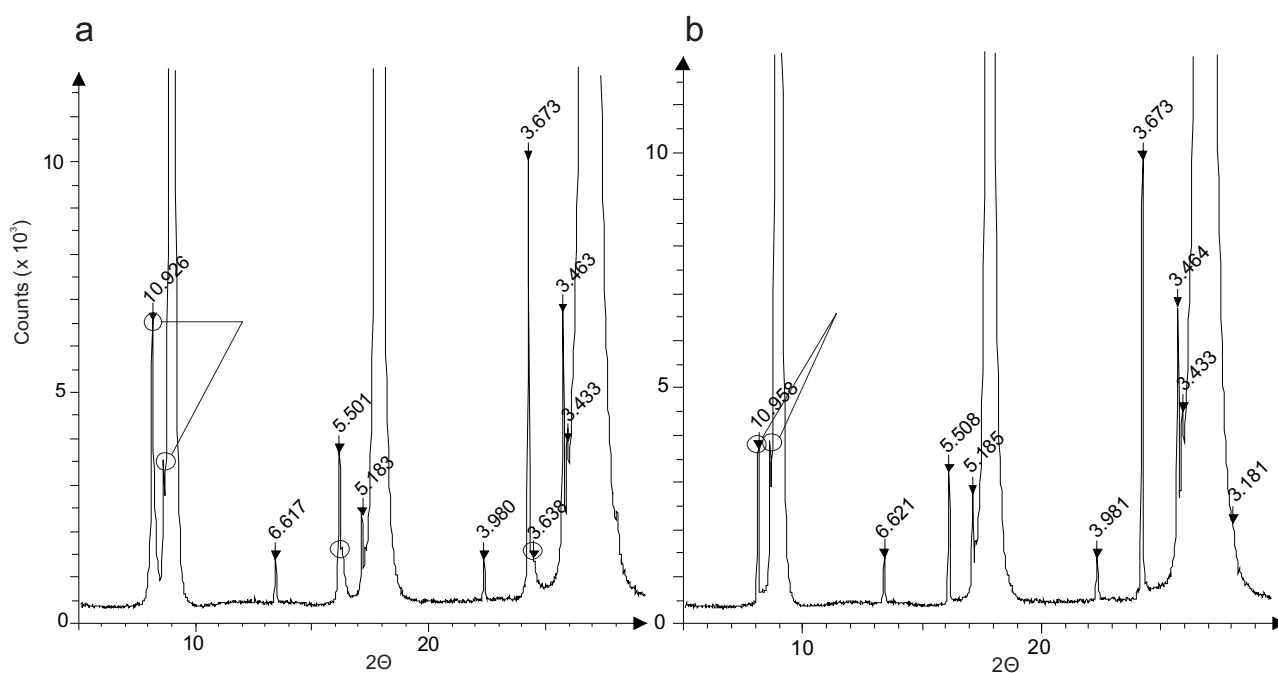
⁵ Intensities relative in %.

These peak differences and similarities exhibit a main structural relationship but with some lattice variations that can only be related to the participation in the structure of the monovalent cation present in solution. It cannot be related to other phases present because most of the peaks that have been defined as GR_{SO_4} -related are influenced by the specific cation. It is beyond the scope of the present project to propose new structural models of either of the GR_{SO_4} compound. It is, however, important to establish these models to correct the thermodynamic properties of GR_{SO_4} . This work will be extended later.

7.4 Natural occurrence of Green Rust

While preparing samples for AFM, I observed an increased stability of GR_{SO_4} when sorbed to muscovite. It oxidised more slowly when adsorbed to the substrate than when it was suspended in solution or as a dry powder. Chemically, this makes sense because the surface of freshly cleaved muscovite resembles the brucite-like structure of GR and the surface stabilises the structure of GR_{SO_4} as a result of the similar structure. It was possible to examine muscovite with adsorbed GR_{SO_4} using XRD, and to identify the basal planes of adsorbed GR_{SO_4} between the muscovite peaks (Fig. 42a). There is no question that the phase is GR because the peaks fit precisely where they should. As a final proof, the sample was exposed to air for 3 weeks and the GR peak relative intensities changed (compare Fig. 42a and b). It was not possible to observe new Fe^{3+} -phases on the oxidised sample.

Figure 42. XRD trace of muscovite with a droplet of a GR_{SO_4} solution.



Having discovered a way to analyse small quantities of GR and keep them stable during sampling and transport, it promised the opportunity to explore for natural occurrence of GR in groundwater. The first sample tested was from a droplet of groundwater from an artesian well located just north of Rønne airport, Bornholm (Fig. 43). XRD showed weak but clear peaks at 7.55 and 3.98 Å (Fig. 44a). These intensities cannot be correlated with muscovite and they fit expected d-spacings for

GR_{CO₃}. The two peaks were also observed on an XRD trace of a sample of groundwater placed on a piece of glass (Fig. 44b). The intensities correlate well with that of GR_{CO₃}. XRD of a similar sample obtained from a water droplet originating from fractures in the granitic rocks of the tunnel at SKB's hard rock laboratory exhibited similar features (Fig. 44c).

Figure 43. Map of sampling location on Bornholm. a) overview map, square enlarged on b. Scale bar 1 km. b) detail map, black spot indicates sampling location of the artesian well, scale bar 200 m.

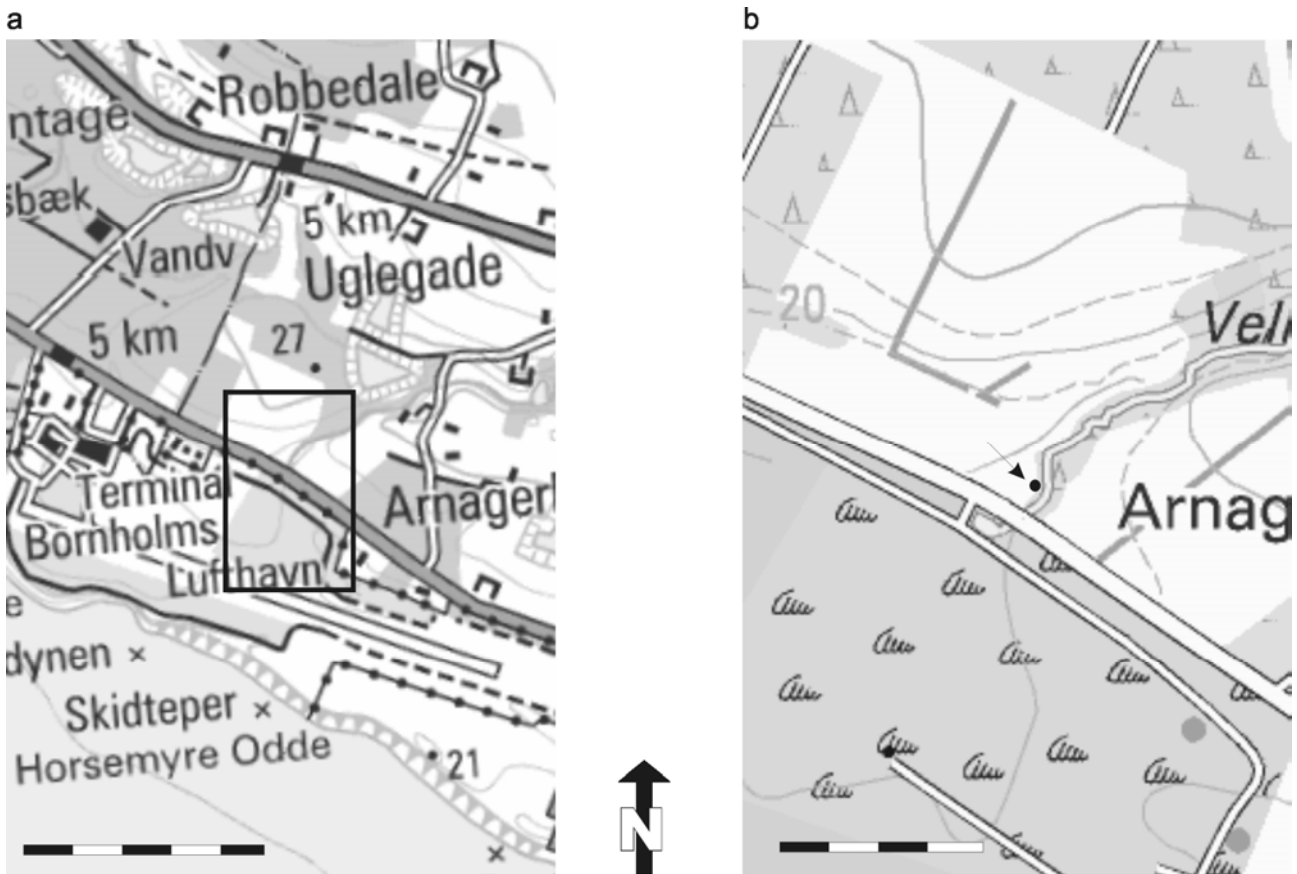
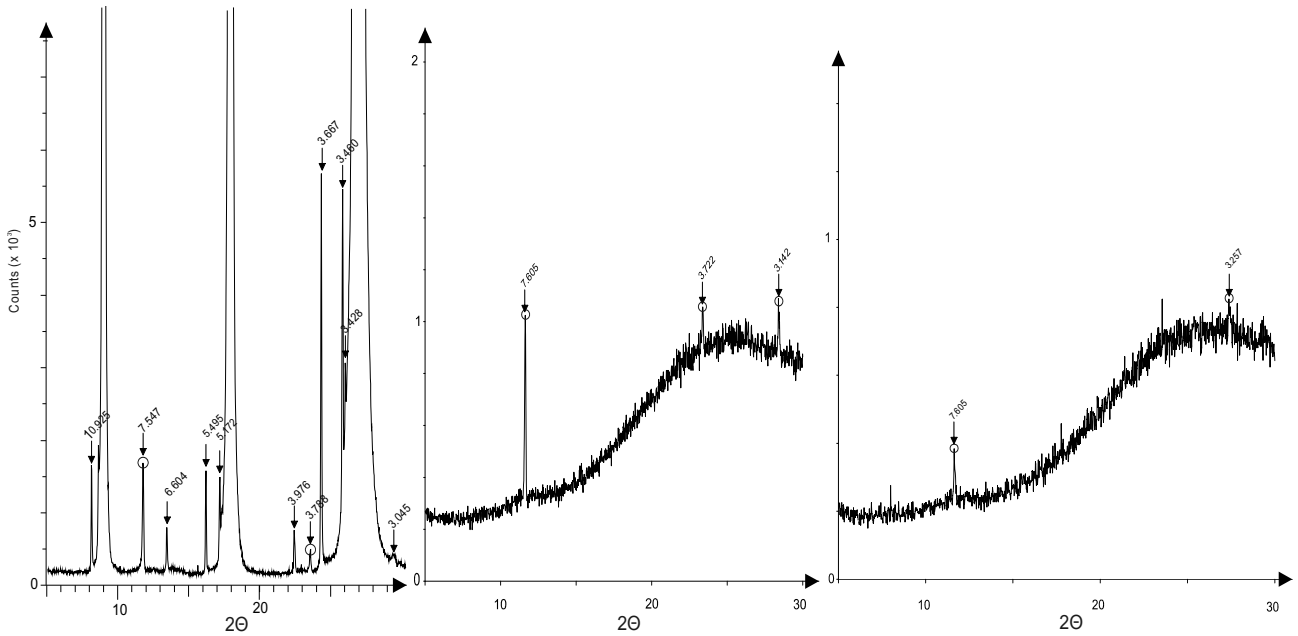
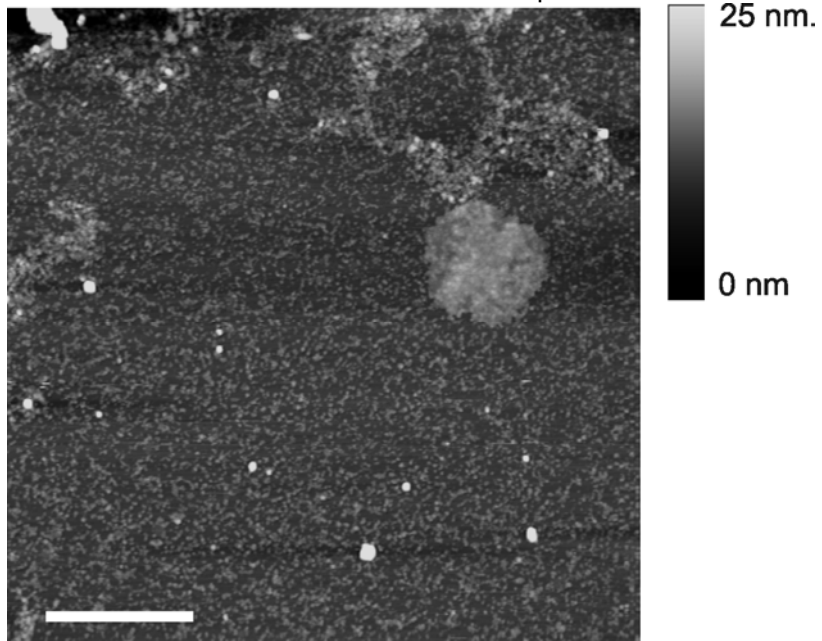


Figure 44. XRD traces of samples obtained at Rønne, Bornholm (a and b) and at the tunnel of Äspö (c). a) Rønne, Bornholm sample on muscovite substrate, b) Rønne, Bornholm sample on glass substrate and c) Äspö sample on glass substrate.



If GR is present in groundwater, it demonstrates its great mobility. If it precipitated during sampling, the process is a good analogue for the behaviour of groundwater rich in Fe^{2+} oxidising on silicates. It is plausible to conclude that GR could precipitate naturally and exist under natural conditions. The results are still preliminary but show promise to solve the discussion whether GR exists in nature or not. Therefore, one of the most important questions is if GR had already formed in the groundwater or if it precipitated on the mica after exposure. The groundwater sample was placed on the muscovite substrate for approximately 30 sec. Excess water was then sucked away by piece of tissue before it was stored dry at approximately 4°C to halt oxidation. An AFM image of a sample from Rønne, Bornholm shows a hexagonal particle (Fig. 45) and it covers a lot of nm size particles suggesting that it is lying on top of something that has adsorbed from the groundwater. Based on these observations it is reasonable to say that the GR was already present in the groundwater sample prior to sampling.

Figure 45. AFM height image of muscovite sample with the residue of a groundwater sample from Rønne, Bornholm. Scale bar is 1 μm .



8 Conclusions

My literature review showed that many GR studies are incomplete or wrong. Some of the best studies were handicapped by the method used to avoid oxidation.

Using AFM and CT-XRD, I showed that when a slightly basic solution becomes oversaturated with $\text{Fe}^{2+}_{(\text{aq})}$, $\text{Fe}(\text{OH})_{2(\text{s})}$ precipitates. Furthermore, during oxidation, $\text{Fe}(\text{OH})_{2(\text{s})}$ transforms topotactically to GR_{SO_4} . Further oxidation of GR_{SO_4} did not provide concrete evidence of the type of transformation to goethite.

Enhanced details of the CT-XRD traces suggest that the monovalent Na is also part of the GR_{SO_4} structure and experiments with other monovalent cations, namely Li and K, showed that they are also part of the GR_{SO_4} structure. This makes it crucial to recalculate the thermodynamic equilibrium constants for GR_{SO_4} .

Atomic scale images of GR_{SO_4} surfaces showed the expected parameters for the surface unit cell. The images also showed the presence of a $\sqrt{3} \times \sqrt{3}$ superstructure, which matches that expected for ordered Fe(III) in the layers and the observed ratio of Fe(II) to Fe(III).

It was possible to use XRD to identify extremely small amounts of GR_{SO_4} sorbed to muscovite. I used this technique to examine samples from two localities having Fe(II)-rich groundwater. GR could be observed with XRD. AFM imaging confirmed these findings.

9 Future work

The results of this thesis point to several directions of future work. The first is to establish the structural model of GR_{SO_4} along with correction of the thermodynamic properties. Having identified monovalent cations part of GR_{SO_4} , a GR-2 compound, it is reasonable to assume that other GR-2 compounds exhibit similar structural properties. It is important to determine if this is also the case for GR-1 compounds. AFM high-resolution images provided the possibility of determining a superstructure of GR_{SO_4} . It would be interesting to examine other GR compound surfaces to establish if they exhibit superstructures as a result of internal ordering and try substituting Cr(III) to see if the ordering is preserved.

With the increasing problems of contaminants in the environment, and the need for cheap and easy remediation techniques, it would be interesting to study the interaction between GR compounds and various contaminants using AFM and CT-XRD. Because of potential of GR to reduce and incorporate trace components, it is important to further investigate the presence of colloidal GR in groundwater systems, because it could influence the transport and immobilisation of such components as heavy metals such as Cr, As, Pb, organic molecules such as pesticides and radionuclides such as U and the tri-valent actinides. Some of these topics will be attacked in work following acceptance of this thesis.

10 Acknowledgements

I am very grateful for the fruitful discussions and comments from my advisor Susan L. S. Stipp and especially for bringing my attention to the complex and very interesting world of Green Rust compounds. Fruitful discussions for improving the text with Jannik Vindeløv, Knud Dideriksen and Rune Kristensen are fully acknowledged. I am most indebted for technical assistance offered by Birgit Damgaard, Peer Jørgensen and Helene Almind. Mössbauer spectroscopy was most kindly done at the Technical University of Denmark by Helge Rasmussen. Discussion of the Mössbauer results with Cathrine Frandsen and Steen Mørup are fully appreciated. Stimulating talks with Tonci Balić-Žunić, Hans Christian Bruun Hansen and the members of the NanoScienceGroup at the Geological Institute of University of Copenhagen, especially Lone L. Skovbjerg are likewise appreciated. Last but not least I am obliged of the support I have received from friends and family, especially my parents and sister effort of keeping me above water through out the whole process of writing and making this thesis. I would also like to thank Eva-Lena Tullborg and Ignasi Puigdomenech for showing interest for this GR project as well as giving me the opportunity to obtain samples at the hard rock laboratory at Äspö, Sweden. Svensk Kärnbränslehantering AB (SKB). The microscope lab was funded by a grant from the Natural Sciences section of the Danish Research Council.

11 Literature cited

- ABDELMOULA, M., REFAIT, PH., DRISSI, S.H., MIHE, J.P. AND GÉNIN, J.-M.R. (1996) Conversion electron Mössbauer spectroscopy and x-ray diffraction studies of the formation of carbonate-containing Green Rust One by corrosion of metallic iron in NaHCO₃ and (NaHCO₃+NaCl) solutions. *Corrosion Science* **38**, 623-633.
- ABDELMOULA, M., TROLARD, F., BOURRIÉ, G. AND GÉNIN, J.-M.R. (1998) Evidence for the Fe(II)-Fe(III) Green Rust “Fougerite” mineral occurrence in the hydromorphic soil and its transformation with depth. *Hyperfine Interactions* **112**, 235-238.
- AGRAWAL, A., FERGUSON, W. GARDNER, B.O., CHRIST, J.A., BANDSTRA, J.Z. AND TRATNYEK, P.G. (2002) Effects of Carbonate Species on the Kinetics of Dechlorination of 1,1,1-Trichloroethane by Zero-Valent Iron. *Environmental Science and Technology* **36**, 4326-4333.
- ALLMANN, R. (1968) The Crystal Structure of Pyroaurite. *Acta Crystal* **B24**, 972-977.
- ANTHONY, J.W., BIDEAUX, R.A, BLADH, K.W. AND NICHOLS, M.C. (1997). *In: Handbook of Mineralogy Volume III, Halides, Hydroxides, oxides*, 13.
- ARDEN, T.V. (1950) The Solubility Products of Ferrous and Ferrosic Hydroxides. *Journal of the Chemical Society* **1**, 882-885.
- ARRHENIUS, G., BACHMAN, J., GEDULIN, B., HUI, S. AND PAPLAWSKY, W. (1989) Anion selective minerals as concentrators and catalysts for RNA precursor components. *Origins of Life and Evolution of the Biosphere* **19**, 235-236.
- ARRHENIUS, G., GEDULIN, B. AND MOJZSIS, S (1993) Phosphate in models for chemical evolution. *In: Chemical Evolution: Origin of Life (Eds. Ponnampereuma, C and Chela-Flores A Deepak Publishing)*, 25-50.
- ARRHENIUS, G., SALES, B., MOJZSIS, S. AND LEE, T. (1997) Entropy and Charge in Molecular Evolution – the Case of Phosphate. *Journal of Theoretical Biology* **187**, 503-522.
- BAILEY, S.W. (1988) Chlorites: Structures and Crystal Chemistry. *In Reviews in Mineralogy volume 19 (Ed. Bailey, SW)*, 347-403.
- BENALI, O., ABDELMOULA, M., REFAIT, P., GÉNIN, J-M. R. (2001) Effect of orthophosphate on the oxidation products of Fe(II)-Fe(III) hydroxycarbonate: The transformation of green rust to ferrihydrite. *Geochimica et Cosmochimica Acta* **65**, 1715-1726.
- BENDER KOCH, C. AND HANSEN, H.C.B. (1997) Reduction of Nitrate to Ammonium by Sulphated Green Rust. *Advances in GeoEcology* **30**, 373-393.
- BENDER KOCH, C. AND MØRUP, S. (1991) Identification of green rust in an ochre sludge. *Clay Minerals* **26**, 577-582.

- BERNAL, J.D., DASGUPTA, D.R., MACKAY, A.L. (1959) The oxides and hydroxides of iron and their structural inter-relationships. *Clay Mineral Bulletin* **4**, 15-30.
- BOND, D.L. AND FENDORF, S. (2003) Kinetics and Structural Constraints of Chromate Reduction by Green Rusts. *Environmental Science and Technology* **37**, 2750-2757.
- BOURRIÉ, G., TROLARD, F., GÉNIN, J.-M.R., JAFFREZIC, A., MAITRE, V. AND ABDELMOULA, M. (1999) Iron control by equilibria between hydroxy-Green Rusts and solutions in hydromorphic soils. *Geochimica et Cosmochimica* **63**, 3417-3427.
- BRINDLEY, G.W. AND BISH, D.L. (1976) Green rust: a pyroaurite type structure. *Nature* **263**, 353.
- BURNS, R.G. (1980a) Does feroxyhyte occur on the surface of Mars? *Nature* **285**, 647.
- BURNS, R.G. (1980b) Feroxyhyte on Mars? *Nature* **288**, 196.
- CARLSON, L. AND SCHWERTMANN, U. (1980) Natural Occurrence of Feroxyhyte (δ^+ -FeOOH). *Clays and Clay Minerals* **28**, 272-280.
- CARLSON, L. AND SCHWERTMANN, U. (1990) The Effect of CO₂ and Oxidation Rate on the Formation of Goethite versus Lepidocrocite from an Fe(II) System at pH 6 and 7. *Clay Minerals* **25**, 65-71.
- CHALAMET, A. (1973) (AS CITED BY HANSEN ET AL., 1994). Reduction sous atmosphere inerte de l'acide nitreux par les ions ferreux. *Ann. Chim* **8**, 353-358.
- CHAUDHURI, S.K., LACK, J.G., COATES, J.D. (2001) Biogenic Magnetite Formation through Anaerobic Biooxidation of Fe(II). *Applied and Environmental Microbiology* **67**, 2844-2848.
- CHUKHROV, F.V., ZVYAGIN, B.B., GORSHKOV, A.I., YERMILOVA, L.P., KOROVUSHKIN, V.V., RUDNITSKAYA, YE.S. AND YAKUBOVSKAYA, N.YU. (1977) Feroxyhyte, a new modification of FeOOH. *International Geology Review* **19**, 873-890.
- COOPER, D.C., PICARDAL, F., RIVERA, J. AND TALBOT, C. (2000) Zinc Immobilization and Magnetite Formation via Ferric Oxide Reduction by *Shewanella putrefaciens* 200. *Environmental Science and Technology* **34**, 100-106.
- CORNELL, R.M. AND SCHNEIDER, W. (1989) Formation of goethite from ferrihydrite at physiological pH under the influence of cysteine. *Polyhedron* **8**, 149-155.
- CORNELL, R.M. AND SCHWERTMANN, U. (1996) The Iron Oxides. Structure, Properties, Reactions, Occurrences and Uses. VCH, Weinheim, Germany, 573 pp .
- CUTTLE, A.H., MAN, V., CRANSHAW, T.E. AND LONGWORTH, G. (1990) A Mössbauer study of green rust precipitates; I, Preparations from sulphate solutions. *Clay Minerals* **25**, 289-301.

- DASGUPTA, D.R. AND MACKAY, A.L. (1959) β -Ferric Oxyhydroxides and green rust. *Journal of the Physical Society of Japan* **14**, 932-935.
- DYAR, M.D. AND BURNS R.G. (1986) Mössbauer spectral study of ferroginous one-layer trioctahedral micas. *American Mineralogist* **71**, 955-965.
- DETOURNAY, J., DE MIRANDA, L., DERIE, R. AND GHODSI, M. (1975) The region of stability of green rust II in the electrochemical potential-pH equilibrium diagram of iron in sulphate medium. *Corrosion Science* **15**, 295-306.
- DODGE, C.J., FRANCIS, A.J., GILLOW, J.B., HALADA, G.P., ENG, C. AND CLAYTON, C.R. (2002) Association of Uranium with Iron Oxides Typically Formed on Corroding Steel Surfaces. *Environmental Science and Technology* **36**, 3504-3511.
- DOMINGO, C., RODRIGUEZ-CLEMENTE, R. AND BLESAS, M.A. (1993) Kinetics of oxidative precipitation of iron oxide particles. *Colloids and Surfaces A - Physicochemical and Engineering Aspects* **79**, 177-189.
- DRISSI, H., REFAIT, P. AND GÉNIN, J.-M.R. (1994) The oxidation of Fe(OH)(2) in the presence of carbonate ions - structure of carbonate green rust one. *Hyperfine Interactions* **90**, 395-400.
- DRISSI, H., REFAIT, P., ABDELMOULA, M. AND GÉNIN, J.-M.R. (1995) The preparation and thermodynamic properties of Fe(II)-Fe(III) hydroxide-carbonate (Green Rust 1); Pourbaix diagram of iron in carbonate-containing aqueous media. *Corrosion Science* **37**, 2025-2041.
- DRITS, V.A., SOKOLOVA, T.N., SOKOLOVA AND CHERKASHIN, V.I. (1987) New members of the hydrotalcite-manasseite group. *Clays and Clay Minerals* **35**, 401-417.
- EGGLESTON, C.M. (1994) High-Resolution Scanning Probe Microscopy: Tip-Surface Interaction, Artefacts, and Application in Mineralogy and Geochemistry. In: *CMS Workshop Lectures volume 7. Scanning Probe Microscopy of Clay Minerals* (Eds. Nagy, K.L. and Blum, A.E. Clay Mineral Society, Aurora, CO, USA), 1-90.
- ELLIS, A.S., JOHNSON, T.M., BULLEN, T.D. AND HERBEL, M.J. (2003) (AS CITED BY JOHNSON AND BOND, 2003) Selenium isotope fractionation by natural microbial consortia in unamended sediment slurries. *Chemical Geology* **in press**.
- ERBS, M., HANSEN, H.C.B. AND OLSEN, C.E. (1999) Reductive dechlorination of carbon tetrachloride using iron (II) iron (III) hydroxide sulfate (green rust). *Environmental Science and Technology* **33**, 307-311.
- FEDER, F., KLINGELHOEFER, G., TROLARD, F. AND BOURRIÉ, G. (2002) In situ Mössbauer spectroscopy and soil solution monitoring to follow spatial and temporal iron dynamics. *17th World Congress of Soil Sciences*, 1654-1 - 1654-10.
- FEITKNECHT, W. AND KELLER, G. (1950) Über die dunkelgrünen Hydroxyverbindungen des Eisens. *Zeitschrift für Anorganische Chemie* **262**, 61-68.

FEITKNECHT, W. AND SCHINDLER, P. (1963) (AS CITED BY CORNELL AND SCHWERTMANN, 1996) Löslichkeitskonstanten von Metalloxiden, -hydroxiden, und – hydroxysalzen in wässrigen Lösungen. *Pure Applied Chemistry* **6**, 125-199.

FERROW, E.A. (2002) Experimental weathering of biotite, muscovite and vermiculite: a Mössbauer spectroscopy study. *European Journal of Mineralogy* **14**, 85-95.

GANCEDO, J.R., MARTINEZ, M.L. AND OTON, J.M. (1983) Formation of Green Rust in NH_4NO_3 solutions. *Anales de Quimica série A* **79**, 470-472.

GÉHIN, A., RUBY, C., ABDELMOULA, M., BENALI, O., GHANBAJA, J., REFAIT, PH. AND GÉNIN, J.-M.R. (2002) Synthesis of Fe(II-III) hydroxysulphate green rust by coprecipitation. *Solid State Sciences* **4**, 61-66.

GÉNIN, J.-M.R., BOURRIÉ, G., TROLARD, F., ABDELMOULA, M., JAFFREZIC, A., REFAIT, P., MAITRE, V. AND HERBILLON, A. (1998a) Thermodynamic Equilibria in Aqueous Suspensions of Synthetic and Natural Fe(II)-Fe(III) Green Rusts: Occurrences of the Mineral in Hydromorphic Soils. *Environmental Science and Technology* **32**, 1058-1068.

GÉNIN, J.-M.R., OLOWE, A.A., RESIAK, B., CONFENTE, M., ROLLET-BENBOUZID, N., HARIDON, S.L. AND PRIEUR, D. (1994) Products obtained by microbially-induced corrosion of steel in a marine environment: Role of green rust two. *Hyperfine Interactions* **93**, 1807-1812.

GÉNIN, J.-M.R., OLOWE, A.A., BENBOUZID-ROLLET, N.D., PRIEUR, D., CONFENTE, M. AND RESIAK, B. (1991) The simultaneous presence of green rust 2 and sulfate reducing bacteria in the corrosion of steel sheet piles in the harbour area. *Hyperfine Interactions* **69**, 875-878.

GÉNIN, J.-M.R., OLOWE, A.A., REFAIT, PH. AND SIMON, L. (1996) On the stoichiometry and Pourbaix diagram of Fe(II)-Fe(III) hydroxyl-sulphate or sulphate containing green rust 2: an electrochemical and Mössbauer spectroscopy study. *Corrosion Science* **38**, 1751-1762.

GÉNIN, J.-M.R., REFAIT, P., BOURRIÉ, G., ABDELMOULA, M. AND TROLARD, F. (2001) Structure and stability of the Fe(II)-Fe(III) green rust “fougerite” mineral and its potential for reducing pollutants in soil solutions. *Applied Geochemistry* **16**, 559-570.

GÉNIN, J.-M.R., REFAIT, P., SIMON, L. AND DRISSI, S.H. (1998b) Preparation and E-h-pH diagrams of the Fe(II)-Fe(III) green rust compounds; hyperfine interaction characteristics and stoichiometry of hydroxy-chloride, -sulphate and –carbonate. *Hyperfine Interactions* **111**, 313-318.

HANSEN, H.C.B. (1989) Composition, stabilization, and light absorption of Fe(II)Fe(III) hydroxy-carbonate (green rust). *Clay Minerals* **24**, 663-669.

HANSEN, H.C.B. (2001) Environmental chemistry of iron(II)-iron(III) LDHs (Green Rusts). *In: Layered double hydroxides: present and future* (Ed. Rives, V. Nova Science Publishers, Inc New York), 413-434.

HANSEN, H.C.B. AND KOCH, C.B. (1998) Reduction of nitrate to ammonium by sulphate green rust; activation energy and reaction mechanism. *Clay Minerals* **33**, 87-101.

- HANSEN, H.C.B. AND KOCH, C.B. (1999) (AS CITED BY WILLIAMS AND SCHERER, 2001) A comparison of nitrate reduction by carbonate and sulphate forms of green rust. *IN Clays for our future, proceedings of the 11th International Clay Conference; (Eds. Kodama, H. Mermut, A.R. and Torrance, J.K. Ottawa, Canada 1999).* 295-302.
- HANSEN, H.C.B. AND POULSEN, I.F. (1999) Interaction of synthetic sulphate “green rust” with phosphate and the crystallization of vivianite. *Clays and Clay Minerals* **47**, 312-318.
- HANSEN, H.C.B., BORGGAARD, O.K. AND SØRENSEN, J. (1994) Evaluation of the free energy of formation of Fe(II)-Fe(III) hydroxide-sulphate (green rust) and its reduction of nitrite. *Geochimica et Cosmochimica Acta* **58**, 2599-2608.
- HANSEN, H.C.B., GULDBERG, S., ERBS, M. AND KOCH, C.B. (2001) Kinetics of nitrate reduction by green rusts – effects of interlayer anion and Fe(II):Fe(III) ratio. *Applied Clay Science* **18**, 81-91.
- HANSEN, H.C.B., KOCH, C.B., NANCKE-KROGH, H., BORGGAARD, O.K. AND SØRENSEN, J. (1996) Abiotic nitrate reduction to ammonium: Key role of green rust. *Environmental Science and Technology* **30**, 2053-2056.
- HARDY, L.I. AND GILLHAM, R.W. (1996) Formation of Hydrocarbons from the Reduction of Aqueous CO₂ by Zero-Valent Iron. *Environmental Science and Technology* **30**, 57-65.
- HASHI, K., KIKKAWA, S. AND KOIZUMI, M. (1983) Preparation and properties of pyroaurite-like hydroxy minerals. *Clays and Clay Minerals* **31**, 152-154.
- HELLER-KALLAI, L. AND ROZENSON, I. (1981) The Use of Mössbauer Spectroscopy of Iron in Clay Mineralogy. *Physics and Chemistry of Minerals* **7**, 223-238.
- HENRIKSEN, K. AND STIPP, S.L.S. (2002) Image distortion in scanning probe microscopy. *American Mineralogist* **87**, 5-16.
- JOHNSON, T.M. AND BULLEN, T.D. (2003) Selenium isotope fractionation during reduction by Fe(II)-Fe(III) hydroxide-sulfate (green rust). *Geochimica et Cosmochimica Acta* **67**, 413-419.
- KARIM, Z. (1986) Formation of ferrihydrite by inhibition of green rust structures in the presence of silicon. *Soil Science Society of America Journal* **50**, 247-250.
- KELLER, G. (1948) Über Hydroxyde und basische Salze des 2wertigen Eisens und deren dunkelgrünen Oxydationsprodukte. *Doctoral thesis, Bern*, 109 pp.
- KLEIN, C. AND HURLBUT, C.S. JR. (1993) *Manual of Mineralogy, John Wiley and Sons Inc. Canada.* 681 pp.
- KOLB, V., ZHANG, S., XU, Y. AND ARRHENIUS, G. (1997) Mineral induced phosphorylation of glycolate ion – A metaphor in chemical evolution. *Origins of Life and Evolution of the Biosphere* **27**, 485-503.

KOUNDE, B., RAHARINAIVO, A., OLOWE, A.A., REZEL, D., BAUER, PH. AND GÉNIN, J.-M.R. (1989) Mössbauer characterization of the corrosion products of steel in civil works: Suspension bridge and reinforced concrete. *Hyperfine Interactions* **46**, 421-428.

KUROKAWA, H. AND SENNA, M. (1999) Self-stabilization of green rust (II) as a precursor of acicular goethite particles with highest possible aspect ratio. *Powder Technology* **103**, 71-79.

LEGRAND, L., ABDELMOULA, M., GÉHIN, A., CHAUSSÉ, A. AND GÉNIN, J.-M.R. (2001) Electrochemical formation of a new Fe(II)-Fe(III) hydroxy-carbonate green rust: characterisation and morphology. *Electrochimica Acta* **46**, 1815-1822.

LEGRAND, L., SAVOYE, S., CHAUSSE, A AND MESSINA, R. (2000) Study of the oxidation products formed on iron in solutions containing bicarbonate/carbonate. *Electrochimica Acta* **46**, 111-117.

LEWIS, D.G. (1997) Factors Influencing the Stability and Properties of Green Rusts. *Advances in GeoEcology* **30**, 345-372.

LIN, R.G., SPICER, R.L., TUNGATE, F.L. AND DAVIS, B.H. (1996) A study of the oxidation of ferrous hydroxide in slightly basic solution to produce gamma-FeOOH. *Colloids and Surfaces A - Physicochemical and Engineering Aspects* **113**, 79-96.

LIN, Z. AND PULS, R.W. (2003) Potential indicators for the assessment of arsenic attenuation in the subsurface. *Advances in Environmental Research* **7**, 825-834.

LOYAUX-LAWNICZAK, S., REFAIT, P., EHRHARDT, J.J., LECOMTE, P. AND GÉNIN, J.-M.R. (2000) Trapping of Cr by formation of ferrihydrite during the reduction of chromate ions by Fe(II)-Fe(III) hydroxysalt green rusts. *Environmental Science and Technology* **34**, 438-443.

MCGILL, I.R., MCENANEY, B. AND SMITH, D.C. (1976a) Crystal structure of green rust formed by corrosion of cast iron. *Nature* **259**, 200-201.

MCGILL, I.R., MCENANEY, B. AND SMITH, D.C. (1976b) Green rust: a pyroaurite type structure. *Nature* **263**, 353-354.

MENDIBOURE, A. AND SCHÖLLHORN, R. (1986) Formation and anion exchange reactions of layered transition metal hydroxides. *Revue de Chimie Minérale* **23**, 819-827.

MIYATA, S. (1983) Anion-exchange properties of hydrotalcite-like compounds. *Clays and Clay Minerals* **31**, 305-311.

MORAGHAN, J.T. AND BURESH, R.J. (1977) Chemical Reduction of Nitrite and Nitrous Oxide by Ferrous Iron. *Soil Science Society of America, Journal* **41**, 47-50.

MURAD, E. AND TAYLOR, R.M. (1984) The Mössbauer spectra of hydroxycarbonate green rusts. *Clay Minerals* **19**, 77-83.

- MURAD, E. AND TAYLOR, R.M. (1986). (AS CITED BY DRISSI ET AL., 1995). *Hyperfine Interactions*, 585.
- MYNENI, S.C.B., TOKUNAGA, T.K. AND BROWN JR., G.E. (1997) Abiotic selenium redox transformations in the presence of Fe(II,III) oxides. *Science* **278**, 1106-1109.
- MYNENI, S.C.B., TOKUNAGA, T.K. AND BROWN JR., G.E. (1998) "Green Rust" in the Lab and in the Soil. *Science* **281**, 1111a.
- MØRUP, S. (1997) Mössbauer Spectroscopy and its Application in Materials Science. *Department of Physics, Technical University of Denmark*, 72 pp.
- NISHIMURA, T. AND ROBINS, R.G. (2000) Removal of Arsenic in Gold Cyanide Processes. *In: Minor elements 2000. Processing and Environmental Aspects of As, Sb, Se, Te* **135-140**, .
- O'LOUGHLIN, E.J., KELLY, S.D., COOK, R.E., CSENCISITS, R. AND KEMNER, K.M. (2003a) Reduction of Uranium(VI) by Mixed Iron(II)/Iron(III) Hydroxide (Green Rust): Formation of UO₂ Nanoparticles. *Environmental Science and Technology* **37**, 721-727.
- O'LOUGHLIN, E.J., KELLY, S.D., KEMNER, K.M., CSENCISITS, R. AND COOK, R.E. (2003b) Reduction of AgI, AuIII, CuII and HgII by FeII/FeIII hydroxysulfate green rust. *Chemosphere* **53**, 437-446.
- OLOWE, A.A., MARIE, Y., REFAIT, PH. AND GÉNIN, J.-M.R. (1991) The influence of concentration on the oxidation of ferrous hydroxide in basic sulphated medium: Particle size analysis of goethite and δ -FeOOH. *Corrosion Science* **9**, 1003-1020.
- ONA-NGUEMA, G., ABDELMOULA, M., JORAND, F., BENALI, O., GÉHIN, A., BLOCK, J.-C. AND GÉNIN, J.-M.R. (2002) Iron (II,III) hydroxycarbonate green rust formation and stabilisation from lepidocrocite bioreduction. *Environmental Science and Technology* **36**, 16-20.
- OREMLAND, R.S., STOLZ, J. AND LOVLEY, D. (1998) "Green Rust" in the Lab and in the Soil. *Science* **281**, 1111a.
- PARMAR, N., GORBY, Y.A., BEVERIDGE, T.J., FERRIS, F.G. (2001) Formation of Green Rust and Immobilisation of Nickel in Response to Bacterial Reduction of Hydrous Ferric Oxide. *Geomicrobiology Journal* **18**, 375-385.
- PEPPER, S.A., BUNKER, D.J., BRYAN, N.D., LIVENS, F.R., CHARNOCK, J.M., PATTRICK, R.A.D. AND COLLISON, D. (2003) Treatment of radioactive wastes: An X-ray absorption spectroscopy study of the reaction of technetium with green rust. *Journal of Colloid and Interface Science* **268**, 408-412.
- PITSCH, S., KRISHNAMURTHY, R. AND ARRHENIUS, G. (2000) Concentration of Simple Aldehydes by Sulfite-Containing Double-Layer hydroxide Minerals: Implications for Biopoesis. *Helvetica Chimica Acta* **83**, 2398-2411.

- PONNAMPERUMA, F.N, TIANCO, E.M. AND LOY, T. (1967) Redox equilibria in flooded soils: I The iron hydroxide systems. *Soil Science* **103**, 374-382.
- RANDALL, S.R., SHERMAN, D.M. AND RAGNARSDOTTIR, K.V. (2001) Sorption of As(V) on green rust (Fe₄(II)Fe₂(III)(OH)₁₂SO₄•3H₂O) and lepidocrocite (γ-FeOOH): Surface complexes from EXAFS spectroscopy. *Geochimica et Cosmochimica Acta* **65**, 1015-1023.
- REFAIT, PH. AND GÉNIN J.-M.R. (1993) The oxidation of ferrous hydroxide in chloride-containing aqueous media and Pourbaix diagrams of green rust one. *Corrosion Science* **34**, 797-819.
- REFAIT, PH., ABDELMOULA, M. AND GÉNIN, J.-M.R. (1998a) Mechanisms of formation and structure of green rust one in aqueous corrosion of iron in the presence of chloride ions. *Corrosion Science* **40**, 1547-1560.
- REFAIT, PH., DRISSI, H., MARIE, Y. AND GÉNIN, J.-M.R. (1994) The substitution of Fe²⁺ ions by Ni²⁺ ions in green rust one compounds. *Hyperfine Interactions* **90**, 389-394.
- REFAIT, PH., DRISSI, S. H., PYTKIEWICZ, J. AND GÉNIN, J.-M.R. (1997) The anionic species competition in iron aqueous corrosion: Role of various green rust compounds. *Corrosion Science* **39**, 1699-1710.
- REFAIT, PH., SIMON, L. AND GÉNIN, J.-M.R. (2000) Reduction of SeO₄²⁻ anions and anoxic formation of iron(II)-iron(III) hydroxy-selenate green rust. *Environmental Science and Technology* **34**, 819-825.
- REFAIT, PH., BON, C., SIMON, L., BOURRIÉ, G., TROLARD, F., BESSIERE, J. AND GÉNIN, J.- M.R. (1999) Chemical composition and Gibbs standard free energy of formation of Fe(II)-Fe(III) hydroxysulphate green rust and Fe(II) hydroxide. *Clay Minerals* **34**, 499-510.
- REFAIT, PH., CHARTON, A. AND GÉNIN, J.-M.R. (1998b) Identification, Composition, thermodynamic and structural properties of a pyroaurite- like iron(II)-iron(III) hydroxy-oxalate Green Rust. *European Journal of Solid State and Inorganic Chemistry* **35**, 655-666.
- RIVES, V. (2001) Layered Double Hydroxides: Present and Future. *Nova Science Publishers, Inc. New York*, 438 pp.
- ROH, Y., LEE, S.Y. AND ELLESS, M.P. (2000a) Characterisation of corrosion products in the permeable reactive barriers. *Environmental Geology* **40**, 184-194.
- ROH, Y., LEE, S.Y., ELLESS, M.P. AND FOSS, J.E. (2000b) Incorporation of radioactive contaminants into pyroaurite-like phases by electrochemical synthesis. *Clays and Clay Minerals* **48**, 266-271.
- SCHWERTMANN, U. AND FECHTER, H. (1994) The formation of green rust and its transformation to lepidocrocite. *Clay Minerals* **29**, 87-92.

- SIMON, L., FRANÇOIS, M., REFAIT, P., RENAUDIN, G., LELAURAIN, M. AND GÉNIN, J.-M.R. (2003) Structure of the Fe(II-III) layered double hydroxysulphate green rust two from Rietveld analysis. *Solid State Sciences* **5**, 327-334.
- SIMON, L., GÉNIN, J.-M.R. AND REFAIT, PH. (1997) Standard free enthalpy of formation of Fe(II)-Fe(III) hydroxysulphite green rust one and its oxidation into hydroxysulphate green rust two. *Corrosion Science* **39**, 1673-1685.
- SONNE LARSEN, M. (2003) Substitution af karbonat i sulfat grøn rust, samt omdannelsesprodukter ved varierende karbonatkoncentration. *Bachelorprojekt*, 31 pp.
- SQUIRES, R.C., GROVES, R. AND JOHNSTON, W.R. (1989) Economics of Selenium Removal from Drainage Water. *Journal of Irrigation and Drainage Engineering* **115**, 48-57.
- SRINIVASAN, R, LIN, R. G., SPICER, R. L. AND DAVIS, B. H. (1996) Structural features in the formation of the green rust intermediate and gamma-FeOOH. *Colloids and Surfaces A - Physicochemical and Engineering Aspects* **113**, 97-105.
- STAMPFL, P. P. (1969) Ein Basisches Eisen-II-III-Karbonat in Rost. *Corrosion Science* **9**, 185-187.
- STIPP, S.L.S., HANSEN, M., KRISTENSEN, R., HOHELLA JR., M.F., BENNEDSEN, L., DIDERIKSEN, K., BALIC-ZUNIC, T., LÉONARD, D. AND MATHIEU, H.-J. (2002) Behaviour of Fe-oxides relevant to contaminant uptake in the environment. *Chemical Geology* **190**, 321-337.
- STUMM, W. AND MORGAN, J.J. (1996) *Aquatic Chemistry. Chemical Equilibria and Rates in Natural Waters. John Wiley and Sons, Inc. New York, USA.* 1024 pp.
- TAMAURA, Y. (1985) Ferrite formation from the intermediate, Green rust II, in the transformation reaction of γ -FeO(OH) in aqueous suspension. *Inorganic Chemistry* **24**, 4363-4366.
- TAMAURA, Y., SATURNO, M., YAMADA, K. AND KATSURA, T. (1984b) The transformation of γ -FeO(OH) to Fe₃O₄ and green rust II in an aqueous solution. *Bulletin of the Chemical Society of Japan* **57**, 2417-2421.
- TAMAURA, Y., YOSHIDA, T. AND KATSURA, T. (1984a) The synthesis of Green Rust II(Fe^{III}₁-Fe^{II}₂) and its spontaneous transformation into Fe₃O₄. *Bulletin of the Chemical Society of Japan* **57**, 2411-2416.
- TAYLOR, R.M. AND SCHWERTMANN, U. (1974) Maghemite in soils and its origin II Maghemite syntheses at ambient temperature and pH 7. *Clay Minerals* **10**, 299-310.
- TAYLOR, R. M. (1980) Formation and properties of Fe(II)Fe(III) hydroxy-carbonate and its possible significance in soil formation. *Clay Minerals* **15**, 369-382.
- TAYLOR, R. M. (1984a) Influence of chloride on the formation of iron oxides from Fe(II) chloride; I, Effect of [Cl]/[Fe] on the formation of magnetite. *Clays and Clay Minerals* **32**, 167-174.

TAYLOR, R. M. (1984b) Influence of chloride on the formation of iron oxides from Fe(II) chloride; II, Effect of [Cl] on the formation of magnetite. *Clays and Clay Minerals* **32**, 175-180.

THOMPSON-EAGLE, E.T. AND FRANKENBERGER JR., W.T. (1992) Bioremediation of Soils Contaminated with Selenium. In: *Advances in Soil Science 17. Soil Restoration*. (Eds. Lal, R. and Stewart, B.A. Springer-Verlag, New York), 261-310.

TOCHIHARA, S., IMAOKA, Y. AND NAMIKAWA, M. (1970). (AS CITED BY KUROKAWA AND SENNA, 1999). *IEEE Trans. Magn* **6**, 808.

TROLARD, F., GÉNIN, J. M. R., ABDELMOULA, M., BOURRIÉ, G., HUMBERT, B. AND HERBILLON, A. (1997) Identification of a green rust mineral in a reductomorphic soil by Moessbauer and Raman spectroscopies. *Geochimica et Cosmochimica Acta* **61**, 1107-1111.

VINŠ, J., ŠUBRT, J., ZAPLETAL, V. AND HANOUSEK, F. (1987) Preparation and properties of green rust type substances. *Collection Czechoslovak Chemical Communication* **52**, 93-102.

WANG, Z., MOORE, R.C., FELMY, A.R., MASON, M.J. AND KUKKADAPU, R.K. (2001) A study of the corrosion products of mild steel in high ionic strength brines. *Waste Management* **21**, 335-341.

WECKHUYSSEN, B.M., WACHS, I.E. AND SCHOONHEYDT, R.A. (1996) Surface Chemistry and Spectroscopy of Chromium in Inorganic Oxides. *Chemical Review* **96**, 3327-3349.

WILLIAMS, A.G.B. AND SCHERER, M.M. (2000) Chromate reduction by Hydroxycarbonate Green Rust. *Proceedings of the 2000 conference on hazardous waste research*.

WILLIAMS, A.G.B. AND SCHERER, M.M. (2001) Kinetics of the Cr(VI) reduction by carbonate green rust. *Environmental Science and Technology* **35**, 3488-3494.

ØSTERGAARD, L.F. (2003) A study of iron oxides formed in solutions representing hydrothermal conditions. *Master Thesis*, 115 pp.

